

ATTITUDE DETERMINATION AND POINTING CONTROL SYSTEM FOR



AALBORG UNIVERSITY
STUDENT REPORT

BSc 2013 | Electronic Engineering & IT | Supervisor: Palle Andersen
Project Group: Michael Nauheimer | Kevin Lyn-Knudsen | Mathias
Mølgaard | Kasper Hemme | Britt Jakobsen |

Aalborg University
The Faculty of Engineering and Science
School of Information and
Communication Technology
Frederik Bajers Vej 7
9220 Aalborg Ø
Tlf.: 9940 9730
Telefax: 9940 9725
<http://www.es.aau.dk>



Subject: Electronics & IT, Control Engineering
Title: Attitude Determination and Pointing Control System for AAUSAT4
Project period: February 4th – May 29th 2013
Semester: 6th Semester (P6)
Project group: 632
Authors:

Kevin Lyn-Knudsen

Michael Nauheimer

Kasper Hemme

Mathias Mølgaard

Britt Jakobsen

Supervisor: Palle Andersen
Number of copies: 9

Pages: 114

Appendix pages: 20

Attachment: 1 cd

Synopsis:

Aalborg University has a history of developing CubeSat satellites. These are sought designed modularly in the view of facilitating reuse of subsystems or parts thereof for new satellites with different missions.

This project deals with the Attitude Determination and Control System (ADCS) for AAUSAT4, scheduled to be part of the ESA QB50 mission. The system is an enhancement of the existing ADCS developed for AAUSAT3. With the detumbling algorithm of AAUSAT3 demonstrated to be well-functioning, the focus of this project is the development of a pointing algorithm which meets the QB50 pointing requirements.

The software is developed to be compatible with the existing hardware platform designed for AAUSAT3. Additionally it has been investigated which sensors and actuators could be relevant for future enhancement of the hardware platform for AAUSAT4.

This report documents the theory behind attitude description, determination and control, and simulations of the developed attitude determination and pointing software. An ADCS hardware platform is assembled for implementation of the software on the intended hardware in the form of an acceptance test. The acceptance test verifies the functionality of the attitude determination system, while the attitude control is verified through simulations only, in lack of an actuator PWM driver for the topical micro controller.

The contents of this report are freely available, but publication (with specification of source) may only take place after arrangement with the authors.

Preface

This BSc report documents the work on the Attitude Determination and Control System (ADCS) for AAUSAT4 developed by 6th semester group 632 in Control Engineering within Electronics & IT at Aalborg University. The primary focus of the report is to make improvements to the existing ADCS system for AAUSAT3, which has been developed at Aalborg University by previous students. The central aspects of the project are: representation of orientation in space in terms of reference frames, description and simulation of the physics of an orbiting spacecraft, analysing future improvements to the ADCS hardware and in particular developing an attitude determination and pointing algorithm for the AAUSAT4.

Reading Guide

Sources given in the beginning of a section apply to all subsections. Additional sources may be given in subsections. Citations are given in square brackets indicating the author (first) and the year of publication (last two ciphers), i.e. *Spacecraft Attitude Determination and Control* from 1978 by J.R. Wertz is given as [Wertz 78]. Figures, equations and tables are numbered according to chapter and location, e.g. third figure in chapter five is numbered 5.3. Units are given in square brackets in symbolic equations and without brackets otherwise.

Symbols, acronyms, general notation and reference frames used in this report are presented in the nomenclature after this preface. Appendices are placed after the main report, referred to by capital letters, followed by the Bibliography. The attached CD contains relevant data sheets, copies of references found on the Internet, MATLAB and C scripts, Simulink models and a digital version of this report.

Acknowledgements

The project group wishes to thank associate professor at the Department of Electronic Systems Jesper A. Larsen for sharing his insights on quaternions, spacecraft dynamics and his availability to answering questions clarifying physical and mathematical matters.

The project group also wishes to thank PhD. students Kasper Vinther and Anders Bech Borchersen for providing the Simulink simulation environment of the satellite, hardware specific sensor drivers and their availability to answering questions about the AAUSAT3 ADCS and desired improvements.

Nomenclature

ADCS	Attitude Determination and Control System, subsystem on AAUSAT3 and 4	MAC	Media Access Control
ADS	Attitude Determination System	MEMS	Micro ElectroMechanical Systems
CAN	Controller Area Network	NORAD	North American Aerospace Defence Command
CoM	Centre of Mass	ORF	Orbital Reference Frame
CRF	Control Reference Frame	P-POD	Poly Picosatellite Orbital Deployer, a cuboid spring deployment contraption mounted in the launch vehicle containing up to three CubeSat units
CSP	CubeSat Space Protocol	RAAN	Right Ascension of the Ascending Node
ECEF	Earth Centered Earth Fixed	SBRF	Satellite Body Reference Frame
ECI	Earth Centered Inertial	SGP4	Simplified General Perturbation model no. 4, propagation model used for description of near-Earth orbits
EEPROM	Electrically Erasable Programmable Read-Only-Memory	SPI	Serial Peripheral Interface
EPS	Electronic Power System, subsystem on AAUSAT3 and 4	SRAM	
ESA	European Space Agency	SVD	Singular Value Decomposition
EVD	Eigen Value Decomposition	TLE	Two Line Element, contains orbit information about a satellite
I ² C	Inter-Integrated Circuit	TRF	Target Reference Frame
IGRF	International Geomagnetic Reference Field, model of the Earth's magnetic field	UTC	Coordinated Universal Time, follows Greenwich Mean Time, but is occasionally corrected according to Sun and Earth movements, thus being scientifically more correct
IOD	In Orbit Demonstrations		
JTAG	Joint Test Action Group		
LEO	Low Earth Orbit, orbits in ~160-2000km altitude		

Notation

Reference frames

There is a number of different reference frames which are used to describe vectors according to different coordinate systems. The notation of the reference frames are important to understand to know in which coordinate system a vector is given. The notation of each reference frame is shown below, and these notations are used as a pre-superscript to the vector to indicate in which reference frame they are given.

$$\begin{array}{c|c|c} \text{ECI : } & i & \text{SBRF: } s \\ \text{ECEF : } & e & \text{CRF: } c \\ & & \text{ORF: } o \\ & & \text{TRF: } t \end{array}$$

ECI is the Earth Centred Inertial Frame, SBRF is the Satellite Body Reference Frame, ORF is the Orbit Reference Frame, ECEF is the Earth Centred Earth Fixed Frame, CRF is the Control Reference Frame and TRF is the Target Reference Frame. A definition of each of the reference frames is given in section 4.2.

Vectors

A vector is written as a bold upright lower case letter, and all entries of the vector is written as the same lower case letter with a number as subscript to indicate the entry number.

$$\mathbf{b} = \begin{bmatrix} b_1 \\ b_2 \\ b_3 \end{bmatrix} = \begin{bmatrix} b_x \\ b_y \\ b_z \end{bmatrix} \quad \mathbf{b}_c = \begin{bmatrix} b_{c,1} \\ b_{c,2} \\ b_{c,3} \end{bmatrix} = \begin{bmatrix} b_{c,x} \\ b_{c,y} \\ b_{c,z} \end{bmatrix}$$

A vector given in a certain reference frame will be denoted with a letter indicating the reference frame as a pre-superscript to the letter indicating the vector. Every entry of a vector has the letter to indicate the reference as a pre-superscript to the letter indicating the vector as well. The example below shows the vector \mathbf{b} given in the ECI reference frame.

$${}^i\mathbf{b} = \begin{bmatrix} {}^i b_1 \\ {}^i b_2 \\ {}^i b_3 \end{bmatrix} = \begin{bmatrix} {}^i b_x \\ {}^i b_y \\ {}^i b_z \end{bmatrix}$$

Vectors forming part of cross products, may be written as skew symmetric matrices (the 1-2-3 notation is omitted, but still applies):

$$\mathbf{a} = \begin{bmatrix} a_x \\ a_y \\ a_z \end{bmatrix}, \quad \mathbf{b} = \begin{bmatrix} b_x \\ b_y \\ b_z \end{bmatrix}, \quad \mathbf{a} \times \mathbf{b} = [\mathbf{a}]_\times \mathbf{b}, \quad \mathbf{b} \times \mathbf{a} = [\mathbf{a}]_\times^\text{T} \mathbf{b}, \quad [\mathbf{a}]_\times = \begin{bmatrix} 0 & -a_z & a_y \\ a_z & 0 & -a_x \\ -a_y & a_x & 0 \end{bmatrix}$$

Matrices

A matrix is written as a bold upright upper case letter, and all entries of the matrix is written as the same upper case letter with two numbers as subscript to indicate the entry number. When the matrix refers to something with relation to a coordinate system, the entry number might be replaced by x, y and z as shown. If the matrix has a subscript, this will be added to the subscript followed by a comma, before the entry number

$$\bar{\mathbf{A}} = \begin{bmatrix} A_{11} & A_{12} & A_{13} \\ A_{21} & A_{22} & A_{23} \\ A_{31} & A_{32} & A_{33} \end{bmatrix} = \begin{bmatrix} A_{xx} & A_{xy} & A_{xz} \\ A_{yx} & A_{yy} & A_{yz} \\ A_{zx} & A_{zy} & A_{zz} \end{bmatrix}$$

$$\bar{\mathbf{A}}_b = \begin{bmatrix} A_{b,11} & A_{b,12} & A_{b,13} \\ A_{b,21} & A_{b,22} & A_{b,23} \\ A_{b,31} & A_{b,32} & A_{b,33} \end{bmatrix} = \begin{bmatrix} A_{b,xx} & A_{b,xy} & A_{b,xz} \\ A_{b,yx} & A_{b,yy} & A_{b,yz} \\ A_{b,zx} & A_{b,zy} & A_{b,zz} \end{bmatrix}$$

The inverse of a matrix, $\bar{\mathbf{A}}$, is denoted

$$\bar{\mathbf{A}}^{-1}$$

The transpose of a matrix, $\bar{\mathbf{A}}$, is denoted

$$\bar{\mathbf{A}}^T$$

Rotations

A rotation can be given in terms of a rotation matrix or a quaternion (see subsection 4.1.3). The pre-superscript of either denotes the frame in which an orientation is given and the pre-subscript denotes which frame has this orientation. I.e. a matrix $\bar{\mathbf{R}}(\mathbf{q})$ being the matrix representation of the quaternion \mathbf{q} , and \mathbf{q} itself given as:

$${}^i_s\bar{\mathbf{R}}({}^i_s\mathbf{q}) \quad \Leftrightarrow \quad {}^i_s\mathbf{q}$$

describes the rotation needed for the i frame to align with the s frame. A vector \mathbf{v} given in s coordinates rotated by either, will result in the same vector given in i coordinates:

$${}^i\mathbf{v} = {}^i_s\bar{\mathbf{R}}({}^i_s\mathbf{q}) {}^s\mathbf{v} \quad \Leftrightarrow \quad {}^i\mathbf{v} = {}^i_s\mathbf{q}^* \otimes {}^s\mathbf{v} \otimes {}^i_s\mathbf{q}$$

Consecutive rotations of a vector from one frame through another to a third frame is implemented as:

$${}^o\mathbf{v} = {}^o_i\bar{\mathbf{R}}({}^o_i\mathbf{q}) {}^i_s\bar{\mathbf{R}}({}^i_s\mathbf{q}) {}^s\mathbf{v} \quad \Leftrightarrow \quad {}^o\mathbf{v} = {}^o_i\mathbf{q}^* \otimes {}^i_s\mathbf{q}^* \otimes {}^s\mathbf{v} \otimes {}^i_s\mathbf{q} \otimes {}^o_i\mathbf{q}$$

A rotation of a frame over time is likewise implemented, when Δt denotes the time interval and the function of the time interval is the rotation of the frame:

$${}^i_s\bar{\mathbf{R}}({}^i_s\mathbf{q}(t + \Delta t)) = {}^i_s\bar{\mathbf{R}}({}^i_s\mathbf{q}(\Delta t)) {}^i_s\bar{\mathbf{R}}({}^i_s\mathbf{q}(t)) \quad \Leftrightarrow \quad {}^i_s\mathbf{q}(t + \Delta t) = {}^i_s\mathbf{q}(t) \otimes {}^i_s\mathbf{q}(\Delta t)$$

For a further explanation, see section 4.1.

Contents

Preface	iii
Nomenclature	v
Notation	vi
List of Figures	1
List of Tables	3
1 Mission Analysis	5
1.1 The Necessity of Controlling a Satellite	5
1.2 AAUSAT4	6
1.3 QB50	6
1.4 Low Earth Orbital Environment	7
1.5 Low Earth Orbital Perturbations	8
1.6 Actuation Speed	10
2 System Requirements	13
2.1 AAUSAT4 ADCS Requirements	13
2.2 Delimitation to Requirements for this Project	14
3 Hardware Design of the ADCS	17
3.1 MCUs of the ADCS	18
3.2 Interface Protocols	18
3.3 Attitude Determination Sensors of AAUSAT3	20
3.4 Attitude Control Actuator of AAUSAT3	22
4 Defining Attitude	25
4.1 Parameters for Describing Attitude	25
4.2 Reference Frames	29
5 Attitude Determination	33
5.1 Orbit Description by Keplerian Orbit Elements	33
5.2 Attitude Estimation	37
5.3 Rotation Between Each of the Reference Frames	39
6 Attitude Control	43
6.1 Dynamic Model of the Satellite	43
6.2 Attitude Propagation – Kinematic Model of the Satellite	52
6.3 Attitude Control System	53

7 Simulation of the ADS and ACS	63
7.1 Simulation of the Orbital Environment	63
7.2 Simulation of the spacecraft dynamics	64
7.3 Simulation of the ADS	64
7.4 Simulation of the Controller	66
8 Integration of the ADCS	71
9 Acceptance Test	73
10 Closure	75
10.1 Conclusion	75
10.2 Further Development	75
Appendices	76
A Cubesat Standard	77
A.1 CubeSat General Specifications	77
A.2 CubeSat Mechanical Requirements	77
A.3 CubeSat Electrical and Operational Requirements	78
A.4 CubeSat Testing Requirements	78
B QB50	79
B.1 Measuring in the Lower Thermosphere	79
B.2 The QB50 CubeSat Network	79
C AAUSAT3 Sun Sensor design	81
C.1 Determination of the Sun Vector	81
C.2 Sun Sensor Coordinate System and Interfacing	82
D Additional Sensors and Actuators Considered for AAUSAT4	83
D.1 Star Tracker	83
D.2 Sun Sensor Based on Solar Panels or Image Sensor	83
D.3 Horizon Sensor	84
D.4 Accelerometer	84
D.5 Reaction Wheels	85
D.6 Thrusters	85
E Determination of Magnetorquer Torque	87
F Constructing the ADCS PCB for the Acceptance Test	91
G Test Protocol for Acceptance Test	93
I Litterature	97
Bibliography	99

List of Figures

1.1	Figure 1.1(a) depicts the average temperatures in the different layers of the atmosphere [Bouger 97]. Figure 1.1(b) depicts the density of the atmosphere, which decrease with altitude [NASA 71].	7
1.2	Overview of the magnitude of disturbance torques throughout the thermosphere [NASA 71]. The depicted magnitudes correspond to a spacecraft with the stated inertia matrix (given in kg·m ²).	8
3.1	Block diagram of the ADCS, showing sensor, actuator and MCU set-up.	17
4.1	A two dimensional example of rotation. The inertial coordinate system or frame, i , can be rotated into the coordinate system s by the rotation ${}^i_s\bar{\mathbf{R}}$. This is the same rotation needed to rotate the vector \mathbf{v} within the i frame to obtain the vector \mathbf{v}' . The i coordinates of the vector \mathbf{v}' are the same as the s coordinates of \mathbf{v}	25
4.2	Euler angles are easily visualised. Here a 3-1-3 rotation is shown, which maps the inertial frame i into the rotating frame s by first a rotation of α about the i z-axis (3), then rotating β about the x-axis of the new s'' frame (1), and finally rotating γ about the z-axis of the s' frame (3), ending with the orientation of the s frame. The dashed line indicate the line of nodes, i.e. the cross-section between the i xy-plane and the s xy-plane.	26
4.3	Coordinate system for the ECEF reference frame, matching exactly that of ECI at vernal equinox. The x-axis points towards the Sun and the z-axis goes through the geometric North Pole.	29
4.4	Coordinate system for the ORF reference frame, with origin at the CoM of the satellite, x-axis aligned with the orbit velocity vector, \bar{v} , and the z-axis pointing towards the centre of mass of the Earth, i.e. the origin in ECI/ECEF, i.e. nadir.	30
4.5	Coordinate system for the SBRF with origin at the centre of mass of the satellite, and each of the axis perpendicular to a set of satellite sides.	31
5.1	Geometric description of an ellipsis, defined by its semimajor and semiminor axes, a and b . The primary (the Earth) is situated in one of the foci of the satellite trajectory ellipsis.	33
5.2	Contorted sketch of a satellite orbit, describing the Keplerian orbital elements. The centre of the Earth is in one of the two foci of the orbit ellipse. The two angles Ω (RAAN) and ω (argument of perigee) are measured in the equatorial and the orbital plane, respectively.	34
5.3	Geometry of the true anomaly, v , and the eccentricity anomaly, E	34
5.4	TLE format specifying data type with d is a decimal number, c is a character, s is a symbol (plus or minus) and e is an exponent.	35
5.5	Contour plot of the IGRF-10 for an altitude of 630 km, for January 1 st 2010.	36

5.6	Illustration of the vector set-up for calculating when the satellite is in the shadow of Earth. The Sun is considered as a point mass.	39
6.1	When a magnetic field, \mathbf{B}_E , is incident on the magnetorquer wires as shown, the forces \mathbf{F}_1 and \mathbf{F}_2 will result to produce a torque on the satellite body.	46
6.2	Block diagram of the Attitude Determination and Control System, the plant being the satellite.	54
6.3	Block diagram for a one axis PD-controller for a position plus rate attitude control.	55
6.4	The grey surface indicate the plane perpendicular to the geomagnetic field vector, \mathbf{B}_E . In figure 6.4(a) the desired control vector $\boldsymbol{\tau}_c$, is projected onto the magnetic field vector. In figure 6.4(b) the control torque vector, $\boldsymbol{\tau}_p$, has been projected onto the plane perpendicular to \mathbf{B}_E	56
6.5	Closed loop ramp response for the controller.	58
6.6	A plot of the steady state error for the controller with a ramp input, shows a steady state error of 14.19.	58
6.7	Closed loop step response shows an overshoot of less than 5%, a rise time of approximately 18 s and settling time of approximately 66 s.	59
6.8	A plot of the steady state error magnitude with a 0.0012 slope applied to the controller, shows that the steady state error is approximately 0.017 rad.	59
6.9	A plot of the closed loop error with a 0.0012 slope applied to the controller, shows that the closed loop error with aerodynamic torque disturbance is 0.0345 rad, compared to the steady state error of 0.0017, which is without aerodynamic disturbance.	60
7.1	The block diagram above shows the simulation blocks together with the signal paths. The diagram shows the path from the spacecraft dynamics to the actuation on the magnetorquer from the controller.	63
7.2	Simulation of the ADS with a static sun vector and a magnetic vector rotating in the plane perpendicular to the sun vector.	65
7.3	Simulation of the ADS with a static sun vector and a magnetic vector rotating in the same plane as the sun vector. The x-axis is time given in seconds and the y-axis are magnitudes of the quaternion components.	65
7.4	Simulation of the ACS with a static sun vector and a perpendicular static magnetic vector. Initial quaternion attitude is equal to $(\frac{1}{\sqrt{2}}, 0, 0, \frac{1}{\sqrt{2}})$ and target quaternion is equal to $(0, 0, 0, 1)$	67
7.5	Simulation of the ACS with a static sun vector and a perpendicular rotating magnetic vector. Initial quaternion attitude is equal to $(\frac{1}{\sqrt{2}}, 0, 0, \frac{1}{\sqrt{2}})$ and target quaternion is equal to $(0, 0, 0, 1)$. The magnetorquer simulation block is bypassed, and the control torque is fed directly back in the system.	68
7.6	Simulation of the ACS with a static sun vector and a perpendicular rotating magnetic vector. Initial quaternion attitude is equal to $(\frac{1}{\sqrt{2}}, 0, 0, \frac{1}{\sqrt{2}})$ and target quaternion is equal to $(0, 0, 0, 1)$	68
7.7	Simulation of the ACS with a static sun vector and a perpendicular static magnetic vector. Initial quaternion attitude is equal to $(\frac{1}{\sqrt{2}}, 0, 0, \frac{1}{\sqrt{2}})$ and a target frame rotating at the same frequency as the ORF.	69
7.8	Simulation of the ACS with a static sun vector and a perpendicular static magnetic vector. Initial quaternion attitude is equal to $(\frac{1}{\sqrt{2}}, 0, 0, \frac{1}{\sqrt{2}})$ and a target frame rotating at a frequency significantly slower than the ORF.	69
7.9	Simulation of the finetuned ACS with a static sun vector and a perpendicular static magnetic vector. Initial quaternion attitude is equal to $(\frac{1}{\sqrt{2}}, 0, 0, \frac{1}{\sqrt{2}})$ and a target frame rotating at a frequency significantly slower than the ORF.	70
8.1	General flowchart for the ADCS.	71

9.1	The figure shows the test set-up for the acceptance test. In the figure the satellite has been rotated 45° counterclockwise.	74
C.1	Figure C.1(a) depicts a sun sensor, where the distance from the slot to the diode array, h , and the distance x determines the angle β . In figure C.1(a) the angle gives the xz-direction to the sun in the sun sensor reference frame. Figure C.1(b) depicts both sun sensors, the right giving the xz-angle and the left the yz-angle, which can be combined to the sun vector.	81
C.2	In figure C.2(a) the reference frame of the sun sensors is depicted, the green axis-coordinates indicating SBRF. This reference frame is directly applied in in C.2(c), which depicts the orientation of each sensor pair and the number convention of side-PCBs on AAUSAT3. Figure C.2(b) displays the numbering of the photo diodes on each side-PCB.	82
D.1	Sun sensor based on an image sensor. The sunray let in through the pinhole illuminates a certain area on the image sensor. With the measured x_m and y_m values from the image sensor, the angles α and β can be determined.	84
E.1	Definition of positive current direction through the magnetorquer coils in each axis. The lever arm length, r , is indicated for all current directions in the magnetorquers.	88
F.1	Assembly of SMD components on the ADCS PCB.	91
F.2	Sun sensor side PCB and aluminium cover.	91
F.3	Assembled mock-up of the CubeSat with ADCS PCB, sun sensor and their interconnection.	92
G.1	Test set-up for the acceptance test in the satellite laboratory.	93
G.2	The picture shows the angle chart used to compare the measured angle to the real angle of the sun vector.	94

List of Tables

3.1	HMC6343 magnetometer properties. Source: [Honeywell 07]	20
3.2	IDG-1215 and ISZ-1215 gyroscope properties, and ADS1115 ADC properties. Sources: [InvenSense 08] [InvenSense 09] [Texas Instruments 09].	21
3.3	SLCD-61N8 photodiode properties. [Silonex 09, Texas Instruments 10]	21
6.1	Intensity of radiation sources for a satellite over the subsolar point integrated over all wavelengths. (Data from NASA)[Wertz 78]	48
C.1	Sun sensor measure planes, all given in the sun sensor reference frame, see figure C.2(a) and C.2(c). The positive angles relate to the diode numbering convention, see figures C.2(b) and C.1.	82

Chapter 1

Mission Analysis

In this chapter a brief introduction to the necessity of an Attitude Determination and Control System will lead to an analysis of the proposed mission for the AAUSAT4 project. The analysis will include mission analysis of the QB50 ESA project and the expected orbit of the satellite to give an overview of some of the factors that will contribute to a requirement specification for the Attitude Determination and Control System on AAUSAT4.

1.1 The Necessity of Controlling a Satellite

The mission of a satellite that is sent into orbit about the Earth may be to measure something by means of on-board sensors, or to act as a repeater for radio communication. Clearly, in the latter case, the satellite must be able to communicate with a ground station by a two-way communication link. In the former, it must also be able to communicate with a ground station by either a down-link or bidirectionally, else the data it collects will not have any value. In any case, a satellite cannot be tested under orbit conditions on the ground, which is why a bidirectional link is always preferred to be able to download and evaluate sensor data from the satellite, and to be able to upload software enhancements accordingly. For the sake of this communication link, the design of the satellite antenna must either allow for isotropic radiation, or be directed toward the ground station, if data transfer is to be continuous.

Due to the Poly Picosatellite Orbital Deployer (P-POD) deployment from the launch rocket, the satellite will inevitably attain a spin. If the satellite antenna should communicate in the VHF-UHF band, the length of the antennas has to be extended to full length after deployment. This extension will add to the spin rate of the satellite. Collectively, the satellite will spin at some rate, and orbital disturbances may accelerate it.

Apart from complicating or even obstructing the communication to the ground station, there may be sensors onboard the satellite that do not work properly if the spin rate gets too high. Accordingly, it will be highly advantageous for the satellite to be able to brake this spin by means of detumbling. The slower the satellite spins results in longer communication time. The best communication link possible will be obtained by controlling the orientation of the satellite so that the antennas are pointing toward the ground station. Some sensors may also be required to point in a certain direction for highest efficiency.

An Attitude Determination and Control System (ADCS) has the purpose of determining the orientation or attitude of the satellite by means of attitude sensors, and controlling it by means of detumbling and pointing algorithms and attitude actuators. An ADCS is one of the basic systems of any spacecraft, and is vital for it to be able to fulfil its mission.

1.2 AAUSAT4

AAUSAT4 is the fourth student-built satellite from Aalborg University, and like its predecessors it will be based on the CubeSat standard. For more information on the CubeSat standard see appendix A. The satellite will be based on experience obtained during the development of previous satellite projects at Aalborg University. The AAUSAT4 project will reuse subsystems from AAUSAT3 to form the basic framework for the satellite. This framework is to be extended or modified with either newly designed subsystems or improved iterations of the old AAUSAT3 subsystems.

Because of the desire to reuse subsystems, it is necessary for AAUSAT4 to use the same internal interface between subsystems as AAUSAT3, to accommodate for a modular satellite design, with reusable subsystems. AAUSAT4 will, like the previous satellites from Aalborg University Space Center, be built exclusively by students using off-the-shelf components.

The main objectives for the AAUSAT projects are to educate students, and give an insight into satellite and space engineering. The scientific experiments conducted by the satellite are merely secondary objectives for the projects, but primary for the AAUSAT4 mission.

1.3 QB50

Sources: [Singarayar 13], [Smith 12].

The AAUSAT4 satellite is a candidate for the QB50 mission. QB50 is a joint ESA project with several universities developing and manufacturing up to 50 CubeSat satellites. The 40 of the satellites are to function as a sensor network to conduct in-situ measurements in the lower thermosphere (90 km to 320 km altitude) and to study the process of re-entry into the atmosphere. These satellites are denoted QB50 type 1. Another 10 satellites are to make In Orbit Demonstrations (IOD) of new technologies, denoted QB50 type 2. A further description of the QB50 mission can be found in Appendix B.

The QB50 type 1 satellites will be grouped into two groups, with each group of 20 satellites carrying the same scientific measurement equipment as a scientific payload. Each of these satellites will be two CubeSat units in size ($10 \times 10 \times 20$ cm), where one unit consists of the scientific payload, and the other as the 'functional unit' of the satellite. The 'functional unit' consists of all the basic subsystems of a satellite. These functions include control of the satellite, keeping the payload in the desired direction, maintaining a radio-link to ground stations, and delivering power to both the scientific payload and the 'functional unit'.

The QB50 type 2 satellites will be of varying size, depending on the technologies they are to demonstrate, but they are all restricted to the CubeSat standard sizes of 1, 2 or 3 units.

With respect to the ADCS aspect of QB50, there are two possible scenarios of controlling the satellite. While detumbling remains a priority in both cases, one scenario is that the satellite will have to point the payload in the direction of travel at all times. The other scenario is that the payload will point in the direction of a mission control center on earth on any given pass.

It has been deemed necessary for AAUSAT4 to work as a 'functional unit' in the QB50 project, to at least consist of: Electronic Power System (EPS), Communication System (COM), and Attitude Determination and Control System (ADCS). Furthermore, Aalborg University has been designated to design two of the QB50 satellites; a QB50 type 1 satellite and a QB50 type 2 satellite. It is expected that the QB50 type 1 will be required to point in the direction of travel, while the QB50 type 2 will be required to point in the direction of a mission control center.

1.3.1 Expected QB50 Orbit

The satellite will be launched into a circular orbit at 320 km altitude from Murmansk in Russia, with an inclination of 79° (see section 5.1 for a description of inclination). The orbit altitude of

spacecrafts in Low Earth Orbit (LEO) is usually no less than 300 km because of the amount of atmospheric drag at these low orbits. This causes a significant orbital decay, which reduces the lifetime of the satellite to only a few months. Consequently, the QB50 mission satellites have an expected lifetime of around three months. It is expected that the lowest altitude where the satellites are still operational will be 90km.

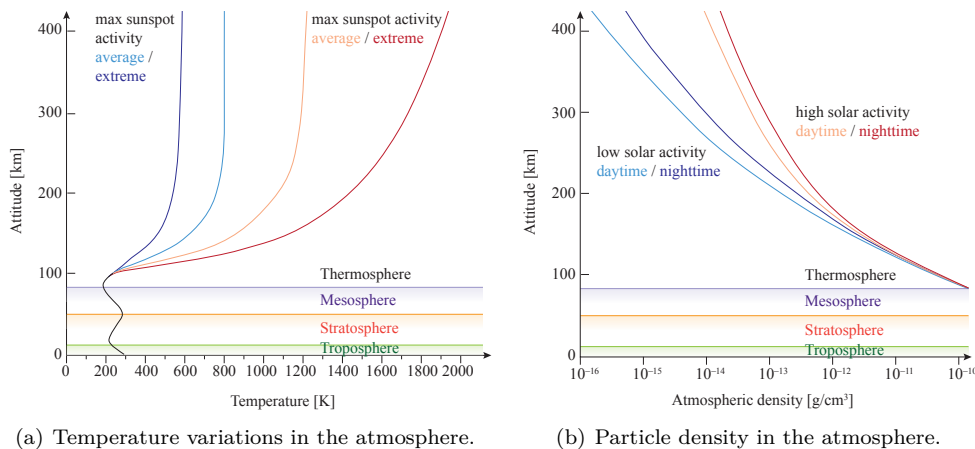
1.4 Low Earth Orbital Environment

Sources: [Wertz 99], [Wertz 78].

The environment which the spacecraft will be exposed to when in orbit has a great influence on both lifetime and performance of the spacecraft. Thus the environment has to be accounted for when designing and constructing a spacecraft, to keep lifetime and performance satisfactory.

1.4.1 Temperature Variations

In the thermosphere (expected orbit) the temperatures can get extremely high as nitrogen and oxygen molecules absorb solar electromagnetic radiation, the temperature increasing with altitude, see figure 1.1(a). In addition to this, the magnitude of the increase depends especially on the sunspot activity cycle, and the variation also on whether the satellite is in or outside eclipse.



(a) Temperature variations in the atmosphere.

(b) Particle density in the atmosphere.

Figure 1.1: Figure 1.1(a) depicts the average temperatures in the different layers of the atmosphere [Bougher 97]. Figure 1.1(b) depicts the density of the atmosphere, which decrease with altitude [NASA 71].

The extreme temperature reflects the energy level of each particle, but as the particle density decreases exponentially with altitude to near-vacuum (see figure 1.1(b)) the molecules get very sparse, and the probability of colliding with particles decreases. Hence the temperature transfer from high-energy particles to the satellite body is relatively small. Measurements from AAUSAT3 (in 790 km altitude) gives the internal satellite temperature to be between -10 and 50°C. Orbit temperature variations are expected to be smaller for lower altitudes, but as AAUSAT3 is in a solar synchronous orbit its temperature variations may be much smaller than what should be expected from a non-solar synchronous orbit.

1.4.2 Atmospheric Drag

Atmospheric drag is the deceleration of the spacecraft caused by collisions between the spacecraft itself and particles in the atmosphere. The amount of deceleration the spacecraft is exposed to by atmospheric drag is highly dependent on several factors. These factors include the velocity, mass

and cross-sectional area in the direction of travel of the spacecraft, as well as the composition of the atmosphere.

Basically a low orbit will cause a higher amount of atmospheric particle collisions on a given spacecraft because of a more dense atmosphere. As the orbit gets higher the atmosphere gets less dense and the amount of collisions is reduced. But factors like the solar cycle and geomagnetism also has an effect on the atmospheric density.

1.4.3 Hyper Velocity Collisions

Once in orbit the spacecraft has to maintain a high velocity of $\sim 7.8 \text{ km/s}$ (velocity required to sustain a LEO). This results in collisions with atmospheric particles, which erodes the spacecraft surface. Collisions of larger particles, such as micrometeorites or spacecraft debris has a high probability of being fatal for the spacecraft, due to the high velocity of both objects.

1.5 Low Earth Orbital Perturbations

Sources: [Wertz 99], [Sørensen 06], [NASA 71], [Wertz 78].

When in orbit several factors affect the flight of a spacecraft, these disturbances contribute to the tumbling of the spacecraft i.e. rotations around its centre of mass. The forces which act upon a spacecraft in orbit are dependent on a variety of parameters, such as spacecraft geometry, solar activity, and orbit altitude comprising composition of the atmosphere, spacecraft velocity, magnetic fields and gravitational pull. The different disturbance factors are described and their influence on a spacecraft attitude will be investigated in the following sections. The perturbation factors are listed in descending order.

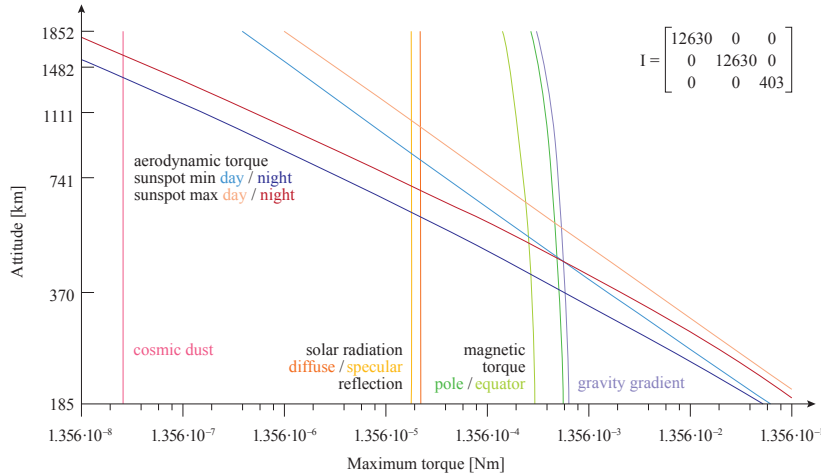


Figure 1.2: Overview of the magnitude of disturbance torques throughout the thermosphere [NASA 71]. The depicted magnitudes correspond to a spacecraft with the stated inertia matrix (given in $\text{kg}\cdot\text{m}^2$).

1.5.1 Aerodynamic Torque

Aerodynamic torque is caused by collisions of atmospheric molecules on the spacecraft surface. The resulting torque from these collisions are based on several factors: the aerodynamics and mass of the spacecraft, the molecular composition of the atmosphere and atmospheric motion, and the velocity of the spacecraft travelling through the atmosphere.

As the atmospheric particles are the reason for aerodynamic torque, the torque diminishes as the orbit altitude is increased, because the atmospheric density decreases. Consequently a low altitude

orbiting spacecraft is subject to a high atmospheric torque, and as the orbit altitude increases, other disturbing torques will become more dominant. Usually at altitudes below 600 km, the aerodynamic torque is predominant, and above 1000 km the solar radiation is the predominant torque. In between 600 km and 1000 km altitude, the aerodynamic and solar radiation forces are likely to be of the same magnitude.

1.5.2 Solar Radiation and Solar Wind

When in orbit a spacecraft is exposed to solar radiation, which is an electromagnetic radiation ranging from X-rays to radio waves, emitted from the Sun. The pressure upon the spacecraft from solar radiation will produce a torque, which is proportional to the momentum flux. The magnitude of momentum flux is proportional to the inverse square of the distance from the Sun.

Solar wind is a stream of charged particles expelled from the Sun. This radiation consists mainly of ionized nuclei and electrons. The torque on the spacecraft directly produced by these charged particles is far less than the torque produced by the solar radiation pressure, and the lower the orbit, the more of the ionized particles will already be absorbed by the atmospheric layers above the orbiting spacecraft. However, solar wind has a large effect on the Earth's magnetic field and atmosphere, as well as the highly charged particles can 'blind' or obscure the spacecraft sensors. The effect on Earth's magnetic field and atmosphere from solar winds, causes an indirect disturbance to the spacecraft through atmospheric drag and magnetic disturbances. When solar wind reaches the atmosphere it heats up the outer layers of the atmosphere, which causes the atmosphere to expand outwards. As the heated air in the atmosphere rises, the atmospheric density in the orbit is increased, thus increasing the atmospheric drag on the spacecraft.

1.5.3 Gravity Gradient

The gravity gradient is the variation in the gravitational pull on a spacecraft. This variation in the gravitational force has an influence on the orbit altitude, inclination, and the spacecraft's moment of inertia. During a revolution around the Earth the orbit altitude will vary according to the gravitational pull on the spacecraft. This variation in altitude is mainly caused by the Earth's gravitational field, but also the Sun and the Moon can have an effect as well as all other planets. At low orbits the oblateness of the Earth has a greater effect on the spacecraft than the gravitational pull of the other bodies in space, as the oblateness of the Earth has a 0.1% variation in gravitational potential, whereas the Moon only has a gravitational potential of 0.02%, at the surface of the Earth. Thus the orbiting Moon has a lesser tidal pull on the spacecraft than the variations in the Earth's gravitational field. With time, changes in the orbit inclination can also occur, although these are small compared to the altitude perturbations.

Thus the gravitational or tidal pull from everything but the Earth are deemed negligible at orbit altitudes less than ~700 km, whereas for orbits above this usually has to include disturbances from the gravitational pull of the Sun and the Moon. At an altitude of 8000 km the magnitude of the gravitational pull of the Earth is the same as that of the Moon.

1.5.4 Eddy Currents and Residual Magnetics

Eddy Currents are currents induced in the spacecraft body frame, and are caused by the spacecraft travelling through the Earth's magnetic field at high velocity. This will cause a disturbance to the spacecraft in the form of an electromagnetic coupling between the spacecraft and the Earth's magnetic field. This electromagnetic coupling produces a torque as the two magnetic fields, i.e. the magnetic field created from the induced currents in the spacecraft and Earth's magnetic field, will try to align.

Residual Magnetics are magnetic fields caused by the currents powering the electronics within a spacecraft. The currents in the electronics creates magnetic fields around the powerlines, which like the Eddy Currents causes a disturbance to the spacecraft from an electromagnetic coupling.

This coupling between the Earth's magnetic field and the spacecraft's Residual Magnetic fields can be kept small, if the spacecraft electronics are designed properly.

Perturbations Considered in this Project

A further analysis will be made of the magnitude of the aerodynamic torque as this is the most dominant force given the orbit of the spacecraft. The second largest contributor to orbital perturbations is the solar radiation. The force of solar radiation will also be calculated to investigate the influence of this factor compared to aerodynamic torque. This will be treated in section 6.1.2. All other orbital perturbation forces are deemed too insignificant in the relevant altitude for further analysis, and will as far as possible be accounted for through the design of the spacecraft.

1.6 Actuation Speed

As mentioned in section 1.3 there are two possible scenarios involving the ADCS of QB50. While the challenge of pointing the satellite in both scenarios is about the same, it poses different requirements with respect to the actuators of the satellite.

QB50 type 1

For the QB50 type 1 the mission dictates that the payload is required to always point in the direction of travel. This leads to the satellite making a full rotation about its centre of mass over the duration of an orbit. By using Equation 1.1 it is possible to find the maximum actuation speed of the satellite in order to maintain pointing of the payload in the direction of travel.

$$\omega = \frac{v}{r \cdot 2\pi} \cdot 2\pi \quad [\frac{\text{rad}}{\text{s}}] \quad (1.1)$$

where

ω	is the angular rate of the satellite	[rad/s]
r	is distance from the centre of Earth to the satellite	[m]
v	is the velocity of the satellite	[m/s]

Using the satellite velocity as defined in section 1.4, it is possible to calculate the actuation speed for the upper and lower bound of the orbital altitudes expected for the QB50. These bounds are 320 km maximum altitude, 200 km minimum pointing requirement and 90 km minimum altitude.

$$\begin{aligned}\omega_{320 \text{ km}} &= \frac{7800 \frac{\text{m}}{\text{s}}}{6691000 \text{ m} \cdot 2\pi} \cdot 2\pi = 0.001166 \frac{\text{rad}}{\text{s}} \\ \omega_{200 \text{ km}} &= \frac{7800 \frac{\text{m}}{\text{s}}}{6571000 \text{ m} \cdot 2\pi} \cdot 2\pi = 0.0012 \frac{\text{rad}}{\text{s}} \\ \omega_{90 \text{ km}} &= \frac{7800 \frac{\text{m}}{\text{s}}}{6461000 \text{ m} \cdot 2\pi} \cdot 2\pi = 0.001207 \frac{\text{rad}}{\text{s}}\end{aligned} \quad (1.2)$$

As seen in Equation 1.2, a maximum actuation speed of 0.0012 rad/s is required in order to maintain pointing in the direction of travel. As the actuation speed varies very little, it is expected that a system that complies with the actuation speed demand for 200 km altitude, will probably also be able to keep up with the required actuation speed in 90 km altitude.

It should be noted that the actuation speed for this type of pointing is constant.

QB50 type 2

The mission for QB50 type 2 requires the satellite to point towards a mission control centre (e.g. AAU) on earth. In this scenario the satellite will be required to actuate the fastest when

passing directly overhead of the mission control centre. The actuation speed in this scenario can be calculated using Equation 1.3.

$$\tan(\omega) = \frac{v}{h} \quad \Leftrightarrow \quad \omega = \tan^{-1}\left(\frac{v}{h}\right) \quad [\frac{\text{rad}}{\text{s}}] \quad (1.3)$$

where

ω	is the angular rate of the satellite	[rad/s]
h	is distance from the surface of the Earth to the satellite	[m]
v	is the velocity of the satellite	[m/s]

Again using the orbital data from section 1.4 it is possible to calculate the actuation speed for the upper bound, lower bound and lower pointing requirement, of the orbital altitudes expected for the QB50.

$$\begin{aligned} \omega_{320\text{ km}} &= \tan^{-1}\left(\frac{7800 \frac{\text{m}}{\text{s}}}{320000 \text{ m}}\right) = 0.02437 \frac{\text{rad}}{\text{s}} \\ \omega_{200\text{ km}} &= \tan^{-1}\left(\frac{7800 \frac{\text{m}}{\text{s}}}{200000 \text{ m}}\right) = 0.0390 \frac{\text{rad}}{\text{s}} \\ \omega_{90\text{ km}} &= \tan^{-1}\left(\frac{7800 \frac{\text{m}}{\text{s}}}{90000 \text{ m}}\right) = 0.08645 \frac{\text{rad}}{\text{s}} \end{aligned} \quad (1.4)$$

As seen in Equation 1.4 a maximum actuation speed of 0.0390 rad/s is required in order to maintain pointing in the direction of a mission control centre. Apart from the varying very much with altitude, the actuation speed of a QB50 type 2 varies very much within an orbit. The actuation speed defined in Equation 1.4 is the maximum needed within one orbit.

By designing an ADCS with the capability of actuating with speeds of 0.0390 rad/s it is possible to have a final system that can accommodate both the QB50 type 1 and type 2 missions.

Chapter 2

System Requirements

The satellites developed in Aalborg University are sought designed modularly with the prospect of reusing subsystems or parts of subsystems for future satellites. The purpose of this project is to design an Attitude Determination and Control System for AAUSAT4, building on the existing hardware and software of the AAUSAT3 ADCS. Hence the project serves as analysis and test as to what parts of the AAUSAT3 ADCS can be reused and what should be appended.

The requirement specification is divided into two parts. The first part outlines the ADCS requirements for AAUSAT4 comprising general CubeSat requirements, mission specific requirements and proposed enhancements for the AAUSAT3 ADCS. The second part delimits the outlined demands to requirements specific for this project and specifies how these requirements should be tested.

2.1 AAUSAT4 ADCS Requirements

As described in section 1.2, AAUSAT4, like the other satellites developed in Aalborg University, is a CubeSat, and must conform to the CubeSat standard, which is given in brief in Appendix A. Satellites participating in the QB50 mission, as described in section 1.3, must attain a specified pointing accuracy, and the robustness of the satellite must grant a lifetime of about 3 months.

Since the ADCS for AAUSAT4 is meant to be based on the AAUSAT3 ADCS, the designed algorithms should be compatible with the existing hardware. Additionally, the developers of the AAUSAT3 ADCS has given insights into obvious software improvement measures, and what tests are needed to gain insight into further enhancement of the existing hardware and software interaction.

CubeSat Requirements

- 2.1.1 The dimensions of a CubeSat are restricted to $10 \times 10 \times 11.35$ cm for a 1 unit CubeSat cf. section 1.2.
 - ⇒ The total size of the ADCS PCB cannot exceed the dimensions of 10×10 cm.
- 2.1.2 The total weight of the satellite should not exceed 1.33 kg per unit cf. Appendix A.
 - ⇒ The weight of the ADCS should be less than 100 g.
- 2.1.3 The satellite centre of mass should be within a sphere of 2 cm from the geometric centre cf. section A.2.
 - ⇒ The ADCS PCB should have its centre of mass within 2 cm from its geometric centre.

QB50 Requirements

- 2.1.4 The CubeSat shall be able to recover from tip-off rates of up to $10^\circ/\text{s}$ within 2 days cf. [Singarayar 13].
⇒ The ADCS actuators must provide detumbling within 2 days.
- 2.1.5 The CubeSats carrying the science sensors shall have an attitude control with pointing accuracy of $\pm 10^\circ$ and pointing knowledge of $\pm 2^\circ$ from its initial launch altitude at 350 km down to at least 200 km cf. [Singarayar 13].
⇒ The ADCS actuators must provide a pointing accuracy of $\pm 10^\circ$ with a required actuation speed as defined in section 1.6.
⇒ The ADCS sensors must provide an accuracy of attitude determination within $\pm 2^\circ$.
- 2.1.6 The CubeSat shall not use any materials that have the potential to degrade during the 2 years storage duration after assembly cf. [Singarayar 13].
⇒ Robust components compatible with the space environment described in section 1.4 should be used for the ADCS.

AAU Requirements and Requests

- 2.1.7 The AAUSAT3 utilises CANBUS communication protocol between subsystems, CSP protocol for internal subsystem communication and uses FreeRTOS as the operational system.
⇒ Software must be designed to comply with the stated communication protocols and be compatible with FreeRTOS.
- 2.1.8 It is desired to implement a pointing algorithm, which has not been implemented on AAUSAT3 due to time constraints cf. the AAUSAT3 team.
⇒ It is proposed to use Singular Value Decomposition (SVD) to estimate the orientation of the satellite.
- 2.1.9 It is desired to test the AAUSAT3 sun sensors on the ground and find a solution if they saturate as the AAUSAT3 team suspect.
⇒ A thorough test of the sun sensors should be performed, requiring appropriate testing facilities.

2.2 Delimitation to Requirements for this Project

As described in section 1.3, Aalborg University has been assigned a two-unit and a three-unit CubeSat in the ESA QB50 mission. However, basing the algorithms of this project on the existing AAUSAT3 ADCS hardware, this project will only cover a one-unit CubeSat. It should take into account the attitude perturbations from section 1.5 relevant for the QB50 orbit, as described in subsection 1.3.1. Seeing that the detumbling algorithm designed for AAUSAT3 has been demonstrated to be well-functioning, the functionality needed developed for the ADCS is delimited to the pointing of the satellite. The requirements which must be met by the system developed in this project can thus be specified as:

- 2.2.1 An attitude determination system must be developed, which can obtain an attitude estimation accuracy of $\pm 2^\circ$ with the sensors present on the AAUSAT3 ADCS.
- 2.2.2 An attitude control system must be developed, which can obtain an attitude accuracy of $\pm 10^\circ$ with the actuators present on the AAUSAT3 ADCS.
- For a QB50 Type 1 satellite, with pointing in the direction of travel, an actuation speed of 0.0012 rad/s should be possible cf. Equation 1.2.
 - For a QB50 Type 2 satellite, with pointing in the direction of a mission control center on Earth, an actuation speed of 0.0390 rad/s should be possible cf. Equation 1.4.

2.2.3 A hardware ADCS platform must be assembled in order to test the algorithms developed according to item 2.2.1 and item 2.2.2.

All requirements should be tested considering the conditions and constraints posed by the orbital environment, as described in section 1.4.

Testing the requirements

Testing of requirement 2.2.1

The plan for testing the attitude determination is to use a powerful source of light and a set of Helmholtz coils. The light source is set to point at a fixed point. This fixed direction of the "sun" is then integrated in the software. The Helmholtz coil is then placed to generate a magnetic field perpendicular to the sun. The satellite shall then be able to determine its attitude in the with the methods defined for this. The actual attitude are then measured externally, and the same methods as the satellite uses, are used for determining the attitude that can be expected from the attitude estimation performed in the satellite software.

Testing of requirement 2.2.2

The control is going to be tested using a fixed attitude, and the satellite positioned away from the target orientation. The controller will then position the satellite in the target orientation. The step response of the satellite is then analyzed to see if the controllers rise time, overshoot and settling time, are as calculated.

The accuracy for pointing the satellite has to be $\pm 10^\circ$. There exist a simulation environment used for the AAUSAT3, which can simulate an orbit for the satellite. The simulation can test if the determination and control works or not, before implementation. The environment is made using the Simulink[®] toolbox in Matlab[®]. It simulates the environment in orbit along with the orientation of the satellite. The reason for using a simulation environment is that it is difficult to make control in three axes at ones when placed on Earth. The environment is also different on Earth compared to the environment in orbit e.g It is not possible to test the atmospheric drag and solar radiation because they are not present when testing the rotation only.

It is also wanted to test the satellite on Earth, this can only be done in one axis at a time. This is done by putting the satellite in a mount where it can rotate almost friction free around one axis and is fixed in the two other axes. This is combined with a set of Helmholtz coils which makes it possible to oppress the Earth's magnetic field and create one which is possible to vary. A last thing needed to test the determination and control of the satellite is to test it in a dark room, where a bright light source is set up so it imitates the sun.

Testing of requirement 2.2.3

This requirement is automatically tested when trying to get the system up and running. The software available for the ADCS will be used for testing the system after it has been produced.

Chapter 3

Hardware Design of the ADCS

As described, this project does not deal with actual hardware design of an ADCS, as the purpose is to develop new software for parts of the system and to test this on the existing ADCS of AAUSAT3. A block diagram of hardware setup of the AAUSAT3 ADCS is shown in figure 3.1.

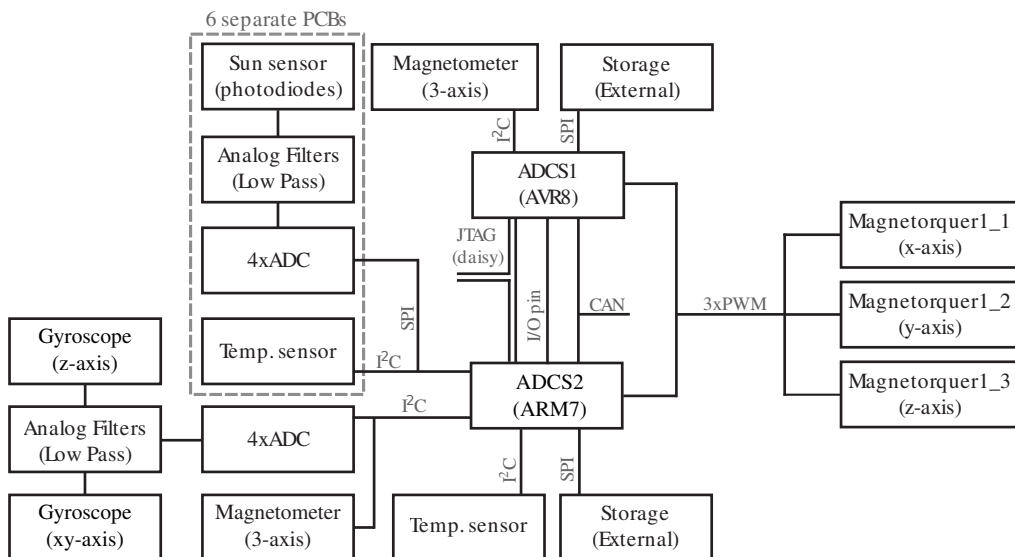


Figure 3.1: Block diagram of the ADCS, showing sensor, actuator and MCU set-up.

The ADCS consists of two subsystems, ADCS1 and ADCS2.

The ADCS1 is responsible for detumbling the satellite, using a magnetometer sensor input to determine the angular rotation of the satellite, and counteracting this rotation by applying a current to the magnetorquers, thus creating a torque in the opposite direction of the angular rotation.

ADCS2 is used for pointing purposes, and uses several sensor inputs to determine the satellite attitude: a sun sensor on the surface of each of the six sides of the satellite, a magnetometer and gyroscopes. With the attitude determined, the microcontroller (MCU) is able to calculate the rotation required for the satellite to be pointing in the desired direction. This rotation is acquired using the magnetorquers, as it is done for the detumbling, thus rendering it impossible to do both operations simultaneously. An I/O connection between the two ADCS subsystems is used to dictate which one has the control of the magnetorquers. ADCS2 can also be used to detumble

the satellite, but as the ADCS2 requires more power to run the extra sensors, the detumbling is primarily handled by the ADCS1 subsystem.

To obtain a thorough understanding of the principles behind the existing hardware from the AAUSAT3 ADCS, this chapter will introduce the sensors and actuators used. Along with the present hardware, additional sensors and actuators commonly used for attitude determination and control has been analysed. The additional sensors and actuators analysed can be found in Appendix D. Finally a short introduction to the MCU and the interface protocols used for AAUSAT3 is presented.

3.1 MCUs of the ADCS

The ADCS of AAUSAT3 has two MCUs as the heart of the system. These are an AVR8 and an ARM7. For redundancy, both MCUs can run a detumble algorithm, but only the ARM7 is able to conduct attitude estimation and pointing. This set up also serves as two power modes for the ADCS, a low power mode only for detumbling (ADCS1), and a high power consumption mode for attitude estimation and pointing (ADCS2).

3.1.1 AVR8

The AVR8 MCU is an AT90CAN128 from Atmel. It is an 8-bit RISC processor with 128 kB flash, 4 kB EEPROM and 4 kB SRAM. The clock frequency is software selectable with a maximum of 8 MHz at 2.7 V operating voltage and a maximum of 16 MHz at 4.5 V. It comprises 64 pins, including 53 programmable I/O lines, 8 external interrupt sources, and contains JTAG, CAN and SPI.

The AVR8 is the main part of ADCS1, which is only able to detumble the satellite as it is only connected to the magnetic field sensor, and thus only able to run a detumbling algorithm. The ADCS1 subsystem consists of the AVR8 micro controller, a 3-axis magnetometers, three magnetorquers (one at each axis), and data storage.

3.1.2 ARM7

The ARM7 MCU is an AT91SAM7A3 from Atmel. It is a 32-bit Reduced Instruction Set Computing (RISC) processor with 256 kB flash, a two-wire EEPROM and 32 kB SRAM. The clock frequency can be set at up to 60 MHz at 1.65 V operating voltage, and it has three external clock inputs. It comprises 100 pins, including 62 programmable I/O lines, and contains JTAG, CAN and SPI-interfaces.

This MCU is the heart of the ADCS2 subsystem, which consists of the ARM7 MCU, six sun sensors, xyz-axes gyroscopes, internal and external temperature sensors, a 3-axis magnetometers, three magnetorquers (one for each axis), and data storage. The determined attitude is used primarily for pointing operations through the magnetorquers, but it can also be used for detumbling the satellite.

The two ADCS subsystems have an I/O connection in between the two MCUs, to make sure only one ADCS subsystem actuates with the magnetorquers at the time. The two MCUs have a CAN interface, allowing for sensor data exchange between the two subsystems.

3.2 Interface Protocols

The internal on-board communication on AAUSAT3 is specified by the Controller Area Network (CAN) interface between all subsystems. On the ADCS subsystem both CAN, Inter-Integrated Circuit (I²C), and Serial Peripheral Interface (SPI) buses are used for sensor and MCU interfaces, with CAN and I²C using the CubeSat Space Protocol (CSP).

3.2.1 Inter-Integrated Circuit Bus - I²C

The I²C interface is used for the magnetometers, gyroscope-ADC and temperature sensors, on both ADCS subsystems.

I²C uses two (serial) data link lines: data (SDA) and clock (SCL). It is a master-slave bus, where a master node, which provides a clock, dictates which device uses the data lines at all times, by requesting data from the slaves or sending data to the slaves. Communication on I²C is done by a master node sending out a start bit followed by a 7-bit slave address, and then a bit to indicate read or write operation. The slave responds with an acknowledge bit, and the master and slave will then continue in the mode which the master dictated, i.e. the master in receive and slave in transmit mode or vice versa. The master node can then end the transmission by sending a stop bit and leaving the bus open for another master to use, or it can send another start bit to continue either receiving or sending data to the addressed slave node.

3.2.2 Controller Area Network Bus - CAN

The CAN bus interface is used between all systems in AAUSAT3, and some subsystems also use CAN interface internally for sensors or controllers. In the ADCS a CAN bus is used between the two MCUs.

The CAN bus is (unlike the I²C) a multi-master bus. When the connection is free, a node is able to transmit a message beginning with the nodes own ID, representing the node's message priority. If several nodes transmit simultaneously, the node with the highest priority, i.e. the lowest ID number, will dominate the transmission line, while the other nodes will stop transmitting and wait for a clear line before retransmitting their messages.

3.2.3 Seriel Peripheral Interface Bus - SPI

The SPI interface is used for the external storage and the ADC of the sun sensors.

The SPI interface is a full duplex bus and uses at least four data link lines for communication. These lines consist of a clock (SCLK), a master-output slave-input (MOSI), a master-input slave-output (MISO) and a slave select (SS). All devices on the bus connection are connected to SCLK, MOSI and MISO lines, and then each device has its own slave select (SS) line. This allows for the master to select which device that has the right to transmit and receive on the data lines (MISO and MOSI). Message transmissions consist of the master selecting a device by pulling the SS line low, it is then able to start sending data to the slave via the MOSI line. The slave responds to the master on the MISO line with the data requested. As this is a full duplex interface, both master and slave can transmit at the same time.

The sun sensors for the ADCS are grouped together with three on its own SPI bus, this gives a total of six data lines between the master and the slaves on the bus. An alternative way is using a daisy-chain setup where each slave relay its data forward to the next slave, and in the end to the master. In this setup a total of four data lines would be used, as all devices are selected at all times.

3.2.4 Cubesat Space Protocol - CSP

The CSP is used on the CAN and some of the SPI buses in AAUSAT3.

The CSP protocol is designed to ease communication between subsystems within the satellite, such that these embedded systems are all connected through a network, and not dependent on a single master with several slaves. The protocol design follows the TCP/IP model with a layer-arranged design comprising transport, routing and MAC layers. It is designed to give the same features as the TCP/IP model offers, but only using a small header of 32 bit.

3.3 Attitude Determination Sensors of AAUSAT3

The AAUSAT3 ADCS developed for the Danish Maritime Safety Administration AIS (Automatic Identification System) mission for an orbit height of approximately 800 km, contains three sensors as seen from Figure 3.1: a magnetometer, a gyroscope and a sun sensor. The specific functionality of each sensor is described in the following.

3.3.1 Magnetometer

Sources: [Cai 12] [Honeywell 07]

The magnetometer measures the magnitude of the magnetic field relative to its sensitive axis. A three-axis magnetometer gives the magnetic field vector as the field strength for each of its sensitive axes in the magnetometer coordinate system.

The magnetometer used on AAUSAT3 is the HMC6343 from Honeywell, which is a tilt compensated electronic compass. It outputs either a compass direction (angle) and a tilt angle, or a three dimensional vector indicating the direction of the geomagnetic field. In AAUSAT3 the latter output format is used.

As seen from Table 3.1 the HMC634 has an I²C interface (see subsection 3.2.1), which obviates an external ADC (Analog to Digital Converter).

While the magnetic field range of the HMC6343 is sufficient, the refresh rate is barely so, since it does not allow for a high tumbling rate, ≥ 5 Hz, before entering the aliasing region of the magnetometer.

HMC6343	
Interface	I ² C
Refresh Rate	5 Hz
Field Range	± 2 G (max)
Max Field Exposure	>5 G
Operating Temperature	-40°C to 80°C

Table 3.1: HMC6343 magnetometer properties. Source: [Honeywell 07]

3.3.2 Gyroscope

Sources: [Lewin 99] [Sensors 99] [Sensors 03] [InvenSense 08] [InvenSense 09] [Texas Instruments 09]

The gyroscope measures the rotational orientation or rotational velocity about its sensitive axis. A classical mechanical gyroscope can be visualised as a wheel or a disc placed in three gimbals, spinning about some axis. Its angular momentum, caused by the spin rate and the disc's moment of inertia, will impede the effect of external torques about any other axes. This can be used as a gyroscopic compass, or used to measure angular rates across two of the three gimbal axes, while no measurement can be made about the spin axis of the disc. A MEMS (Micro ElectroMechanical Systems) gyroscope can have one, two, or three sensitive axes.

For the AAUSAT3 ADCS PCB, two angular rate gyroscopes are used: the IDG-1215 two-axis gyroscope and the ISZ-1215 single-axis gyroscope, allowing for angular rate measurements about any axis. The gyroscopes both use the Coriolis effect and a vibrating mass to measure angular rate about each sensitive axis, and outputs an analogue voltage proportional to the angular rate. A list of the general properties of the two gyroscopes can be seen in Table 3.2.

As both gyroscopes are analogue, the ADS1115 multiple input ADC is used, its general properties are also presented in Table 3.2. The ADS1115 features I²C interface along with a refresh rate of up to 860 Hz which should be sufficient for any type of application on the MCU.

	IDG-1215	ISZ-1215	ADC ADS1115
Interface	Analogue	Analogue	I ² C
Refresh Rate	Analogue	Analogue	8 Hz - 860 Hz
Relative measurement axes	x and y	z	
Full scale Range	$\pm 67^\circ/\text{s}$	$\pm 67^\circ/\text{s}$	
Sensitivity	15 mV/ $^\circ\text{s}$	15 mV/ $^\circ\text{s}$	
Operating Temperature	-40°C to 105°C	-40°C to 105°C	-40°C to 125°C

Table 3.2: IDG-1215 and ISZ-1215 gyroscope properties, and ADS1115 ADC properties. Sources: [InvenSense 08] [InvenSense 09] [Texas Instruments 09].

3.3.3 Sun Sensor Based On Photocells

Source: [Winetraub 06] [Silonex 09]

Sun sensors are used to determine the orientation of a satellite with respect to the Sun. A sun sensor determines the attitude of the satellite, with respect to the Sun, by measuring the inclination of the incident sunlight. Sun sensors can use different sensor technologies, the one used in the AAUSAT3 ADCS being based on photo diodes. These sensors use two photocell modules to determine the inclination of the incident sunlight. This is done by letting the sunlight illuminate the photocell modules through a small slot in the sensor cover, which will only illuminate a small part of the photocell module. The single-axis angle is found as a ratio between the measured intensity on each photocell. To determine the angle of the satellite with respect to the Sun, a two axis reading is necessary. This is done with two perpendicular slots with photocell modules. A description of the sun sensors designed for AAUSAT3 can be found in Appendix C.

The photo diodes used for the AAUSAT3 sun sensor is the SLCD-61N8, its significant properties being listed in Table 3.3. The SLCD-61N8 photocells are analogue, which is why the ADS1148 ADC used, its significant properties also presented in Table 3.3. This determines the total refresh rate of the sun sensors to a maximum of 2 kHz, along with defining the interface to the sun sensor as SPI (see subsection 3.2.3).

	SLCD-61N8	ADC ADS1148
Interface	Analogue	SPI
Refresh Rate	Analogue	2kHz
Acceptance half angle	60°	
Operating Temperature	-40°C to 125°C	-40°C to 125°C

Table 3.3: SLCD-61N8 photodiode properties. [Silonex 09, Texas Instruments 10]

3.3.4 Additional Attitude Determination Sensors Considered for AAUSAT4

There exist a variety of sensors traditionally used for attitude determination apart from the types used for the AAUSAT3 mission. Due to the progress in MEMS technology, and the different requirements of the ESA QB50 mission compared to that of AAUSAT3, a few more sensor types

are evaluated as potential sensors for the AAUSAT4 ADCS. These additional considerations can be found in Appendix D.

The conclusion to this analysis is that the sensors of AAUSAT3 are the most relevant for AAUSAT4 as well. A horizon sensor will not have a field of view that is wide enough to detect the horizon and hence determine the attitude in very low orbits like that of AAUSAT4. An accelerometer is inferior to the gyroscope to determine angular rates. A star tracker is still too expensive for an un-sponsored mission as AAUSAT4, but the development within this field makes it a viable option as an attitude sensor in near future, and it is recommended for future satellite projects of AAU to survey the price development of MEMS star trackers.

A sun sensor based on solar panels is assessed as a feasible redundancy system for the photo cell sun sensors of AAUSAT3. However, it must be examined if it is possible with the current hardware to configure the connections in order to allow for separate power output measurements for the solar panels. If this is achieved, it will enhance the EPS to allow for checks for defective panels and optimise algorithms for charging. The ADCS may then further optimise the power output by pointing three panels in the direction of the Sun (one side of the cube does not contain solar panels).

An image sensor used as a sun sensor is able to determine the sun vector with greater precision than the current photo cell sun sensor. However, test facilities must be obtained to thoroughly test the AAUSAT3 sun sensors to determine the precision of these before it is possible to advise whether to develop new sun sensors based on image sensors.

3.4 Attitude Control Actuator of AAUSAT3

The AAUSAT3 mission entails that its attitude control must be able to point the satellite antennas in the direction of Aalborg during a pass, and generally point its AIS receivers towards the Earth, especially so around the Greenlandic waters. To be able to detumble and control the pointing, magnetorquers are used.

3.4.1 Magnetorquers

A magnetorquer, or magnetic torquer, is simply a coil using electromagnetic force to rotate the satellite. Three perpendicular magnetorquers work by letting currents run through the coils, thus inducing a magnetic field, which will act on the surrounding magnetic field. Hence a force, and thereby a torque, will be applied to the satellite, as the induced magnetic field is trying to align with the surrounding magnetic field.

One of the advantages of a magnetorquer is that it does not have any moving parts, it is lightweight compared to other actuators, and it is also energy efficient. Furthermore, since the satellite will be in LEO, there is an external magnetic field that can be utilised. The design is simple and a magnetorquer only requires electrical power in order to actuate.

One of the main disadvantages of the magnetorquer is that it is not the most powerful actuator when in Earth orbit. For the magnetorquer to be powerful, i.e. fast acting, very high magnetic flux densities are needed. This can only be obtained by either the induced magnetic field being very strong, which would require a substantial amount of the rationed ADCS power, or by the surrounding magnetic field being very strong, which is not within design control for Earth orbit.

The magnetourquers used are custom made with no iron core. When determining the amount of windings and size for each magnetorquer, the total magnetic field produced needs to be taken into account, as it has to be strong enough to counter act disturbance torques, see section 6.1.2.

3.4.2 Additional Attitude Control Actuators Considered for AAUSAT4

Due to the different mission and requirements of the ESA QB50 compared to that of AAUSAT3, a few more actuator types are evaluated as potential actuators for the AAUSAT4 ADCS. These additional considerations can be found in Appendix D.

The conclusion to this analysis is that the magnetorquers is a good choice of actuator for AAUSAT4 because of the low orbit altitude, but with the pointing requirements of item 2.1.5, the magnetorquer design on AAUSAT3 will not provide sufficient accuracy with the necessary promptness, see section 1.6 and Appendix E.

Reaction wheels will enable the satellite to actuate considerably faster than the magnetorquers. They provide great flexibility regarding position within the satellite, and can be dimensioned to actuate with the desired speed. On top of this they can rid the model of small disturbances. It is recommended that AAUSAT4 should be provided with reaction wheels, together with magnetorquers, in the further development of the AAUSAT4 ADCS succeeding this semester.

Thrusters are generally not considered for CubeSats, due to the requirements of the CubeSat standard (see Appendix A), as they may not contain vessel pressures exceeding 1.2 atm or contain chemical energies exceeding 100 Wh, which gives a thruster a relatively short lifetime. The ion propulsion type would be the best thruster type for a CubeSat, however, a small size ion thruster should first be developed, which is not considered obtainable within the time frame of AAUSAT4.

Chapter 4

Defining Attitude

The motion and in particular the angular motion of an object in three-dimensional Euclidean space must be described with respect to a reference frame, usually an orthogonal Cartesian coordinate system. Several reference frames may be defined for specifying the orientation of a spacecraft. One reference frame may be seen as inertial (fixed), and other reference frames as revolving as seen from the inertial frame.

This chapter will introduce three sets of parameters for describing the attitude of a reference frame (or a vector) relative to another reference frame, namely Euler angles, direct cosine matrices and quaternions. Subsequently, the reference frames used for attitude determination in this project are defined.

4.1 Parameters for Describing Attitude

Sources: [Bak 02] [Wiśniewski 99] [Sidi 97]

Attitude representation is the concept of describing orientation of a coordinate system fixed in the spacecraft with respect to an inertial coordinate system, which is described by means of a rotation. This rotation can be viewed in two different ways, as illustrated in Figure 4.1. The rotation depicted, is the rotation of the inertial coordinate system, denoted by superscript i , into the rotated coordinate system, denoted by superscript s . When this rotation is applied to a vector given in s coordinates, the result will be the same (fixed) vector given in i coordinates – or in other words, the vector is "rotated the opposite way" of the coordinate system in the previous explanation, to obtain the coordinates in the i coordinate system or frame, as the un-rotated vector has in the s frame.

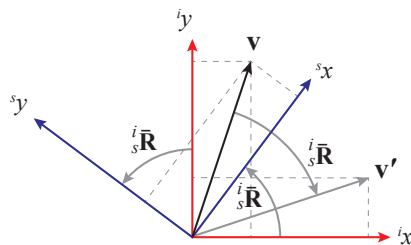


Figure 4.1: A two dimensional example of rotation. The inertial coordinate system or frame, i , can be rotated into the coordinate system s by the rotation $i_s\mathbf{R}$. This is the same rotation needed to rotate the vector \mathbf{v} within the i frame to obtain the vector \mathbf{v}' . The i coordinates of the vector \mathbf{v}' are the same as the s coordinates of \mathbf{v} .

A rotation is an operation that preserves distance, angles and handedness, i.e. rotating vectors (e.g. a coordinate system) about a fixed point, will not scale the vector in any direction. When a spacecraft is seen as a rigid body the same applies, as the mutual distances between each point of mass are preserved.

4.1.1 Euler Angles

Any rotation in space can be represented by three consecutive rotations about the orthogonal frame axes, one axis at a time. The first rotation is carried out about any of the three axes, the second rotation is about either of the two axes not used for the first rotation and the third rotation is about either of the two axes not used for the second rotation. The angles of this step-wise rotation are called Euler angles. The rotations can be intrinsic, i.e. about the mobile frame axes (body-axes), or extrinsic, i.e. about the inertial frame axes (space-axes), of which the former is the most common way of using Euler angles. An example of intrinsic Euler angles is shown in Figure 4.2.

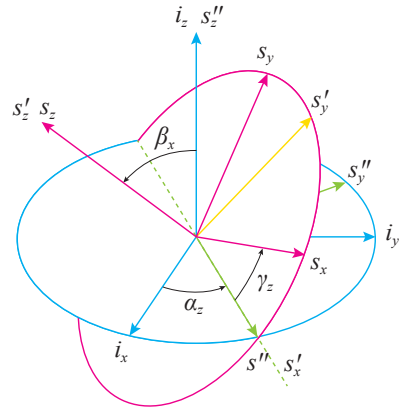


Figure 4.2: Euler angles are easily visualised. Here a 3-1-3 rotation is shown, which maps the inertial frame i into the rotating frame s by first a rotation of α about the i z -axis (3), then rotating β about the x -axis of the new s'' frame (1), and finally rotating γ about the z -axis of the s' frame (3), ending with the orientation of the s frame. The dashed line indicate the line of nodes, i.e. the cross-section between the i xy -plane and the s xy -plane.

The Euler angles can be represented by matrices of one angular rotation retaining the axis of which the rotation is made:

$$\bar{\mathbf{A}}_{\theta_1} = \begin{bmatrix} 1 & 0 & 0 \\ 0 & \cos \theta_1 & \sin \theta_1 \\ 0 & -\sin \theta_1 & \cos \theta_1 \end{bmatrix} \quad \bar{\mathbf{A}}_{\theta_2} = \begin{bmatrix} \cos \theta_2 & 0 & -\sin \theta_2 \\ 0 & 1 & 0 \\ \sin \theta_2 & 0 & \cos \theta_2 \end{bmatrix} \quad \bar{\mathbf{A}}_{\theta_3} = \begin{bmatrix} \cos \theta_3 & \sin \theta_3 & 0 \\ -\sin \theta_3 & \cos \theta_3 & 0 \\ 0 & 0 & 1 \end{bmatrix}$$

The order of the Euler angles is non-commutative, as the sequence of the three rotations equals three matrices being multiplied. There exist 12 different sequences of Euler angles, a very popular set being the 3-1-3 sequence, shown in Figure 4.2, mathematically defined as $s = \bar{\mathbf{A}}_\gamma \bar{\mathbf{A}}_\beta \bar{\mathbf{A}}_\alpha i$, (s denoting the rotating frame, and i denoting the inertial frame, see section 4.2) where both α and γ are substituting θ_3 in the above matrices, and β is substituting θ_1 . This sequence is commonly used by astronomers to define orbit planes of planets relative to each other. NASA use a 2-3-1 sequence by convention. Only for infinitesimal Euler angles the order of the sequence becomes unimportant.

A sequence of three Euler angles defines a unique orientation, but there is no unique set of Euler angles for a given orientation.

4.1.2 Direction Cosine Matrix

A direction cosine matrix is composed of unit vectors of one reference frame in motion, s , projected onto another reference frame, i , and hence ${}^i_s\bar{\mathbf{R}}$ maps vectors described in s to i coordinates. Each of the elements in the matrix, $R_{jk} = i_j \cdot s_k$, is the cosine of the angle between i_j and s_k :

$${}^i_s\bar{\mathbf{R}} = \begin{bmatrix} i_1 \cdot s_1 & i_1 \cdot s_2 & i_1 \cdot s_3 \\ i_2 \cdot s_1 & i_2 \cdot s_2 & i_2 \cdot s_3 \\ i_3 \cdot s_1 & i_3 \cdot s_2 & i_3 \cdot s_3 \end{bmatrix} \quad (4.1)$$

A direction cosine matrix is a real orthonormal matrix which implies the properties that its inverse is equal to its transpose, and for a right handed system that its determinant is equal to +1. This means that the space of the direction cosine matrix belongs to the Special Orthogonal group SO(3). Referring to Figure 4.2, the direction cosine matrix ${}^i_s\bar{\mathbf{R}} = \bar{\mathbf{A}}_\gamma \bar{\mathbf{A}}_\beta \bar{\mathbf{A}}_\alpha$ will rotate the coordinate system i into s . Then ${}^s_i\bar{\mathbf{R}} = {}^s_s\bar{\mathbf{R}}^T$ will rotate the coordinate system s into alignment with i , consistent with rotating a vector given in s coordinates into i coordinates.

The matrix describing the rotation by an Euler angle as well as the product of three Euler angles (in a specified order) describing the full rotation, are rotation matrices. Successive rotations by direction cosine matrices are possible following the same convention as for Euler angles. Hence a vector can be transformed from coordinates of frame i to frame c , via frame s , by matrix multiplication of the two rotation matrices: ${}^c_i\bar{\mathbf{R}} = {}^c_s\bar{\mathbf{R}} {}^s_i\bar{\mathbf{R}}$. Again, the order of the multiplication (successive rotations) is non-commutative.

Euler's Eigenaxis Rotation Theorem

An arbitrary orientation of a rigid body or reference frame can be obtained by a rotation about a given vector, $\hat{\mathbf{e}}$, called the eigenaxis of the rotation, by an angle, θ . The eigenaxis is unchanged by the rotation.

The direction cosine matrix can be parameterised in terms of the eigenaxis, $\hat{\mathbf{e}} = [e_1 \ e_2 \ e_3]^T$ and the angular rotation about this, θ , when $\hat{\mathbf{e}} = \bar{\mathbf{R}}\hat{\mathbf{e}}$. When \mathbf{I} denotes the identity matrix, \mathbf{R} can be expressed as:

$$\bar{\mathbf{R}}(\hat{\mathbf{e}}, \theta) = \cos \theta \bar{\mathbf{I}}_{3 \times 3} + (1 - \cos \theta) \hat{\mathbf{e}} \hat{\mathbf{e}}^T - \sin \theta [\hat{\mathbf{e}}]_\times, \quad [\hat{\mathbf{e}}]_\times = \begin{bmatrix} 0 & -e_3 & e_2 \\ e_3 & 0 & -e_1 \\ -e_2 & e_1 & 0 \end{bmatrix} \quad (4.2)$$

Given a direction cosine matrix the elements of the eigenaxis can be found as:

$$\hat{\mathbf{e}} = \frac{1}{2 \sin \theta} \begin{bmatrix} R_{23} - R_{32} \\ R_{31} - R_{13} \\ R_{12} - R_{21} \end{bmatrix} \quad (4.3)$$

The direction cosine matrix will always have an eigenvalue equal to +1, and the eigenvector corresponding to this eigenvalue is the eigenaxis, $\hat{\mathbf{e}}$.

4.1.3 Quaternions

A quaternion is a hyper-complex number consisting of a real and an imaginary part like complex numbers, the complex part being a three-dimensional vector of imaginary units i , j and k :

$$\mathbf{q} = q_4 + iq_1 + jq_2 + kq_3 \quad \Leftrightarrow \quad \mathbf{q}^* = q_4 - iq_1 - jq_2 - kq_3 \quad (4.4)$$

$$i^2 = j^2 = k^2 = ijk = -1 \quad ij = -ji \quad jk = -kj \quad ki = -ik \quad (4.5)$$

A true quaternion (representing a rotation), also called the Euler-Rodriguez symmetric parameters, is of unit length: $\mathbf{q}_{1:3}^* \mathbf{q}_{1:3} + q_4^2 = 1$, where $\mathbf{q}_{1:3} = [q_1 \ q_2 \ q_3]^T$. This also means that

$\mathbf{q}^{-1} = \mathbf{q}^*$. Geometrically the unit length constraint means, that quaternions can be interpreted as a four-dimensional sphere, the rotation describing a trajectory on the surface of this sphere. Described in terms of the eigenaxis rotation, the quaternion elements can be written:

$$\mathbf{q} = \begin{bmatrix} \hat{\mathbf{e}} \sin \frac{\theta}{2} \\ \cos \frac{\theta}{2} \end{bmatrix} \quad (4.6)$$

Quaternion multiplication is defined as:

$$\mathbf{p} \otimes \mathbf{q} = \underbrace{p_4 q_4 - \mathbf{p}_{1:3} \cdot \mathbf{q}_{1:3}}_{\text{scalar part}} + \underbrace{p_4 \mathbf{q}_{1:3} + q_4 \mathbf{p}_{1:3} + \mathbf{p}_{1:3} \times \mathbf{q}_{1:3}}_{\text{vector part}} = [\mathbf{q}]_{\otimes R} \mathbf{p} = [\mathbf{p}]_{\otimes L} \mathbf{q} \quad (4.7)$$

$$[\mathbf{q}]_{\otimes R} = \begin{bmatrix} q_4 & q_3 & -q_2 & q_1 \\ -q_3 & q_4 & q_1 & q_2 \\ q_2 & -q_1 & q_4 & q_3 \\ -q_1 & -q_2 & -q_3 & q_4 \end{bmatrix} \quad [\mathbf{p}]_{\otimes L} = \begin{bmatrix} p_4 & -p_3 & p_2 & p_1 \\ p_3 & p_4 & -p_1 & p_2 \\ -p_2 & p_1 & p_4 & p_3 \\ -p_1 & -p_2 & -p_3 & p_4 \end{bmatrix}$$

Like the direction cosine matrix, quaternions are non-commutative, and successive rotations can be combined as: ${}^c_i \mathbf{q} = {}^s_i \mathbf{q} \otimes {}^c_s \mathbf{q} \Leftrightarrow {}^s_i \mathbf{q} = {}^c_i \mathbf{q} \otimes {}^c_s \mathbf{q}^*$. Quaternion representation of rotations is written by transforming a vector into a quaternion with zero real part. The angular velocity of a reference frame s as seen from a inertial reference frame i , denoted ${}^i \boldsymbol{\omega}_s$, can be found in the reference frame s by rotating the vector from i to s :

$$\begin{bmatrix} {}^s \boldsymbol{\omega}_s \\ 0 \end{bmatrix} = {}^s_i \mathbf{q}^* \otimes \begin{bmatrix} {}^i \boldsymbol{\omega}_s \\ 0 \end{bmatrix} \otimes {}^s_i \mathbf{q} \quad \Leftrightarrow \quad \begin{bmatrix} {}^i \boldsymbol{\omega}_s \\ 0 \end{bmatrix} = {}^s_i \mathbf{q} \otimes \begin{bmatrix} {}^s \boldsymbol{\omega}_s \\ 0 \end{bmatrix} \otimes {}^s_i \mathbf{q}^* \quad (4.8)$$

Consecutive rotations described by quaternions give a non-singular, bi-linear method to go from one reference frame to another through successive rotations. Rotating from i to b to c is implemented as:

$$\begin{bmatrix} {}^c \boldsymbol{\omega}_s \\ 0 \end{bmatrix} = {}^c_b \mathbf{q}^* \otimes {}^b_i \mathbf{q}^* \otimes \begin{bmatrix} {}^i \boldsymbol{\omega}_s \\ 0 \end{bmatrix} \otimes {}^s_i \mathbf{q} \otimes {}^s_b \mathbf{q} \quad (4.9)$$

The quaternion \mathbf{q} and the quaternion $-\mathbf{q}$ represent the same rotation about $\hat{\mathbf{e}}$ in SO(3): the former of an angle θ , and the latter of an angle $2\pi + \theta$.

Quaternions in Terms of the Direction Cosine Matrix and Vice Versa

The quaternion representation, \mathbf{q} , can be transformed into a direction cosine matrix, $\bar{\mathbf{R}}$, by:

$$\bar{\mathbf{R}}(\mathbf{q}_{1:3}, q_4) = (q_4^2 - \mathbf{q}_{1:3}^* \mathbf{q}_{1:3}) \bar{\mathbf{I}}_{3 \times 3} + 2\mathbf{q}_{1:3} \mathbf{q}_{1:3}^* - 2q_4 [\mathbf{q}_{1:3}]_\times, \quad [\mathbf{q}_{1:3}]_\times = \begin{bmatrix} 0 & -q_3 & q_2 \\ q_3 & 0 & -q_1 \\ -q_2 & q_1 & 0 \end{bmatrix} \quad (4.10)$$

Inversely, given a direction cosine matrix, $\bar{\mathbf{R}}$, the corresponding quaternion can be found as:

$$q_4 = \frac{1}{2} \sqrt{1 + \text{trace} \bar{\mathbf{R}}}, \quad 0 \leq \theta \leq \pi \quad \text{and} \quad \mathbf{q}_{1:3} = \frac{1}{4q_4} \begin{bmatrix} R_{23} - R_{32} \\ R_{31} - R_{13} \\ R_{12} - R_{21} \end{bmatrix}, \quad q_4 \neq 0 \quad (4.11)$$

It should be noted that there are four different ways of rewriting a rotation matrix into a quaternion. The greatest value of the following:

$$\begin{aligned} q_4 &= \frac{1}{2} \sqrt{1 + R_{11} + R_{22} + R_{33}} \\ q_1 &= \frac{1}{2} \sqrt{1 + R_{11} - R_{22} - R_{33}} \\ q_2 &= \frac{1}{2} \sqrt{1 - R_{11} + R_{22} - R_{33}} \\ q_3 &= \frac{1}{2} \sqrt{1 - R_{11} - R_{22} + R_{33}} \end{aligned} \quad (4.12)$$

should be the one defined as the square-root term in Equation 4.10, and the remaining values should then be found according to [Sidi 97].

Comparison of the Attitude Parameters

Attitude described by either Euler angles or the direction cosine matrix require matrix multiplications, resulting in successive calculations involving several trigonometric functions, which is heavy calculation-wise. Additionally the direction cosine matrix contains highly redundant information, with only three degrees of freedom out of the nine components of the matrix. The Euler angles contain only the minimal number of attitude parameters, but suffer from singularities in its derivatives, used in kinematic equations.

Instead attitude representation is desired with as little redundant information is possible, but without suffering from singularities. This can be achieved by the use of quaternions, which are also much lighter computationally, as they contain only multiplication.

4.2 Reference Frames

In the following the reference frames of this project are defined. The reference frames are used to describe different objects relative orientation to one another. Among other things this is used in order to interpret sensor data relative to the satellite itself. All reference frames are described by three right-hand orthogonal unit vectors in \mathbb{R}^3 . The general focus of the reference frames is rotation and not translation.

4.2.1 Earth Centred Inertial reference frame (ECI)

The Earth Centred Inertial reference frame (ECI) is defined as having its origin in the centre of mass of the Earth. The z-axis of the ECI is pointing towards the geometric North Pole and the x-axis is pointing towards the Sun at the vernal equinox which happens around March 20th. The y-axis is the right-hand cross product between the z- and x-axis, making it extend through the equator somewhere in the Indian ocean (see Figure 4.3).

The ECI is not a true inertial reference frame seeing that it is orbiting the Sun. However, since a rotation around the Sun takes a whole year, the change in direction of Earth's movement is minuscule, and the ECI can be assumed inertial close to Earth, as is the case for this project. The ECI frame can be used to describe the position of celestial bodies relative to the Earth, since the reference frame is not rotating with the surface of the Earth.

Vectors specified in the ECI frame will be denoted as: ${}^i\mathbf{v}$.

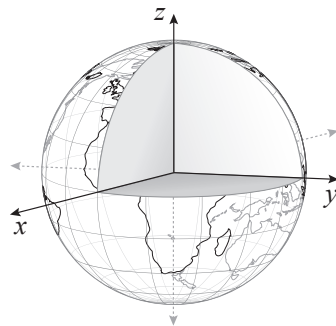


Figure 4.3: Coordinate system for the ECEF reference frame, matching exactly that of ECI at vernal equinox. The x-axis points towards the Sun and the z-axis goes through the geometric North Pole.

4.2.2 Earth Centred Earth Fixed reference frame (ECEF)

The Earth Centred Earth Fixed reference frame (ECEF) also has its origin placed at the centre of mass of the Earth. It shares the same orientation for its z-axis as the ECI, however, the x-axis is crossing the point where the Greenwich meridian and the equator meets. The y-axis is the right-hand cross product of the z- and x-axis. Due to these features the ECEF is exactly equal to the ECI reference frame at vernal equinox. The ECEF frame is used to describe the position of objects with fixed orientation to the surface of the Earth, e.g. magnetic field vectors or the Mission Control Center (MCC) at AAU.

Vectors specified in the ECEF will be denoted as: $^f\mathbf{v}$.

4.2.3 Orbit Reference Frame (ORF)

The Orbit Reference Frame (ORF) is a reference frame which has its origin in the orbiting body (the satellite in this case) and has a fixed orientation towards the Earth. The origin of the reference frame is located at the centre of mass (CoM) of the satellite with its z-axis pointing towards the CoM of the earth. The x-axis is pointing in the same direction as the velocity vector, and the y-axis is the right-handed cross product of the z- and x-axis. On Figure 4.4 an illustration of the ORF, placed on an orbiting satellite, can be seen.

Vectors specified in the ORF will be denoted as: $^o\mathbf{v}$.

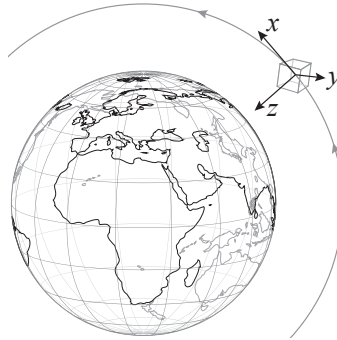


Figure 4.4: Coordinate system for the ORF reference frame, with origin at the CoM of the satellite, x-axis aligned with the orbit velocity vector, \bar{v} , and the z-axis pointing towards the centre of mass of the Earth, i.e. the origin in ECI/ECEF, i.e. nadir.

4.2.4 Satellite Body Reference Frame (SBRF)

The Satellite Body Reference Frame (SBRF) is a satellite body fixed reference frame used to describe the orientation and position of different elements within the satellite. Since the final physical design for AAUSAT4 has not been determined yet, the SBRF for AAUSAT3 is used in this project. The SBRF axes for AAUSAT3 has been aligned parallel with the satellite frame. The origin of the SBRF is placed in the CoM of the satellite with the x-axis pointing in the direction along the batteries. Furthermore the z-axis is pointing orthogonally in the opposite direction of the plane spanned by the antennas of the satellite, and the y-axis is the right-handed cross product of the z- and x-axis.

Vectors specified in the SBRF will be denoted as: $^s\mathbf{v}$.

4.2.5 Control Reference Frame (CRF)

The Control Reference Frame (CRF) is a reference frame placed with its origin in the CoM of the satellite, like the SBRF. The relation or rotation between SBRF and CRF is stationary, and is

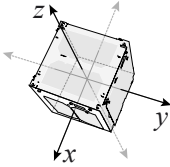


Figure 4.5: Coordinate system for the SBRF with origin at the centre of mass of the satellite, and each of the axis perpendicular to a set of satellite sides.

determined by the eigenvectors of the inertia matrix given in SBRF (see section 6.1). The z-axis of the CRF is pointing in the direction of the major axis of the satellite, i.e. the axis with the largest inertia eigenvalue, and the x-axis is pointing in the direction of the minor axis of inertia. The y-axis is the right-hand cross product of the z- and x-axis, and is oriented along the intermediate axis of inertia.

With the three axes pointing in the same direction as the inertial axes, the CRF is body fixed as the inertia of the satellite is fixed. However, had the satellite been able to change shape (i.e. deploy solar panels), then the CRF would change.

Vectors specified in the CRF will be denoted as: ${}^c\mathbf{v}$.

4.2.6 Target Reference Frame (TRF)

The Target Reference Frame (TRF) is a reference frame used to define a target for the satellite pointing. The goal is for the SBRF to align with the TRF, thereby obtaining a satellite attitude in the desired direction. The origin of the TRF is placed in the CoM of the satellite. The z-axis is defined as a vector aligned with the line drawn between the MCC and the CoM of the satellite, with the direction always pointing away from the MCC. The x-axis is defined as the vector that is orthogonal on the z-axis while pointing in the direction of travel. The y-axis is the right-handed cross product of the z- and x-axis.

Vectors specified in the TRF will be denoted as: ${}^t\mathbf{v}$.

Chapter 5

Attitude Determination

This chapter will introduce the Keplerian orbit parameters necessary to be able to determine the position of the satellite within the inertial reference frame. A method for estimating the rotation of the satellite relative to the inertial frame is given, such that the attitude of the satellite can be determined. Subsequently the relation between each of the reference frames, as described in section 4.2, given as the rotation required to align one with the other, will be derived. This relation depends on the position of the satellite, which is found using orbit data and current time.

5.1 Orbit Description by Keplerian Orbit Elements

Source: [Wertz 78].

To be able to position the satellite and hence the SBRF within the ECI, a number of parameters must be provided. This data may be given as Keplerian elements, all given in the inertial frame, in this case the ECI.

An orbit described by Keplerian elements is an ideal (reference) orbit defined by two gravitationally interacting spherically symmetric objects, where their relative velocity and position define the orbit plane. The shape of the orbit must be an ellipsis for permanently associated objects. The ellipsis is defined by two focus points, one being the position of the larger of the two objects (when $m_{\text{large}} \gg m_{\text{small}}$; in this case the Earth), and the ellipsis boundary being the trajectory of the satellite.

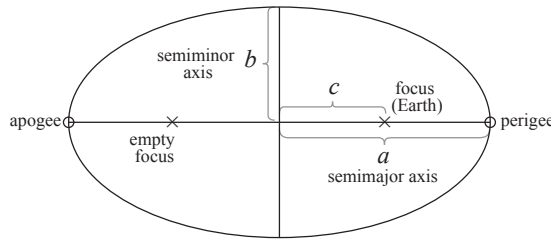


Figure 5.1: Geometric description of an ellipsis, defined by its semimajor and semiminor axes, a and b . The primary (the Earth) is situated in one of the foci of the satellite trajectory ellipsis.

The shape of the orbit ellipsis is uniquely defined by the *eccentricity* parameter, e , described in terms of the *semimajor axis*, a , defining the size of the ellipsis; and the distance from the focus point to the centre of the ellipsis, c ; see Figure 5.1. The magnitude of the eccentricity will be

$0 < e < 1$ for an ellipsis, and the smaller the value, the more circular the orbit:

$$e = \frac{c}{a} = \frac{\sqrt{a^2 - b^2}}{a} \quad (5.1)$$

The orientation of the orbit plane in space is defined by the *inclination* parameter, i , and the east-west orientation Ω . The inclination is the angle from the equatorial plane to the orbit plane. The intersection line between the two planes, called the line of nodes, intersects the orbit trajectory in two points: the ascending node, where the satellite crosses the equatorial plane going from south to north; and the descending node, where it crosses the plane going from north to south. The east-west orientation is defined by the *right ascension of the ascending node* (RAAN), which is the angle measured in the equatorial plane eastward from the ECI x-axis (equal to the ECEF x-axis at vernal equinox) to the ascending node, see Figure 5.2.

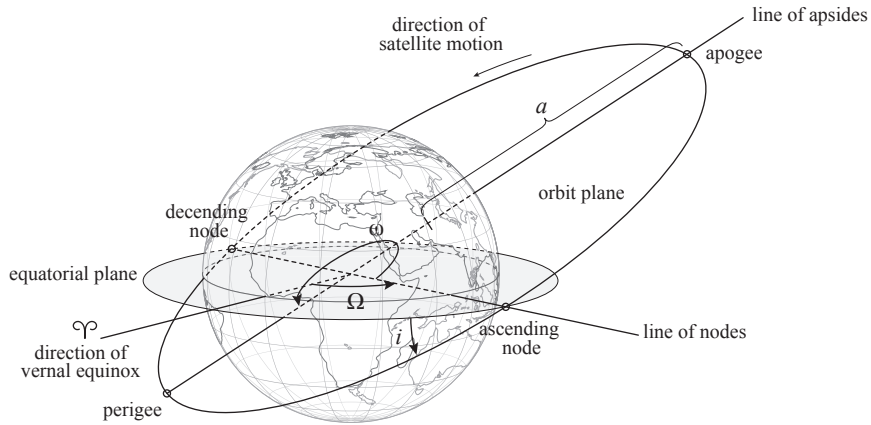


Figure 5.2: Contorted sketch of a satellite orbit, describing the Keplerian orbital elements. The centre of the Earth is in one of the two foci of the orbit ellipse. The two angles Ω (RAAN) and ω (argument of perigee) are measured in the equatorial and the orbital plane, respectively.

The terms perigee and apogee height describes the lowest and highest altitudes, respectively, during an orbit of the satellite, measured from the surface of the Earth. The rotation of the orbit ellipsis within the orbital plane is defined by the *argument of perigee*, ω . This is the angle measured in the orbital plane in the direction of motion of the satellite from the ascending node to perigee.

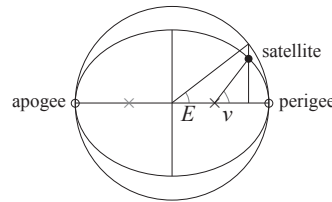


Figure 5.3: Geometry of the true anomaly, v , and the eccentricity anomaly, E .

The position of the satellite within the orbit is specified by the *true anomaly*, v , which is the angle measured at the focus point (the Earth) in the orbital plane from perigee to the satellite, see Figure 5.3. To be able to calculate the true anomaly, the *mean anomaly*, M , and the eccentricity

anomaly, E , are introduced:

$$M = 360 \cdot \frac{\Delta t}{P} = E - e \sin E \quad [^\circ] \quad (5.2)$$

$$\tan\left(\frac{v}{2}\right) = \sqrt{\frac{1+e}{1-e}} \cdot \tan\left(\frac{E}{2}\right) \quad (5.3)$$

where

Δt is the time between satellite perigee passage and epoch time (see subsection 5.1.1)

P is the orbital period of the satellite

The largest disturbance causing deviations from the ideal Keplerian orbit for low altitude orbits, are the predominant atmospheric drag, which tend to decrease the semimajor axis of the orbit.

5.1.1 Two Line Element – TLE

Sources: [Hoots 80] [Kelso 12].

The classical Keplerian orbital elements are available, along with a time stamp (epoch), through the Two Line Element (TLE) format. TLE data is published by the North American Aerospace Defence Command (NORAD), which monitors and tracks man-made objects in space. The TLE data is available online a few weeks after launch, and is transmitted to the satellite by the ground station on the fly. The initial TLE data is generated pre-launch on basis of the launch vehicle provider information on inclination, eccentricity and launch time, and the calculations are updated by the ground station until the telemetered data from NORAD is available. Each of the two lines of the TLE consist of 69 characters, specified in Figure 5.4.

NORAD classifies all space objects to be near-Earth or deep-space, defined by the revolution time being less or greater than 225 min, respectively. According to this, the TLE will be propagated using either the Simplified General Perturbation model (SGP4) for near-Earth orbits or the Simplified Deep-space Perturbation model (SDP4) for deep-space orbits. The prediction of position and velocity must be calculated using the corresponding decoding, also published by NORAD, i.e. if the TLE was obtained using the SGP4 propagator model, the SGP4 decoding model must be used to reconstruct data correctly.

Line number	Satellite number		Classification		International designator		Epoch time												First derivative of mean motion		Second derivative of mean motion		BSTAR drag term		Ephemeris type		Element no.	Checksum																																								
	Year	Launch no.	Year	Piece	Year	Julian date in current year [JD]	[rev/day] ²	[rev/day] ³	[Earth_radii ⁻¹]	Line	Check																																																									
1	2	3	4	5	6	7	8	9	10	11	12	13	14	15	16	17	18	19	20	21	22	23	24	25	26	27	28	29	30	31	32	33	34	35	36	37	38	39	40	41	42	43	44	45	46	47	48	49	50	51	52	53	54	55	56	57	58	59	60	61	62	63	64	65	66	67	68	69
1	d	d	d	d	d	c	d	d	d	d	d	d	d	d	d	d	d	d	d	d	d	d	d	d	d	d	d	d	d	s	*	d	d	d	d	d	d	d	d	s	e	s	d	d	d	d	s	e	d	d	d	d	d															
2	d	d	d	d	d	d	d	d	d	d	d	d	d	d	d	d	d	d	d	d	d	d	d	d	d	d	d	d	d	d	d	d	d	d	d	d	d	d	d	d	d	d	d	d	d	d	d	d	d	d	d	d	d	d	d	d	d	d	d	d	d							

Line number	Satellite number		Inclination i		RAAN Ω		Eccentricity e		Argument of perigee ω		Mean anomaly M		Mean motion n		Epoch revision		Checksum																																																			
	[Deg]	[Deg]	[Deg]	[Deg]	[Deg]	[Deg]	[Deg]	[Deg]	[Deg]	[Deg]	[Deg]	[Deg]	[Deg]	[Deg]	[rev/day]	[rev/day]																																																				
1	2	3	4	5	6	7	8	9	10	11	12	13	14	15	16	17	18	19	20	21	22	23	24	25	26	27	28	29	30	31	32	33	34	35	36	37	38	39	40	41	42	43	44	45	46	47	48	49	50	51	52	53	54	55	56	57	58	59	60	61	62	63	64	65	66	67	68	69
2	d	d	d	d	d	d	d	d	d	d	d	d	d	d	d	d	d	d	d	d	d	d	d	d	d	d	d	d	d	d	d	d	d	d	d	d	d	d	d	d	d	d	d	d	d	d	d	d	d	d	d	d																

Figure 5.4: TLE format specifying data type with d is a decimal number, c is a character, s is a symbol (plus or minus) and e is an exponent.

The *satellite number* is a catalogue number sequentially assigned by NORAD. The *classification* field may contain either C (classified) or U (unclassified, the latter being the case for all public TLEs). The *international designator* holds the last two digits of the launch year, the number of launch of that year, and piece of that launch. The *epoch time* indicates the UTC (Coordinated Universal Time) time when the orbit elements of the TLE were true, consisting of the last two digits of the year and the number of day of the year with decimals. The *mean motion* and its

first and second derivatives are only used in older SGP versions. The B_{star} or B^* is a drag-like coefficient used by SGP4, relating to the ballistic coefficient, C_B .

The *ephemeris type* is not used in the public TLE. The *element number* is the number of TLE for the particular object (satellite). The inclination, RAAN, eccentricity, argument of perigee and mean anomaly are as described in section 5.1. The *epoch revision* is the number of revolutions about the Earth, where a revolution begins at the ascending node, from launch to first pass of the ascending node being revolution 0, as defined by NORAD.

Below is an example of a TLE for the AAUSAT3 [Celestrak 13]:

```
1 39087U 13009B    13143.08539338 .00000611 00000-0 23441-3 0     818
2 39087   98.6314 333.2535 0013266 24.6778 335.5032 14.34037573 12399
```

5.1.2 International Geomagnetic Reference Field – IGRF

Sources: [of Geomagnetism 10]

An IGRF model is a mathematical description of the geomagnetic field (the Earth's main magnetic field), and its variations. It is given as a spherical harmonics series, from the The International Association of Geomagnetism and Aeronomy.

The IGRF models are considered linear for a 5 year period, and the IGRF-11 model consists of the coefficients for the mathematical description for the period 2010 to 2015. This also includes the annual changes in the geomagnetic field for this time period. An example of an IGRF plot is shown in figure 5.5 as a contour plot.

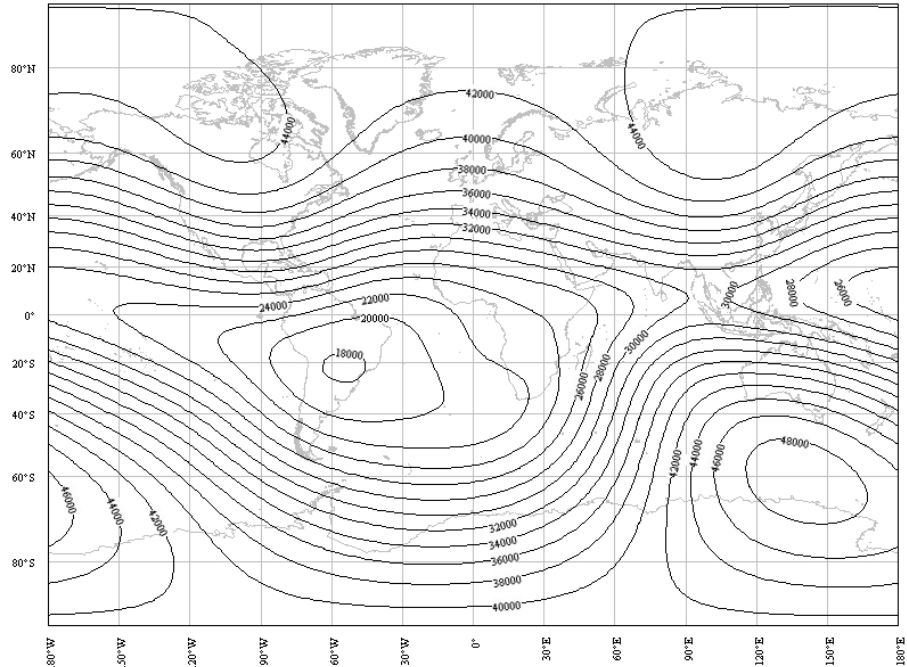


Figure 5.5: Contour plot of the IGRF-10 for an altitude of 630 km, for January 1st 2010.

5.1.3 Ephemeris Model

An ephemeris model is used to determine the Earth's rotation and the Sun's position in the ECI frame for a given time. The Earth's rotation is used to determine the geomagnetic field vector,

which rotates with the Earth. The Sun's position is used to determine a sun vector, which changes with the Sun's position relative to the Earth. These two vectors, the sun vector and magnetic vector are used for attitude determination, as these are known vectors in the ECI frame.

5.2 Attitude Estimation

The attitude of the satellite can be described as a rotation of the inertial frame, ECI, into alignment with the rotating SBRF. To determine the rotation which will align the two frames, it is necessary to know at least two vectors in each frame. At the present satellite, AAUSAT3, there are two sensors which can be used for estimating the (SBRF) attitude of the satellite; the sun sensors, giving the sun vector, and the magnetometers, giving the magnetic field vector. Both vectors can be calculated for the ECI for a known position, using the International Geomagnetic Reference Field (IGRF) model to calculate the ECI magnetic field vector and an ephemeris model to calculate the position of the Sun, as described in subsection 5.1.2 and subsection 5.1.3. The problem with using only the magnetometer measurements for determination of the attitude is that, if the satellite is rotating about the axis of the direction of the magnetic field, it will not be possible to sense this by using magnetometer measurements. The same problem applies to only using the sun sensors if rotation is about the sun vector. This also means, that the attitude cannot be determined if the two vectors are parallel. Finally, the sun vector will be unavailable if the satellite is in eclipse, which also means that the attitude cannot be determined by measurements. A means to determine when the satellite is in eclipse, is presented in subsection 5.2.3.

In the following, a method for determining the attitude of the SBRF will be described. The method involves solving Wahba's problem with a singular value decomposition (SVD) algorithm in order to determine the optimal rotation matrix describing the SBRF of the satellite in ECI coordinates.

5.2.1 Wahba's Problem

Sources: [Wahba 65] [Markley 99]

Wahba's problem in general is a loss function describing the square magnitude difference of vectors measured by sensors on the satellite with expected vectors in the ECI reference frame. The goal of this method of attitude determination is to find an optimal matrix ${}^i_s\bar{\mathbf{R}}_{\text{opt}}$ that minimizes the loss function given as:

$$J({}^i_s\bar{\mathbf{R}}) \triangleq \frac{1}{2} \sum_{k=1}^n \| {}^i\mathbf{v}_k - {}^i_s\bar{\mathbf{R}} {}^s\mathbf{v}_k \|^2 \quad k \geq 2 \quad (5.4)$$

where

- ${}^i_s\bar{\mathbf{R}}$ is the matrix which will rotate a vector given in SBRF into ECI coordinates
- ${}^i\mathbf{v}_k$ is the expected vector of measurement in ECI
- ${}^s\mathbf{v}_k$ is the measured vector in SBRF

Equation 5.4 can be stated with a weighing of the vectors, a_k , which may be used to emphasise vectors with known high precision and dampen vectors measured with sensors known to add much noise to the measurement. This will result in the equation:

$$J({}^i_s\bar{\mathbf{R}}) = \frac{1}{2} \sum_{k=1}^n a_k \| {}^i\mathbf{v}_k - {}^i_s\bar{\mathbf{R}} {}^s\mathbf{v}_k \|^2 \quad k \geq 2 \quad (5.5)$$

As shown in [Wahba 65], Wahba's problem can instead be described as:

$$J({}^i_s\bar{\mathbf{R}}) = \sum_{k=1}^n {}^i\mathbf{v}_k^T {}^i\mathbf{v}_k + \sum_{k=1}^n {}^s\mathbf{v}_k^T {}^s\mathbf{v}_k - 2 \text{trace}({}^i_s\bar{\mathbf{R}} \bar{\mathbf{B}}^T), \quad \text{where } \bar{\mathbf{B}} = \sum_{k=1}^n {}^i\mathbf{v}_k {}^s\mathbf{v}_k^T \quad (5.6)$$

As the rotational matrix is orthogonal, ${}^i_s\bar{\mathbf{R}}^T {}^i_s\bar{\mathbf{R}}$ disappears from the quadratic term. In order to minimize $J({}^i_s\bar{\mathbf{R}})$ on this form, it is instead a question of maximising $\text{trace}({}^i_s\bar{\mathbf{R}}\bar{\mathbf{B}}^T)$. It is possible to solve this maximisation by applying the SVD to the matrix $\bar{\mathbf{B}}$. This will result in:

$$\text{trace}({}^i_s\bar{\mathbf{R}}\bar{\mathbf{B}}^T) = \text{trace}({}^i_s\bar{\mathbf{R}}\underbrace{\bar{\mathbf{V}}\text{diag}[\Sigma_{11} \Sigma_{22} \Sigma_{33}]\bar{\mathbf{U}}^T}_{\text{svd}(\bar{\mathbf{B}})^T}) = \text{trace}(\bar{\mathbf{U}}^T {}^i_s\bar{\mathbf{R}}\bar{\mathbf{V}}\text{diag}[\Sigma_{11} \Sigma_{22} \Sigma_{33}]) \quad (5.7)$$

where

- $\text{diag}[\Sigma_{11} \Sigma_{22} \Sigma_{33}]$ is a diagonal matrix with the entries Σ_{11} , Σ_{22} , and Σ_{33}
- $\Sigma_{11} \Sigma_{22} \Sigma_{33}$ are the singular values of $\bar{\mathbf{B}}$ with the properties $\Sigma_{11} \geq \Sigma_{22} \geq \Sigma_{33}$
- $\bar{\mathbf{U}}, \bar{\mathbf{V}}$ are right-handed orthogonal matrices

The trace can be maximised by solving Equation 5.8 with respect to ${}^i_s\bar{\mathbf{R}}_{\text{opt}}$:

$$\begin{aligned} \bar{\mathbf{U}}^T {}^i_s\bar{\mathbf{R}}_{\text{opt}} \bar{\mathbf{V}} &= \text{diag}[1 \ 1 \ \det(\bar{\mathbf{U}})\det(\bar{\mathbf{V}})] \\ {}^i_s\bar{\mathbf{R}}_{\text{opt}} &= \bar{\mathbf{U}} \text{diag}[1 \ 1 \ \det(\bar{\mathbf{U}})\det(\bar{\mathbf{V}})] \bar{\mathbf{V}}^T \end{aligned} \quad (5.8)$$

The last entry of the diagonal matrix has the value $\det(\bar{\mathbf{U}})\det(\bar{\mathbf{V}})$ which can either result in +1 or -1. This component will invert the z-axis of ${}^i_s\bar{\mathbf{R}}_{\text{opt}}$ when a left-handed vector-base has been obtained. This ensures that ${}^i_s\bar{\mathbf{R}}_{\text{opt}}$ will always have right-hand orientation. It is possible to determine how good an estimate has been calculated through Equation 5.8 by using the attitude error covariance matrix $\bar{\mathbf{P}}$, which is given in [Markley 99] as:

$$\bar{\mathbf{P}} = \bar{\mathbf{U}} \text{diag}[(s_2 + s_3)^{-1} (s_3 + s_1)^{-1} (s_1 + s_2)^{-1}] \bar{\mathbf{U}}^T \quad (5.9)$$

where

$$\begin{aligned} s_1 &\equiv \Sigma_{11} \\ s_2 &\equiv \Sigma_{22} \\ s_3 &\equiv \det(\bar{\mathbf{U}})\det(\bar{\mathbf{V}})\Sigma_{33} \end{aligned}$$

In case of an unobservable attitude the matrix $\bar{\mathbf{P}}$ will become infinite.

5.2.2 The Singular Value Decomposition Method for Attitude Estimation

The first step in the SVD method is to create the matrix, $\bar{\mathbf{B}}$, consisting of the sum of the outer products of the measured (in SBRF) and expected (in ECI) magnetic field vectors and sun vectors, respectively, as:

$$\bar{\mathbf{B}} = a_{\text{sun}} {}^s\hat{\mathbf{v}}_{\text{sun}} {}^i\hat{\mathbf{v}}_{\text{sun}}^T + a_{\text{mag}} {}^s\hat{\mathbf{v}}_{\text{mag}} {}^i\hat{\mathbf{v}}_{\text{mag}}^T \quad (5.10)$$

where

- a_{sun} is a coefficient determining how to weight the sun sensor measurements
- a_{mag} is a coefficient determining how to weight the magnetometer measurements
- ${}^s\hat{\mathbf{v}}_{\text{sun}}$ is the normalised measured sun vector in the SBRF
- ${}^s\hat{\mathbf{v}}_{\text{mag}}$ is the normalised measured magnetic field vector in the SBRF
- ${}^i\hat{\mathbf{v}}_{\text{sun}}$ is the normalised calculated sun vector in the ECI
- ${}^i\hat{\mathbf{v}}_{\text{mag}}$ is the normalised calculated magnetic field vector in the ECI

There is no definitive way to determine the coefficients a_{sun} and a_{mag} . One way could be to go to the laboratory and do a number of measurements using the two sensors. By doing measurements it is then possible to determine the variance of these measurements. The variance of the measurements, σ , relates to the accuracy performance of the sensor in question. Thereby the inverse variances of the measurements could be used as the coefficients a_{sun} and a_{mag} , respectively. In this project such measurements are not made, so by default these coefficients are set to one, to give an equal weight of the two sensors.

5.2.3 Determining when the Satellite is in Eclipse

It is possible to determine when the satellite is in eclipse by using vector calculations between the three bodies: the Sun, Earth, and satellite. Primarily two factors need to be examined. The distance from the centre of the Earth to the vector stretched from the satellite to the Sun, and also the angle between the latter vector and the vector stretched between the centre of the Earth and the satellite. These vectors are depicted in Figure 5.6.

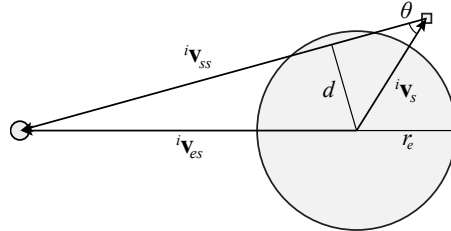


Figure 5.6: Illustration of the vector set-up for calculating when the satellite is in the shadow of Earth. The Sun is considered as a point mass.

The satellite is in eclipse when $d \leq r_e$ and $\theta \leq \theta_{\text{thresh}}$. θ_{thresh} is calculated as:

$$\frac{\sin(90^\circ)}{\|i\mathbf{v}_s\|} = \frac{\sin(\theta_{\text{thresh}})}{r_e} \quad \Leftrightarrow \quad \theta_{\text{thresh}} = \arcsin\left(\frac{r_e}{\|i\mathbf{v}_s\|}\right) \quad (5.11)$$

where

- r_e is the radius of the Earth [m]
- $i\mathbf{v}_s$ is the satellite vector [m]

The angle θ can be determined by calculating the angle between the $-i\mathbf{v}_s$ vector and $i\mathbf{v}_{ss}$ as:

$$\theta = \arccos\left(\frac{\underbrace{(i\mathbf{v}_{es} - i\mathbf{v}_s)}_{i\mathbf{v}_{ss}} \cdot i\mathbf{v}_s}{\|i\mathbf{v}_{es} - i\mathbf{v}_s\| \|i\mathbf{v}_s\|}\right) \quad (5.12)$$

where

- $i\mathbf{v}_{ss}$ is the satellite-sun vector [m]
- $i\mathbf{v}_{es}$ is the Earth-sun vector [m]

When the angle is below θ_{thresh} , the second criteria of $d \leq r_e$ should be determined as:

$$d = \|i\mathbf{v}_s\| \sin(\theta) [\text{m}] \quad (5.13)$$

where

- d is the distance from the centre of Earth to the satellite-sun vector [m]

5.3 Rotation Between Each of the Reference Frames

Some of the reference frames described in section 4.2 are better for describing certain properties of the satellite, while others are more practical to use when comparing different properties. For example it may be desirable to always make one of the sides of the satellite point towards Earth, while another axis is pointing in the travel direction of the satellite. In this case it would mean that the SBRF should align with the ORF, meaning that there should be no rotation between these two reference frames. This section will deal with the methods for rotation between each of the defined reference frames, mainly relating the rotating frames to the inertial frame, ECI.

5.3.1 Rotation Between ECI and ECEF

From the definition of the ECI frame and the ECEF frame in section 4.2, it is known that these reference frames share the same z-axis. This means that the rotation between these reference frames can be described as a positive (counter clockwise) rotation about the z-axis given as the direction cosine matrix shown in equation 5.14

$${}^i_f \bar{\mathbf{R}} = \begin{bmatrix} \cos \theta & -\sin \theta & 0 \\ \sin \theta & \cos \theta & 0 \\ 0 & 0 & 1 \end{bmatrix} \quad (5.14)$$

The rotation matrix, ${}^i_f \bar{\mathbf{R}}$, tells how the ECEF frame is rotated when looking at it in the ECI frame. This also means that if a vector is known in the ECEF frame, this rotation matrix can be multiplied with the vector to find its coordinates in the ECI frame. From section 4.1 it is known that this rotation matrix can be turned in to a quaternion that describes the same rotation of a vector. According to Equation 4.11, the rotation matrix, ${}^i_f \bar{\mathbf{R}}$, can be converted to the quaternion, ${}^i_f \mathbf{q}$, as:

$$\begin{aligned} {}^i_f q_4 &= \frac{1}{2} \sqrt{1 + {}^i_f R_{11} + {}^i_f R_{22} + {}^i_f R_{33}} = \sqrt{\frac{1 + \cos(\theta)}{2}} \\ {}^i_f q_1 &= \frac{1}{4{}^i_f q_4} ({}^i_f R_{23} - {}^i_f R_{32}) = 0 \\ {}^i_f q_2 &= \frac{1}{4{}^i_f q_4} ({}^i_f R_{31} - {}^i_f R_{13}) = 0 \\ {}^i_f q_3 &= \frac{1}{4{}^i_f q_4} ({}^i_f R_{12} - {}^i_f R_{21}) = \frac{-\sin(\theta)}{\sqrt{2 + 2 \cos(\theta)}} \end{aligned} \quad (5.15)$$

where the angle θ depends on the time since the last vernal equinox. In fact the ECI and the ECEF frames align approximately every 23 hours, 56 minutes and 4 seconds (equal to 86,164.09053 seconds – the length of a sidereal day). This means that it is sufficient to know how long it has been since the last time the ECI and ECEF frame were aligned to know what the angle θ is, as shown by equation 5.16.

$$\theta = 2\pi \frac{t_{al}}{86164.04053} \quad (5.16)$$

where

t_{al} is the time since last the ECI and ECEF frames were aligned. [s]

When the quaternion needed for converting a vector from ECEF coordinates to ECI coordinates is known, it is also possible to determine the quaternion for representing ECI coordinates in the ECEF frame. This quaternion is known to be the conjugate, which means that ${}^f_i \mathbf{q} = {}^i_f \mathbf{q}^*$. These ways of converting between the ECI and ECEF frames have been implemented as the functions `eci2ecef()` and `ecef2eci()` in C in the file called `rotdfuncs.c` (which is available on the CD), ready for use on the MCUs implemented on the satellite.

5.3.2 Rotation Between ECI and ORF

From the definition of the ORF it is known that it has its origin in the CoM of the satellite and that the x-axis of the frame is pointing in the travel direction, the z-axis is pointing towards the CoM of Earth and the y-axis is the right handed cross product of the z- and x-axis.

To get to know how the ORF is described in the ECI frame, it is needed to know the location ${}^i(x_0, y_0, z_0)$ and the velocity ${}^i(\dot{x}_0, \dot{y}_0, \dot{z}_0)$ of the satellite. This data can be retrieved from the TLE

data which will be available for the satellite after launch. A C source code file called *sgp4m.c* takes an array of TLE data as input and gives the position and velocity vector of the satellite in the ECI frame as output. With this data achieved, the different axes of the ORF represented in the ECI frame can be determined as:

$${}^i_o\mathbf{x} = \frac{1}{\sqrt{{}^i\dot{x}_0^2 + {}^i\dot{y}_0^2 + {}^i\dot{z}_0^2}} \begin{bmatrix} {}^i\dot{x}_0 \\ {}^i\dot{y}_0 \\ {}^i\dot{z}_0 \end{bmatrix}, \quad {}^i_o\mathbf{z} = \frac{1}{\sqrt{{}^i{x}_0^2 + {}^i{y}_0^2 + {}^i{z}_0^2}} \begin{bmatrix} -{}^i{x}_0 \\ -{}^i{y}_0 \\ -{}^i{z}_0 \end{bmatrix}, \quad {}^i_o\mathbf{y} = {}^i_o\mathbf{z} \times {}^i_o\mathbf{x} \quad (5.17)$$

where the rotation matrix, ${}^i_o\bar{\mathbf{R}}$, describing ORF coordinates in the ECI frame is given as:

$${}^i_o\bar{\mathbf{R}} = [{}^i_o\mathbf{x} \quad {}^i_o\mathbf{y} \quad {}^i_o\mathbf{z}] \quad (5.18)$$

Like the rotation matrix in the previous section, this rotation matrix aligning the ECI frame with the ORF can be converted to a quaternion as well. The methods for converting between the ORF and ECI frame has been implemented in C in the function called `orf2eci()` in the file *rotfuncs.c* (which is available on the CD), ready for use on the MCUs implemented on the satellite.

5.3.3 Rotation Between ECI and SBRF

The rotation of the SBRF relative to the ECI frame is found using singular value decomposition, as described in subsection 5.2.2, starting by determining the matrix $\bar{\mathbf{B}}$ according to Equation 5.10. After determining the matrix $\bar{\mathbf{B}}$, it is possible to take the SVD of said matrix, as shown in equation 5.19 (some C source code for determining the SVD has been obtained and is given as the function `svd()` in the file *svd.c* available on the CD).

$$[\mathbf{U}, \mathbf{S}, \mathbf{V}] = \text{svd}(\bar{\mathbf{B}}) \quad (5.19)$$

This decomposition is carried out in order to be able to determine the optimal rotation matrix, ${}^i_s\mathbf{R}_{\text{opt}}$, giving SBRF in ECI coordinates. The optimal rotation matrix, ${}^i_s\mathbf{R}_{\text{opt}}$, can then be determined as:

$${}^i_s\mathbf{R}_{\text{opt}} = \bar{\mathbf{U}} \begin{bmatrix} 1 & 0 & 0 \\ 0 & 1 & 0 \\ 0 & 0 & \det(\bar{\mathbf{U}}) \det(\bar{\mathbf{V}}) \end{bmatrix} \bar{\mathbf{V}}^T = \bar{\mathbf{U}} \bar{\mathbf{I}} \bar{\mathbf{V}}^T \quad (5.20)$$

As in the previous cases, this rotation matrix can be turned into a quaternion. There are some cases, e.g. when the satellite is in eclipse, where the above calculations might fail to give useful results, see subsection 5.2.3. In these cases the quaternion is set to the value (0,0,0,1), which temporarily tells that the SBRF and the ECI frame are aligned, and no rotation should be imposed, until the satellite gets out of eclipse again.

5.3.4 Rotation Between SBRF and CRF

The CRF is the frame that is used to do the calculations for the control system, and this frame always has the same orientation relative to the SBRF. The calculations for the control are dependent on the moment of inertia for the satellite, and from the definition of the CRF, its axes are the principal axes of the satellite, defined by the satellite inertia. Hence the inertia matrix in the CRF is a diagonal matrix. The matrix that diagonalises the inertia matrix is found through Eigen Value Decomposition (EVD) of the SBRF inertia matrix, and contains the eigenvectors of the SBRF inertia matrix. This matrix is the rotation matrix which can be multiplied with a vector in the CRF to give the coordinates of this vector in the SBRF. This rotation matrix is given by:

$${}^s_c\bar{\mathbf{R}} = \begin{bmatrix} 0.9821 & 0.1666 & 0.0881 \\ -0.1170 & 0.9055 & -0.4078 \\ -0.1477 & 0.3902 & 0.9088 \end{bmatrix} \quad (5.21)$$

The diagonalisation of the inertia matrix and the calculations for determining this rotation matrix can be seen in section 6.1. With the rotation matrix determined, it is also possible to determine the quaternion for the same rotation. This calculation should only be carried out once on the MCU, as the relation between CRF and SBRF does not change over time. The quaternion is calculated according to the methods described in section 4.1:

$$\begin{aligned}\overset{s}{_c}q_4 &= \frac{1}{2}\sqrt{1 + \overset{s}{_c}R_{11} + \overset{s}{_c}R_{22} + \overset{s}{_c}R_{33}} = 0.9744 \\ \overset{s}{_c}q_1 &= \frac{1}{4\overset{s}{_c}q_4}(\overset{s}{_c}R_{23} - \overset{s}{_c}R_{32}) = -0.2039 \\ \overset{s}{_c}q_2 &= \frac{1}{4\overset{s}{_c}q_4}(\overset{s}{_c}R_{31} - \overset{s}{_c}R_{13}) = -0.0606 \\ \overset{s}{_c}q_3 &= \frac{1}{4\overset{s}{_c}q_4}(\overset{s}{_c}R_{12} - \overset{s}{_c}R_{21}) = 0.0727\end{aligned}\quad (5.22)$$

Now the quaternion rotating SBRF into alignment with CRF is determined and ready for use in simulation and the implementation.

5.3.5 Rotation between ECI and TRF

The TRF is a frame which is used for pointing at the MCC. It has its z-axis as the direction from the MCC towards the satellite. The y-axis is determined as the cross product of the z-axis and the travel direction of the satellite. Finally the x-axis can be determined as the cross product of the y-axis and z-axis.

Like when determining the ORF, it is needed to know the location ${}^i(x_0, y_0, z_0)$ and the velocity vector, ${}^i\mathbf{v}_0 = {}^i(\dot{x}_0, \dot{y}_0, \dot{z}_0)$, of the satellite given in the ECI frame. Furthermore it is also needed to know the location of the MCC given in the ECI frame. It is known that the MCC is placed at the location (3427961, 603674, 5326755) given in the ECEF frame. This location will then have to be rotated into the ECI frame to be used for determining the direction from the MCC to the satellite. For convenience, this location is called ${}^i\mathbf{v}_{\text{MCC}}$, indicating that it is the vector from the Earth CoM towards the MCC. Furthermore the location of the satellite is called ${}^i\mathbf{v}_{\text{sat}}$, indicating that it is the vector from the Earth CoM towards the satellite. Thereby it is possible to determine the vector from the MCC towards the satellite and thereby also the z-axis of the TRF:

$${}^i\mathbf{z} = \frac{{}^i\mathbf{v}_{\text{sat}} - {}^i\mathbf{v}_{\text{MCC}}}{\|{}^i\mathbf{v}_{\text{sat}} - {}^i\mathbf{v}_{\text{MCC}}\|} \quad (5.23)$$

With the z-axis determined it is also possible to determine the y axis:

$${}^i\mathbf{y} = {}^i\mathbf{z} \times \frac{{}^i\mathbf{v}_0}{\|{}^i\mathbf{v}_0\|} \quad (5.24)$$

Finally it is possible to determine the x-axis by taking the cross product of the y- and z-axis:

$${}^i\mathbf{x} = {}^i\mathbf{y} \times {}^i\mathbf{z} \quad (5.25)$$

These descriptions of the x-, y- and z-axis of the TRF given in the ECI frame can be used to determine the rotation matrix, ${}^i\bar{\mathbf{R}}$, as:

$${}^i\bar{\mathbf{R}} = [{}^i\mathbf{x} \quad {}^i\mathbf{y} \quad {}^i\mathbf{z}] \quad (5.26)$$

Chapter 6

Attitude Control

This chapter introduces the dynamic model of the satellite, which is then used in order to design the pointing control system. Section 6.1 gives the derivations and equations needed to mathematically model the essential torques which the satellite will be subjected to when in orbit, while section 6.3 describes the control system, which takes the sensed input from the attitude determination system and computes the control signal on basis of the satellite model. The control system is tested in a Simulink simulation environment with the attitude determination system, leading on to the acceptance test.

6.1 Dynamic Model of the Satellite

Sources:[Arovas 08][J. Peraire 09][Wertz 78]

First, dynamic equations are defined relating the satellite moment of inertia to these torques, next the external torques are defined comprising a control torque and an environmental disturbance torque. Finally the model relating all specified torques is concluded. This will lead to the design of the attitude control system, described in section 6.3.

The satellite is built around a cubic framework, with a centre of mass 2 cm off the geometric centre. The satellite framework is modelled as a rigid body. Due to the fact that it can be thought of as solid, meaning that any two points within the body maintain their mutual distance regardless of any external torques exerted on the body.

Newton's second law describes the relation between a force, F , exerted on a body and the translational motion of the body in terms of its acceleration, a , and mass, m , disregarding any friction:

$$F(t) = m \cdot a(t) \quad [\text{N}] \quad (6.1)$$

The counterpart equation for rotational motion, similarly relating a torque, τ , exerted on the body, to the motion of the body in terms of its rotational acceleration, α , and inertia, J , likewise disregarding any friction:

$$\tau(t) = J \cdot \alpha(t) \quad [\text{Nm}] \quad (6.2)$$

Moment of Inertia

The moment of inertia is an expression of how the mass of an object is distributed relative to a rotational axis, and hence the body's reluctance toward acceleration or deceleration. For the simplified case, the moment of inertia for a point mass is considered:

$$J = \sum_{i=1}^n m_i \cdot r_i^2 \quad [\text{kg}\cdot\text{m}^2] \quad (6.3)$$

where

J	is the moment of inertia of the body	[kg·m ²]
m_i	is the mass of the i^{th} particle	[kg]
r_i	is the distance from the rotational axis to the i^{th} particle	[m]

The rotational axis may be any axis, e.g. an axis going through the geometric centre of the body. To find the inertia about the centre of mass of the body, Steiner's theorem, which describes the inertia relation between two parallel axes, is used:

$$J_{\text{CoM}} = J - m \cdot d^2 \quad [\text{kg} \cdot \text{m}^2] \quad (6.4)$$

where

J_{CoM}	is the moment of inertia around the axis, a_1 , going through CoM	[kg·m ²]
J	is the inertia around an arbitrary axis, a_2 , parallel to a_1	[kg·m ²]
m	is the mass of the object	[kg]
d	is the distance between the two axes	[m]

When the body is free to move about more than one axis, as is the case for a satellite in three dimensional space, the inertia is expressed as a matrix. If the rigid body is symmetrical in all three axes, the inertia matrix will be a diagonal matrix. If the diagonal is zero, it means that the body would get an infinite angular velocity when a constant torque is applied over infinitely long time. Off-diagonal elements in the matrix being different from zero, is an expression of how e.g. a torque in the x axis gives a acceleration of the rigid body around the y axis, J_{xy} .

The inertia of AAUSAT3 is represented as the matrix ${}^s\bar{\mathbf{J}}$ in the SBRF, which is determined using Autodesk® Inventor®. The CAD programme calculates the inertia of the object using a 3D model, with the mass properties function, which outputs the inertia matrix:

$${}^s\bar{\mathbf{J}} = \begin{bmatrix} J_{s,xx} & J_{s,xy} & J_{s,xz} \\ J_{s,yx} & J_{s,yy} & J_{s,yz} \\ J_{s,zx} & J_{s,zy} & J_{s,zz} \end{bmatrix} = \begin{bmatrix} 4806.218 & 10636.223 & 13438.363 \\ 10636.223 & 92852.250 & -1627.530 \\ 13438.363 & -1627.530 & 92147.773 \end{bmatrix} \cdot 10^{-6} \quad [\text{kg} \cdot \text{m}^2]$$

The non-zero off-diagonal entries makes this a difficult problem to control. Rotating it into a diagonal matrix greatly simplifies the control problem. The CRF is represented as the principal axes of the rigid body, where a torque exerted in one axis, does not induce a torque in any of the other axes, i.e. a torque applied to x does not cause any acceleration around y . The diagonalisation of the SBRF inertia matrix results in the CRF inertia matrix, by taking EVD of ${}^s\bar{\mathbf{J}}$ as shown in equation 6.5:

$${}^s\bar{\mathbf{J}} = {}_c^s\bar{\mathbf{R}} {}^c\bar{\mathbf{J}} {}_c^s\bar{\mathbf{R}}^{-1} \Leftrightarrow \quad (6.5)$$

$${}^c\bar{\mathbf{J}} = \begin{bmatrix} J_{c,xx} & 0 & 0 \\ 0 & J_{c,yy} & 0 \\ 0 & 0 & J_{c,zz} \end{bmatrix} = \begin{bmatrix} 1518 & 0 & 0 \\ 0 & 94107 & 0 \\ 0 & 0 & 94181 \end{bmatrix} \cdot 10^{-6} \quad [\text{kg} \cdot \text{m}^2]$$

The matrix that diagonalises the matrix ${}^s\bar{\mathbf{J}}$ into ${}^c\bar{\mathbf{J}}$ is the rotational matrix, ${}_c^s\bar{\mathbf{R}}$, consisting of the eigenvectors of ${}^s\bar{\mathbf{J}}$. The rotational matrix can be used to rotated from SBRF to CRF. For rotation from CRF to SBRF, the inverse of the matrix is used.

$${}_c^s\bar{\mathbf{R}} = \begin{bmatrix} 0.9821 & 0.1666 & 0.0881 \\ -0.1170 & 0.9055 & -0.4078 \\ -0.1477 & 0.3902 & 0.9088 \end{bmatrix} \quad (6.6)$$

Dynamic Equations of the Satellite

Attitude dynamics relates the angular velocity of a rigid body relative to its CoM to external torques, evaluated in an inertial reference frame. The basic equation of attitude dynamics is that of angular momentum:

$$\mathbf{L}_{\text{tot}} = \sum_{i=1}^n \mathbf{r}_i \times \mathbf{p}_i = \sum_{i=1}^n \mathbf{r}_i \times m_i \mathbf{v}_i \quad (6.7)$$

where

\mathbf{L}_{tot}	is the total angular momentum of the rigid body	[kg·m ² /s]
\mathbf{r}_i	is the position of the i^{th} point mass in inertial space	[m]
\mathbf{p}_i	is the momentum of the i^{th} point mass	[kg·m/s]
m_i	is the mass of the i^{th} point mass	[kg]
\mathbf{v}_i	is the translational velocity of the i^{th} point mass	[m/s]

The time derivative of the angular momentum in Equation 6.7 is equal to the total torque on the body, given in an inertial reference frame:

$$\begin{aligned} \frac{d\mathbf{L}_{\text{tot}}}{dt} &= \sum_{i=1}^n \frac{d}{dt} (\mathbf{r}_i \times m_i \mathbf{v}_i) = \sum_{i=1}^n (\mathbf{v}_i \times m_i \mathbf{v}_i + \mathbf{r}_i \times m_i \mathbf{a}_i) \\ &= \sum_{i=1}^n \mathbf{r}_i \times \mathbf{F}_i = \sum_{i=1}^n \boldsymbol{\tau}_i = \boldsymbol{\tau}_{\text{tot}} \end{aligned} \quad (6.8)$$

where

\mathbf{v}_i	is the translational velocity, equal to the time derivative of \mathbf{r}_i	[m/s]
\mathbf{a}_i	is the translational acceleration, equal to the time derivative of \mathbf{v}_i	[m/s ²]
\mathbf{F}_i	is the force exerted on the i^{th} point mass	[N]
$\boldsymbol{\tau}_i$	is the torque exerted on the i^{th} point mass	[N·m]

Combining Equation 6.8 and Equation 6.2, where the angular velocity (and inertia) may be that of the spacecraft or any rigid body, the relation is:

$$\boldsymbol{\tau}_{\text{tot}} = \frac{d\mathbf{L}_{\text{tot}}}{dt} = \bar{\mathbf{J}} \frac{d\boldsymbol{\omega}}{dt} \quad \Leftrightarrow \quad \mathbf{L}_{\text{tot}} = \bar{\mathbf{J}} \boldsymbol{\omega} \quad (6.9)$$

According to section 5.3, a vector ${}^i\mathbf{L}$ may be represented in the CRF by a rotation matrix ${}^i\bar{\mathbf{R}}$, as the vector ${}^c\mathbf{L}$. The derivative of the rotation matrix, where ${}^i\boldsymbol{\omega}_c$ is the rotation of the CRF (i.e. the spacecraft) relative to the inertial frame, is given as [Wertz 78]:

$$\frac{d{}^c\bar{\mathbf{R}}}{dt} = [{}^i\boldsymbol{\omega}_c]_{\times}^T {}^c\bar{\mathbf{R}}, \quad [{}^i\boldsymbol{\omega}_c]_{\times}^T = \begin{bmatrix} 0 & \omega_z & -\omega_y \\ -\omega_z & 0 & \omega_x \\ \omega_y & -\omega_x & 0 \end{bmatrix} \quad (6.10)$$

Due to the law of preservation of angular momentum, in an inertial frame ${}^i\mathbf{L}$ is constant in the absence of external torques. This entails that the derivative of ${}^c\mathbf{L}$ can be stated as:

$$\begin{aligned} \frac{d{}^c\mathbf{L}}{dt} &= \frac{d}{dt} ({}^c\bar{\mathbf{R}} {}^i\mathbf{L}) = \frac{d{}^c\bar{\mathbf{R}}}{dt} {}^i\mathbf{L} + {}^c\bar{\mathbf{R}} \frac{d{}^i\mathbf{L}}{dt} = \frac{d{}^c\bar{\mathbf{R}}}{dt} {}^i\mathbf{L} + 0 \\ &= [{}^i\boldsymbol{\omega}_c]_{\times}^T {}^c\bar{\mathbf{R}} {}^i\mathbf{L} = [{}^i\boldsymbol{\omega}_c]_{\times}^T {}^c\mathbf{L} = -{}^i\boldsymbol{\omega}_c \times {}^c\mathbf{L} \end{aligned} \quad (6.11)$$

Equation 6.11 is an expression of the internal torques of the spacecraft, caused by nutation. Nutation arises when the angular momentum vector is not aligned with one of the principal axes

of the spacecraft, which will make the angular momentum vector spin as seen from the CRF, this spin rate being the body nutation rate. Combining Equation 6.11 with Equation 6.9, the Euler differential equation can now be stated as:

$$\tau_{\text{tot}} = \tau_{\text{ext}} + \tau_{\text{int}} \quad \Leftrightarrow \quad {}^c\bar{\mathbf{J}} \frac{d^i \boldsymbol{\omega}_c}{dt} = \tau_{\text{ext}} - {}^i\boldsymbol{\omega}_c \times {}^c\bar{\mathbf{J}} {}^i\boldsymbol{\omega}_c \quad (6.12)$$

Equation 6.12 can be rewritten to vector form and it is then possible to determine the torque applied on every (principal) axis independently of each other:

$${}^c\bar{\mathbf{J}} \frac{d^i \boldsymbol{\omega}_c}{dt} = \begin{bmatrix} \tau_{\text{ext},x} \\ \tau_{\text{ext},y} \\ \tau_{\text{ext},z} \end{bmatrix} + \begin{bmatrix} (J_{yy} - J_{zz})\omega_y\omega_z \\ (J_{zz} - J_{xx})\omega_x\omega_z \\ (J_{xx} - J_{yy})\omega_x\omega_y \end{bmatrix} \quad (6.13)$$

The external torques comprise control torques and environmental disturbance torques, which will be derived in the following.

6.1.1 Magnetorquer Control Torque

Sources: [Markowitz 10] [Jewett 08]

The control torque is the torque that emerges on basis of actuation. As outlined in section 3.4, magnetorquers are used to detumble and point the satellite. A magnetorquer is an electric coil in which a current flows. As long as the current flow through the coil is not parallel with the Earth's magnetic field, the coil can be used to exert a force on the satellite. The direction and magnitude of the force depends on the angle between the magnetic field and the direction of the current, as depicted in Figure 6.1.

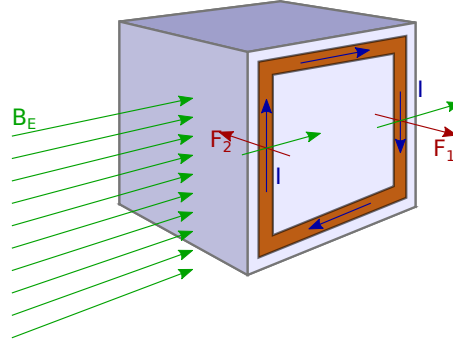


Figure 6.1: When a magnetic field, \mathbf{B}_E , is incident on the magnetorquer wires as shown, the forces \mathbf{F}_1 and \mathbf{F}_2 will result to produce a torque on the satellite body.

As shown in Figure 6.1, the magnetorquer can be seen as four individual wires. The force exerted on each wire in a magnetic field can be calculated as:

$$\mathbf{F} = \mathbf{I}\mathbf{l} \times \mathbf{B}_E \quad [\text{N}] \quad (6.14)$$

where

\mathbf{F}	is the force exerted on the wire	[N]
\mathbf{I}	is the current running through the magnetorquer	[A]
\mathbf{l}	is the length of the wire	[m]
\mathbf{B}_E	is the Earth's magnetic field	[Wb/m]

In the case of \mathbf{B}_E being parallel with the current running through the top and bottom wire, these can be assumed to be zero, as the cross product of two parallel vectors is zero. In this case the

two individual forces \mathbf{F}_1 and \mathbf{F}_2 can be used to calculate the torque. The forces calculated by equation 6.14 can be used to calculate the torque exerted on the satellite by multiplying it with the distance from the center of the magnetorquer to the side of the magnetorquer. In this case the side length of the magnetorquer is called l and thus the distance from the center to the side of the magnetorquer is $l/2$. The torque on the satellite can now be described as:

$$\tau = \frac{l}{2} \cdot (\mathbf{F}_1 + \mathbf{F}_2) = \frac{l}{2} \cdot (I\mathbf{l} \times \mathbf{B}_E - I(-l) \times \mathbf{B}_E) = l^2 \cdot (\mathbf{I} \times \mathbf{B}_E) \quad [\text{Nm}] \quad (6.15)$$

It is also known that l^2 is the area enclosed by the magnetorquer, and that equation 6.15 only describes the torque on a single wire loop. So for a multiple loop coil the torque can be described as:

$$\tau = NI A \times \mathbf{B}_E \quad [\text{N}\cdot\text{m}] \quad (6.16)$$

where

τ	is the torque exerted on the satellite	[Nm]
N	is the number of windings in the magnetorquer	[.]
A	is the area enclosed by the magnetorquer	[m ²]

The above is a simplified way of determining the torque exerted by the magnetorquer. However, the expression shown in equation 6.16 is in fact the general way of determining the torque exerted on the satellite when applying a current to the magnetorquer. The derivation showing that this is the general expression is shown in appendix E.

The magnitude of the control torque of Equation 6.16, can be expressed by rewriting the cross product, with θ being the angle between the two vectors \mathbf{I} and \mathbf{B}_E :

$$||\tau|| = N ||\mathbf{I}|| A ||\mathbf{B}_E|| \sin \theta \quad [\text{N}\cdot\text{m}] \quad (6.17)$$

As the magnetic field of the earth, \mathbf{B}_E , is the only thing which cannot be adjusted, it means that there are three different variables to adjust to get the desired torque from the magnetorquer: the number of windings, N , the current running through the magnetorquer, \mathbf{I} and the area inside the magnetorquer, A . Whenever any of these values is increased or decreased, so is the value of the torque generated by the magnetorquer. Because of the limited power supply on the satellite, it is wanted to keep the current, \mathbf{I} , as low as possible. But in order to keep a low current flow, it is needed to increase either the area, A , or the number of windings, N , or both. When increasing any of them, it also results in an increase of the total weight of the satellite. From equation 6.17 it is also seen that the maximum torque for a fixed set of values of N , \mathbf{I} and A , is obtained when the angle between the two vectors \mathbf{B}_E and \mathbf{I} is 90°.

The equation that is going to be included as the control torque in the dynamic model, is the expression of τ in equation 6.16.

6.1.2 Environmental Disturbance Torque

There are many types of environmental disturbances affecting a satellite in a Low Earth Orbit, as described in section 1.4. The disturbance torque magnitude from solar radiation and aerodynamic torque are determined for the purpose of designing a controller which can suppress these disturbance torques, and for the purpose of designing magnetorquers with adequate amount of torque, to be able to control the satellite.

Solar Radiation Torque

Sources: [Wertz 78]

Any kind of radiation that hits the surface of the satellite will produce a force on this surface, and thereby a torque about the centre of mass. The surface is exposed to a force per unit area which is equal to the difference between the incident and reflected momentum flux vectors. The

intensity of the solar radiation varies according to the inverse square law of distance seen equation 6.18:

$$I \propto \frac{1}{d^2} \quad (6.18)$$

where

- I is the radiation intensity
- d is the distance between the source and the observer

This means that the intensity of the radiation from the sun does not vary a lot for a satellite in orbit around Earth. According to [Wertz 78] there are three major factors determining the radiation torque on a spacecraft: The intensity and spectral distribution of the incident radiation, the geometry of the surface and its optical properties, and the orientation of the Sun vector relative to the spacecraft.

Likewise, there are also three major sources of electromagnetic radiation pressure: solar illumination, solar radiation reflected by the Earth and its atmosphere, and radiation emitted from earth and its atmosphere.

Table 6.1 shows the intensity of the above described sources. From the table it is seen that the direct solar radiation is the most dominant source, and in general this is the only one considered. But as this project concerns designing an ADCS for a satellite in an orbit around the Earth, with an altitude of 90 - 320 km, it might be necessary to take into account both the reflected radiation and Earth's radiation itself. It is important to note that the information about the reflected radiation and Earth's own radiation is when assuming a spherical spacecraft.

Altitude [km]	Solar radiation [W/m ²]	Earth reflectance* [W/m ²]	Earth radiation* [W/m ²]
500	1358	600	150
1000	1358	500	117
2000	1358	300	89
4000	1358	180	62
8000	1358	75	38
15000	1358	30	14
30000	1358	12	3
60000	1358	7	2

*Assuming a spherical spacecraft

Table 6.1: Intensity of radiation sources for a satellite over the subsolar point integrated over all wavelengths. (Data from NASA)[Wertz 78]

There are three different forces which is affecting the satellite when under influence of radiation. One of the forces is caused by absorption and the other two are caused by reflection - specular reflection and diffuse reflection. The differential radiation force (momentum transferred per time) due to the radiation that is absorbed by the satellite is given by equation 6.19

$$d\mathbf{F}_{abs} = -PC_a \cos(\theta_{SN}) \hat{\mathbf{S}} dA \quad (0 \leq \theta \leq 90^\circ) \quad (6.19)$$

where

- $d\mathbf{F}_{abs}$ is the differential radiation force (vector)
- P is the momentum flux incident on an elemental area, dA , with unit outward normal $\hat{\mathbf{N}}$
- C_a is the absorption coefficient
- θ_{SN} is the angle between the vectors $\hat{\mathbf{S}}$ and $\hat{\mathbf{N}}$
- $\hat{\mathbf{S}}$ is the unit vector from the satellite's CoM to the CoM of the Sun

And the mean momentum flux, P , can be determined by equation 6.20

$$P = \frac{F_e}{c} \quad (6.20)$$

where

- F_e is the solar constant
- c is the speed of light

As it is seen, equation 6.19 is only true for θ_{SN} between 0° and 90° . This is because if the angle is bigger than 90° (or smaller than 0°) it means that the surface of the satellite is not illuminated. This means that there will be no force applied to the surface due to solar radiation. Like the equation for the differential radiation force, due to absorption, there is also one for the specular reflection, which is given by equation 6.21

$$d\mathbf{F}_{spec} = -2PC_s \cos^2(\theta_{SN})\hat{\mathbf{N}}dA \quad (0 \leq \theta \leq 90^\circ) \quad (6.21)$$

where C_s is the coefficient of specular reflection. This is determined by the fraction of the entire incident radiation which is specularly reflected. The direction of the reflected radiation is in the direction given by $(-\hat{\mathbf{S}} + 2\hat{\mathbf{N}}\cos[\theta_{sn}])$. In the case of a diffuse, or partially diffuse, surface the radiation will be reflected in all directions with a distribution proportional to $\cos(\phi)$ where ϕ is the angle between the reflected radiation and $\hat{\mathbf{N}}$. The differential radiation force, due to diffusely reflected radiation, is then determined by integrating the contribution of the reflected radiation over all angles, and then finally equation 6.22 can be used to determine the differential radiation force due to diffuse reflection.

$$d\mathbf{F}_{diff} = PC_d \left(-\frac{2}{3} \cos(\theta_{SN})\hat{\mathbf{N}} - \cos(\theta_{SN})\hat{\mathbf{S}} \right) dA \quad (0 \leq \theta \leq 90^\circ) \quad (6.22)$$

where C_d is the coefficient of diffuse reflection. This is determined by the fraction of the entire incident radiation which is diffusely reflected. If it is then assumed that all of these have some contribution to the total differential radiation force and $C_a + C_s + C_d = 1$, it is then possible to determine the total differential radiation force by equation 6.24

$$\begin{aligned} d\mathbf{F}_{tot} &= \int [d\mathbf{F}_{abs} + d\mathbf{F}_{spec} + d\mathbf{F}_{diff}] \\ &= -P \int [(1 - C_s - C_d)\hat{\mathbf{S}} + 2C_s \cos(\theta_{SN})\hat{\mathbf{N}} + \frac{2}{3}C_d\hat{\mathbf{N}} + C_d\hat{\mathbf{S}}] \cos(\theta_{SN}) dA \\ &= -P \int [(1 - C_s)\hat{\mathbf{S}} + 2(C_s \cos(\theta_{SN}) + \frac{1}{3}C_d)\hat{\mathbf{N}}] \cos(\theta_{SN}) dA \\ &= -P[(1 - C_s)\hat{\mathbf{S}} + 2(C_s \cos(\theta_{SN}) + \frac{1}{3}C_d)\hat{\mathbf{N}}] \cos(\theta_{SN}) A \end{aligned} \quad (6.23)$$

In the case of the satellite, A is the area of the side (or sides) affected by the radiation. When knowing the differential solar radiation force, $d\mathbf{F}_{tot}$, it is possible to determine the solar radiation torque, as shown in equation 6.24

$$\tau_{solar} = \int \mathbf{r} \times d\mathbf{F}_{tot} \quad (6.24)$$

where

- τ_{solar} is the solar radiation torque (vector) [Nm]
- \mathbf{r} is the vector from the CoM of the satellite to the elemental area dA [m]

All of the above equations can be used to calculate the torque for each side of the satellite, and these torques can then finally be summed up to determine the full torque caused by solar radiation.

The maximum force has been calculated, from equation 6.24, to a maximum of $1.023 \cdot 10^{-9}$ for one side, where $\hat{\mathbf{s}}$ is parallel to $\hat{\mathbf{n}}$. The maximum force is then determined using equation 6.24.

$$= \underbrace{P}_{4.52 \cdot 10^{-6}} \cdot \underbrace{[(1 - C_s) \hat{\mathbf{s}} + 2(C_s \cos(\theta_{sn}) + \underbrace{\frac{1}{3}C_d}_{\text{Max. } \frac{1}{3}}) \hat{\mathbf{n}}]}_{\text{Max. 1}} \underbrace{\cos(\theta_{sn})}_{\text{Max. 1}} \cdot \underbrace{A}_{113 \cdot 10^{-6}} \quad (6.25)$$

It is then seen that the largest force exerted is when $C_s = 1 \wedge C_d = 0$ and $\theta_{sn} = 0$ and therefore also the largest torque. The value of the largest force is equal to the length of the largest force vector achieved by equation 6.25, and is determined to be $1.0230 \cdot 10^{-9}$. To find the maximum torque of the satellite, the total force is to be crossed with the vector \mathbf{r} , as seen in equation 6.24

$$\tau_{solar} = \int \mathbf{r} \times d\mathbf{F}_{tot} = \begin{bmatrix} 0.05 \\ 0 \\ -0.02 \end{bmatrix} \times \begin{bmatrix} 1.230 \cdot 10^{-9} \\ 0 \\ 0 \end{bmatrix} = \begin{bmatrix} 0 \\ 0 \\ -2.046 \cdot 10^{-11} \end{bmatrix} \quad (6.26)$$

So the total maximum torque around the three axes is $2.046 \cdot 10^{-11}$ Nm.

Aerodynamic Torque Estimation

Sources: [Wertz 78] [Wiśniewski 99], [NASA 71].

The aerodynamic torque affecting the satellite is the sum of all forces around the centre of mass, from atmospheric particle collision, on the satellite surface. An estimation of the total aerodynamic torque which acts upon the satellite can be made using the expression:

$$\tau_{aero} = rF \quad [\text{Nm}] \quad (6.27)$$

where

τ_{aero}	is the total aerodynamic torque	[N·m]
r	is the moment arm length	[m]
F	is the total aerodynamic force	[N]

For this conservative worst case estimation of aerodynamic torque the CoM is assumed to be at the centre of one side of the satellite, hence the moment arm length will then be half the satellite length, i.e. 5 cm. An approximation of the force which acts upon the satellite is used to give an estimate of the aerodynamic disturbance torque magnitude. The total force upon the satellite surface in the direction of travel can be found as:

$$F_{aero} = \frac{1}{2} C_D \rho v^2 A \quad [\text{N}] \quad (6.28)$$

where

C_D	is the drag coefficient for the satellite	[·]
ρ	is the atmospheric particle density	[kg/m ³]
v	is the satellite velocity	[m/s]
A	is the projected area of the satellite normal to the incident flow	[m ²]

As there have been no measurements of drag characteristic for the satellite, a maximum drag coefficient of four is assumed for when the incident flow is perpendicular to the satellite frame, and a minimum drag coefficient of two is assumed for when the incident flow angle, θ , is farthest

from perpendicular. These drag coefficient values are based on the typical ballistic coefficients for low-earth orbit satellites table from [Wertz 99, p. 207].

The atmospheric particle density is read from figure 1.1(b), at an orbit altitude 300 km to 10^{-13} g/cm^3 for high solar activity and $0.6 \cdot 10^{-15} \text{ g/cm}^3$ for low solar activity. These are the maximum and minimum values for the atmospheric density, not taking daily particle density variations into account.

The projected cross sectional area of the satellite is at least 0.01 m^2 (incident flow perpendicular to the satellite frame) and at most 0.026 m^2 (incident flow angle, θ , farthest from perpendicular). The satellite velocity for an circular low earth orbit is $\sim 7.8 \text{ km/s}$.

The maximum aerodynamic force is calculated at the worst conditions possible (highest particle density), for incident particle flow perpendicular and farthest from perpendicular to the satellite. It should be noted that the worst drag coefficient is for lowest cross sectional area of the satellite normal to the incident stream of particles.

$$F_{\text{aero}, \theta \perp} = \frac{1}{2} \cdot 4 \cdot 10^{-13} \frac{\text{kg}}{\text{m}^3} \cdot (7800 \frac{\text{m}}{\text{s}})^2 \cdot 0.01 \text{ m}^2 = 121.68 \cdot 10^{-6} \text{ N} \quad (6.29)$$

$$F_{\text{aero}, \theta \min} = \frac{1}{2} \cdot 2 \cdot 10^{-13} \frac{\text{kg}}{\text{m}^3} \cdot (7800 \frac{\text{m}}{\text{s}})^2 \cdot 0.026 \text{ m}^2 = 158.18 \cdot 10^{-6} \text{ N} \quad (6.30)$$

The estimated worst case aerodynamic torque is calculated from the force found in equation 6.30, which is the worst case estimate for the aerodynamic force:

$$\tau_{\text{aero}} = 0.05 \text{ m} \cdot 158.18 \cdot 10^{-6} \text{ N} = 6.08 \cdot 10^{-6} \text{ Nm} \quad (6.31)$$

This aerodynamic torque estimation shows that the resulting torque due to aerodynamics is considerably larger than the second largest torque, caused by solar radiation, found in Equation 6.26 to $2.046 \cdot 10^{-11} \text{ N}\cdot\text{m}$, which is approximately a factor 300000 smaller than the aerodynamic. This proves that the aerodynamic torque can be considered the only significant disturbance torque to include in the model of the satellite dynamics. This disturbance torque will be derived in the following.

Aerodynamic Disturbance Torque Model Equation

Assuming the particle velocity energy is completely absorbed by the satellite upon impact, a more accurate calculation of the aerodynamic force, $d\mathbf{F}_{\text{aero}}$, on a given surface, dA , can be made. For a pointing purpose it is assumed that the angular spin rate, ω , of the satellite is close to zero, and thus not included in this disturbance model.

$$d\mathbf{F}_{\text{aero}} = -\frac{1}{2} C_D \rho v^2 (\hat{\mathbf{n}} \cdot \hat{\mathbf{v}}) \hat{\mathbf{v}} dA \quad [\text{N}] \quad (6.32)$$

where

- $\hat{\mathbf{n}}$ is the normal vector outwards from the surface of the satellite [·]
- $\hat{\mathbf{v}}$ is the unit vector in the direction of translational velocity, v [·]

With a vector, \mathbf{r} , from the centre of mass of the satellite, to an infinitesimal area on the surface the which is acted upon by the differential aerodynamic force, $d\mathbf{F}_{\text{aero}}$, the total torque acting upon the surface can be found by an integral over the surface.

$$\tau_{\text{aero}, k} = \int \mathbf{r}_k \times d\mathbf{F}_{\text{aero}, k} \quad [\text{N}\cdot\text{m}] \quad (6.33)$$

The total aerodynamic torque upon the satellite is then the sum of individual torques from each of the satellite surfaces.

$$\tau_{\text{aero}} = \sum_{k=1}^n \tau_{\text{aero}, k} \quad [\text{N}\cdot\text{m}] \quad (6.34)$$

As the satellite consists of several rectangular plane surfaces a simplified model can be made from equation 6.32 and 6.34. The total aerodynamic torque is then.

$$\boldsymbol{\tau}_{\text{aero}} = \frac{1}{2} C_D \rho v^2 \sum_{k=1}^n A_k (\hat{\mathbf{n}}_k \cdot \hat{\mathbf{v}}) \hat{\mathbf{v}} \times \mathbf{r}_i \quad [\text{N}\cdot\text{m}] \quad (6.35)$$

As A_i is attributed to the surfaces of the satellite, and since the satellite is a cuboid, equation 6.35 can be rewritten as the sum of three surfaces: A_1 to A_3 , with A_i being the individual surface areas.

$$\boldsymbol{\tau}_{\text{aero}} = \frac{1}{2} C_D \rho v^2 (A_1([1\ 0\ 0]^T \cdot \hat{\mathbf{v}}) \hat{\mathbf{v}} \times \mathbf{r}_1 + A_2([0\ 1\ 0]^T \cdot \hat{\mathbf{v}}) \hat{\mathbf{v}} \times \mathbf{r}_2 + A_3([0\ 0\ 1]^T \cdot \hat{\mathbf{v}}) \hat{\mathbf{v}} \times \mathbf{r}_3) \quad (6.36)$$

In Equation 6.36 A_1 is the surface perpendicular to the x-axis in the SBRF, A_2 is the surface perpendicular to the y-axis in the SBRF, A_3 is the surface perpendicular to the z-axis in the SBRF.

The maximum aerodynamic torque possible around one axis is calculated from equation 6.36 to $0.259 \cdot 10^{-6}$ Nm. As this is the most dominant disturbance torque, the magnetorquer actuation torque has to be able to produce a torque higher than this.

6.1.3 Complete Dynamic Model

The satellite has been modelled together with external torques such as control torque and disturbance torque, and these are assembled to a joint model of the total satellite torque. This joint model will form the basis of the control theory going to be used to control the attitude of the satellite:

$$\begin{aligned} \boldsymbol{\tau}_{\text{tot}} &= \boldsymbol{\tau}_{\text{sat}} + \boldsymbol{\tau}_c + \boldsymbol{\tau}_d \\ \bar{\mathbf{J}}\dot{\boldsymbol{\omega}} &= -\boldsymbol{\omega} \times \bar{\mathbf{J}}\boldsymbol{\omega} + NIA \times \mathbf{B}_E + \boldsymbol{\tau}_d \end{aligned} \quad (6.37)$$

The disturbance torque will not be included in the control torque calculations, but the magnitude of the disturbance torques must be considered when deciding the magnitude of the control torque.

6.2 Attitude Propagation – Kinematic Model of the Satellite

Sources: [Bak 02] [Wiśniewski 99] [Wertz 78]

Prediction or propagation of spacecraft attitude based on present angular velocity and (measured) attitude can be described by kinematic equations. Kinematics concerns the time dependent relative orientation and angular velocity of the rigid body with respect to a reference frame.

When the orientation of a spacecraft, with respect to a reference frame, is changing over time, it can be represented by the quaternion $\mathbf{q}(t)$. The rotation of the body over a small time interval Δt is then $\mathbf{q}(\Delta t)$, and the attitude obtained after Δt is $\mathbf{q}(t + \Delta t)$:

$$\mathbf{q}(t + \Delta t) = \mathbf{q}(t) \otimes \mathbf{q}(\Delta t) \quad (6.38)$$

The rotation can be rewritten to matrix form using the relation between the eigenaxis, $\hat{\mathbf{e}}$, rotation angle, θ , and quaternions from Equation 4.6 and 4.7:

$$\mathbf{q}(\Delta t) = \cos\left(\frac{\theta}{2}\right) \bar{\mathbf{I}}_{4 \times 4} + \sin\left(\frac{\theta}{2}\right) [\hat{\mathbf{e}}]_{\otimes R}, \quad [\hat{\mathbf{e}}]_{\otimes R} = \begin{bmatrix} 0 & e_z & -e_y & e_x \\ -e_z & 0 & e_x & e_y \\ e_y & -e_x & 0 & e_z \\ -e_x & -e_y & -e_z & 0 \end{bmatrix} \quad (6.39)$$

Here $\bar{\mathbf{I}}$ is the identity matrix and the skew symmetric matrix $[\hat{\mathbf{e}}]_{\otimes R}$ multiplied with a quaternion \mathbf{q} represents a quaternion multiplication: $[\hat{\mathbf{e}}]_{\otimes R} \mathbf{q} = \mathbf{q} \otimes \hat{\mathbf{e}}$. As $\theta = \omega \Delta t$ has to be a small angle

(with $\Delta t \rightarrow 0$ in Equation 6.41) the approximations $\cos(\frac{\theta}{2}) \approx 1$ and $\sin(\frac{\theta}{2}) \approx \frac{1}{2}\theta = \frac{1}{2}\omega\Delta t$ are made, and introducing the skew symmetric matrix $[\boldsymbol{\omega}]_{\otimes R} = [\hat{\mathbf{e}}]_{\otimes R} \boldsymbol{\omega}$, containing the components of the spacecraft angular velocity, $\boldsymbol{\omega} = [\omega_1 \ \omega_2 \ \omega_3 \ 0]^T$, Equation 6.39 can be reduced to:

$$\mathbf{q}(\Delta t) \approx \bar{\mathbf{I}}_{4 \times 4} + \frac{1}{2}[\boldsymbol{\omega}]_{\otimes R} \Delta t, \quad [\boldsymbol{\omega}]_{\otimes R} = \begin{bmatrix} 0 & \omega_z & -\omega_y & \omega_x \\ -\omega_z & 0 & \omega_x & \omega_y \\ \omega_y & -\omega_x & 0 & \omega_z \\ -\omega_x & -\omega_y & -\omega_z & 0 \end{bmatrix} \quad (6.40)$$

Now the kinematic differential equation of the spacecraft can be written as:

$$\begin{aligned} \dot{\mathbf{q}}(t) &= \lim_{\Delta t \rightarrow 0} \frac{\mathbf{q}(t + \Delta t) - \mathbf{q}(t)}{\Delta t} = \lim_{\Delta t \rightarrow 0} \frac{\mathbf{q}(\Delta t) \otimes \mathbf{q}(t) - \mathbf{q}(t)}{\Delta t} \\ &\approx \lim_{\Delta t \rightarrow 0} \frac{(\bar{\mathbf{I}}_{4 \times 4} + \frac{1}{2}[\boldsymbol{\omega}]_{\otimes R} \Delta t) - \bar{\mathbf{I}}_{4 \times 4}}{\Delta t} \mathbf{q}(t) = \frac{1}{2}[\boldsymbol{\omega}]_{\otimes R} \mathbf{q}(t) \end{aligned} \quad (6.41)$$

The time interval Δt should be small enough for $[\boldsymbol{\omega}]_{\otimes R}$ to be constant over the interval. When this is the case, the solution to Equation 6.41 can be obtained as:

$$\begin{aligned} \dot{\mathbf{q}}(t) = \frac{1}{2}[\boldsymbol{\omega}]_{\otimes R} \mathbf{q}(t) &\stackrel{\mathcal{L}}{\Rightarrow} s\mathcal{Q}(s) - \mathcal{Q}(0) = \frac{1}{2}[\boldsymbol{\omega}]_{\otimes R} \mathcal{Q}(s) \\ \mathcal{Q}(s) = \frac{\mathcal{Q}(0)}{s - \frac{1}{2}[\boldsymbol{\omega}]_{\otimes R}} &\stackrel{\mathcal{L}^{-1}}{\Rightarrow} \mathbf{q}(t) = e^{\frac{1}{2}[\boldsymbol{\omega}]_{\otimes R} t} \mathbf{q}(0) \end{aligned} \quad (6.42)$$

It can be verified that Equation 6.42 is in fact the same as Equation 6.38, by rewriting the exponent term to the form of $\mathbf{q}(\Delta t)$ in Equation 6.39:

$$e^{\frac{1}{2}[\boldsymbol{\omega}]_{\otimes R} t} = \cos\left(\frac{\omega t}{2}\right) \bar{\mathbf{I}}_{4 \times 4} + \sin\left(\frac{\omega t}{2}\right) [\boldsymbol{\omega}]_{\otimes R} \boldsymbol{\omega}^{-1} \quad (6.43)$$

Remembering that $[\boldsymbol{\omega}]_{\otimes R} \boldsymbol{\omega}^{-1} = [\hat{\mathbf{e}}]_{\otimes R}$, it is indeed verified that the propagated attitude quaternion is equal to the quaternion product of $\mathbf{q}(\Delta t)$ and the current attitude quaternion.

6.3 Attitude Control System

In this section, the design of the controller for the ADCS is determined. The attitude control system has to align the SBRF with a target frame, to acquire the desired pointing direction for the satellite. The target frame is specified for a direction in which the satellite has to point either its payload sensors or antenna, and the SBRF is found using the Attitude Determination System (ADS), which states the current direction of the satellite body. The target frame may be either the TRF for ground station pointing, or the ORF for nadir (or travel direction) pointing. Throughout the remainder of this report, the ORF is used as the target frame, thus obtaining travel-direction pointing.

An overview of the complete attitude control system is shown in figure 6.2. The control system is made as a PD-controller with quaternions as reference and feedback.

The controller uses an attitude quaternion and a target quaternion as feedback and reference, respectively, and from these an error quaternion is created. The control law block uses this error quaternion to determine a torque necessary for rotating the satellite to reduce the error.

A projection of the control torque vector onto the plane perpendicular to the geomagnetic field is used to generate only the torque components perpendicular to the geomagnetic field, thus maximizing the efficiency of the current used in the magnetorquer coils.

The control current block converts the projected torque vector to the current needed for each of the magnetorquers to obtain the projected torque. It uses a measurement of the geomagnetic field

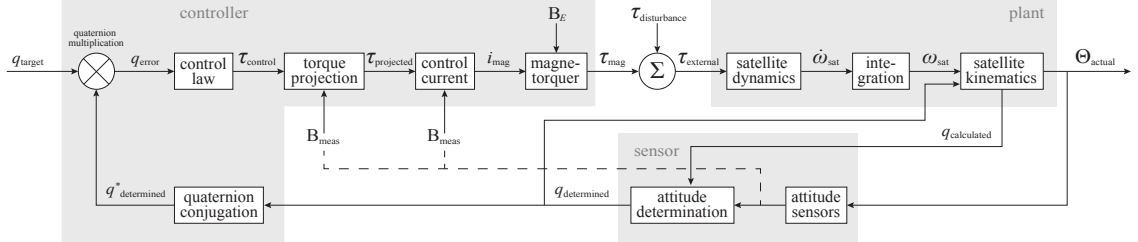


Figure 6.2: Block diagram of the Attitude Determination and Control System, the plant being the satellite.

strength to determine the magnetic moment required by each magnetorquer, and calculates the related current.

Each magnetorquer is controlled through a PWM signal and an H-bridge. A voltage corresponding to the determined current is applied to create the desired magnetic moment, which interacts with the geomagnetic field to create a torque. This torque, along with the satellite dynamics and kinematics will rotate the satellite in the desired direction.

A mathematical model of the satellite kinematics is made to propagate the satellite attitude for the torque applied, using the dynamic model developed in section 6.1.

Attitude sensors measure the geomagnetic field, sun position and angular velocity, and from these measurements the satellite attitude is determined. If the sensors are unable to obtain attitude information, the propagated attitude may be used for the attitude control system instead.

6.3.1 Attitude Controller

The attitude controller has to apply a torque to the satellite to rotate the satellite in the desired direction. As there is low rotational velocity damping for the satellite in space, the controller has to reduce the angular velocity once the satellite has obtained or is near the correct attitude.

From Equation 6.9 the control torque can be defined as the inertia matrix multiplied with the angular acceleration of the satellite. With the inertia matrix diagonalised in Equation 6.5, using principal axes in CRF, the control torque components are simplified into three linear relations between inertia and angular acceleration about each of the principal axes.

A proportional derivative control design has been chosen as the controller, which will increase the torque if the angular error grows, and at the same time decrease the torque if the angular velocity grows. The dynamic equation for the PD-controller, with θ being the angle or attitude of the satellite, θ_{ref} the desired attitude, and K_p and K_d the proportional and derivative gains, is given as:

$$J\ddot{\theta} = K_p(\underbrace{\theta_{ref} - \theta}_{\theta_{error}}) - K_d\dot{\theta} \quad (6.44)$$

By Laplace transforming equation 6.44, a transfer function for the PD-controller is made:

$$\frac{\theta}{\theta_{ref}} = \frac{K_p}{Js^2 + K_d s + K_p} \quad (6.45)$$

Here, the sensors and attitude determination are assumed to be much faster than the dynamics of the satellite, setting feedback gain to unity. A diagram for the PD-controller in one axis is shown in figure 6.3, where θ is the angle of the satellite in this axis, and $\dot{\theta}$ is the angular velocity about the same axis.

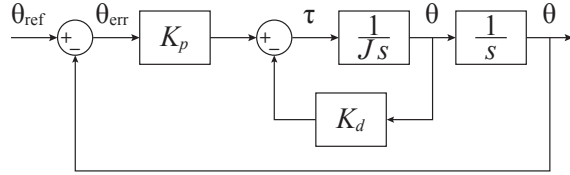


Figure 6.3: Block diagram for a one axis PD-controller for a position plus rate attitude control.

Control Law

The input to the attitude control block is the error quaternion, \mathbf{q}_e , which is the rotation needed to align the determined attitude quaternion, \mathbf{q}_d from the SBRF, with the target attitude quaternion, \mathbf{q}_t in the ORF:

$$\mathbf{q}_t = \mathbf{q}_d \otimes \mathbf{q}_e \quad \Leftrightarrow \quad \mathbf{q}_d^* \otimes \mathbf{q}_t = \mathbf{q}_d^* \otimes \mathbf{q}_d \otimes \mathbf{q}_e = \mathbf{q}_e \quad (6.46)$$

This rotation indicated by the error quaternion is obtained by inducing a control torque to rotate the spacecraft to the target orientation, and doing so by the shortest intermediate angular change, i.e. rotating about the eigenaxis of the two attitudes. The components in the error quaternion describes the rotation around the eigenvector $\hat{\mathbf{e}}$, given in SBRF coordinates.

$$\mathbf{q}_e = \begin{bmatrix} e_1 \sin \frac{\theta}{2} \\ e_2 \sin \frac{\theta}{2} \\ e_3 \sin \frac{\theta}{2} \\ \cos \frac{\theta}{2} \end{bmatrix} \quad (6.47)$$

The three imaginary components of the error quaternion are proportional to the angular error in the three axes. As two quaternions \mathbf{q} and $-\mathbf{q}$ represent the same rotation, the sign of the real part of the quaternion is multiplied with the quaternion term of the control law in Equation 6.44, in order to always represent identical rotations in the same way (see section 4.1). Now, according to Equation 6.44, the desired control torque to be exerted by each of the magnetorquers (given in the SBRF frame) is given by:

$$\begin{aligned} {}^s\tau_{cx} &= K_{px} q_{e1} \text{sign}(q_{e4}) - K_{dx} \omega_x \\ {}^s\tau_{cy} &= K_{py} q_{e2} \text{sign}(q_{e4}) - K_{dy} \omega_y \\ {}^s\tau_{cz} &= K_{pz} q_{e3} \text{sign}(q_{e4}) - K_{dz} \omega_z \end{aligned} \quad (6.48)$$

The angular velocity of the spacecraft (relative to the inertial frame) can be calculated according to the kinematic equation stated in Equation 6.41 as:

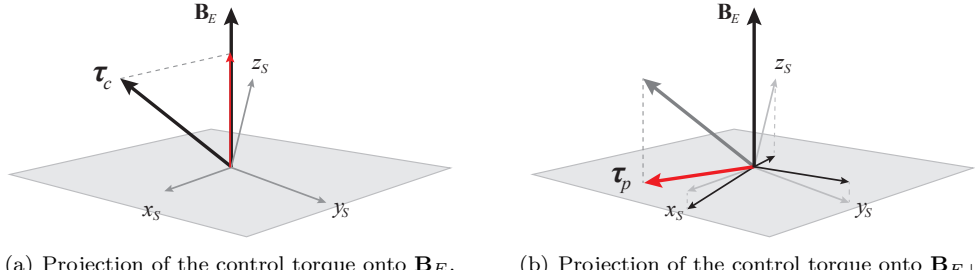
$$\dot{\mathbf{q}}_d = \frac{1}{2} [\boldsymbol{\omega}]_{\otimes R} \mathbf{q}_d = \frac{1}{2} \bar{\mathbf{Q}}_d \boldsymbol{\omega} \quad \Leftrightarrow \quad \boldsymbol{\omega} = 2 \text{inv}(\bar{\mathbf{Q}}_d) \dot{\mathbf{q}}_d, \quad \bar{\mathbf{Q}}_d = \begin{bmatrix} q_{d4} & -q_{d3} & q_{d2} \\ q_{d3} & q_{d4} & -q_{d1} \\ -q_{d2} & q_{d1} & q_{d4} \\ -q_{d1} & -q_{d2} & -q_{d3} \end{bmatrix} \quad (6.49)$$

A direct inverse of $\bar{\mathbf{Q}}_d$ obviously cannot be found, so instead a pseudoinverse can be used. Using the AAUSAT3 ADCS hardware, a gyroscope is available, and the angular velocity may be measured directly.

The torque found in equation 6.48 is the torque which the magnetorquers has to produce to reduce the error quaternion and to align the SBRF with the target frame. This control torque is obtained by an interaction between the geomagnetic field and the magnetic moment induced by the current running through the magnetorquer coils.

Torque Projection

An induced magnetic moment parallel to the geomagnetic field will not produce a torque, and magnetic moments close to the geomagnetic field will only produce a small torque. Thus using the control torque vector, magnetic moments parallel to the geomagnetic field will be induced from the magnetorquers and power will be wasted in the coils without producing a torque. By projecting the control torque vector onto a plane perpendicular to the geomagnetic field, creating a new projected control vector which is perpendicular to the geomagnetic field vector, then the induced magnetic moment will produce the maximum amount of torque.



(a) Projection of the control torque onto \mathbf{B}_E . (b) Projection of the control torque onto $\mathbf{B}_{E\perp}$.

Figure 6.4: The grey surface indicate the plane perpendicular to the geomagnetic field vector, \mathbf{B}_E . In figure 6.4(a) the desired control vector τ_c , is projected onto the magnetic field vector. In figure 6.4(b) the control torque vector, τ_p , has been projected onto the plane perpendicular to \mathbf{B}_E .

The projection of the control torque vector, τ_c , onto the plane perpendicular to the magnetic field vector is illustrated in Figure 6.4, and is calculated as:

$$\tau_p = \tau_c - \underbrace{\frac{\tau_c \cdot \mathbf{B}_E}{\|\mathbf{B}_E\|} \mathbf{B}_E}_{\text{part of } \tau_c \parallel \mathbf{B}_E} \quad (6.50)$$

The projected torque vector will not be able to produce the exact torque required to obtain the desired attitude, but due to the physical constraints of the magnetorquers, it will result in the same magnetorquer moment to use the projected vector and the control law derived control torque vector.

Control Current

The current needed for the magnetorquers to induce the desired magnetic moment can be found from the three elements in the projected torque vector by the relation defined in subsection 6.1.1 as:

$$\tau_p = NIA \times \mathbf{B}_E = \mathbf{M} \times \mathbf{B}_E \quad \Leftrightarrow \quad \|\tau_p\| \hat{\tau}_p = \|\mathbf{M}\| \|\mathbf{B}_E\| \hat{\mathbf{M}} \times \hat{\mathbf{B}}_E \quad (6.51)$$

where

\mathbf{M} is the magnetic moment defined as $\mathbf{M} = NIA$ $[A \cdot m^2]$
 $\hat{\tau}_p, \hat{\mathbf{M}}, \hat{\mathbf{B}}_E$ are the normalised (unit) vectors of τ_p, \mathbf{M} and \mathbf{B}_E , respectively [.]

The cross product of perpendicular unit vectors can be written in terms of either of the unit vectors as:

$$\hat{\tau}_p = \hat{\mathbf{M}} \times \hat{\mathbf{B}}_E \quad \Leftrightarrow \quad \hat{\mathbf{M}} = \hat{\mathbf{B}}_E \times \hat{\tau}_p \quad \Leftrightarrow \quad \hat{\mathbf{B}}_E = \hat{\tau}_p \times \hat{\mathbf{M}} \quad (6.52)$$

Rearranging the terms in Equation 6.51 to isolate first the magnetic moment, \mathbf{M} , leads to obtain the current, \mathbf{I} :

$$\begin{aligned} \|\boldsymbol{\tau}_p\| \hat{\mathbf{B}}_E \times \hat{\boldsymbol{\tau}}_p &= \|\mathbf{M}\| \|\mathbf{B}_E\| \hat{\mathbf{M}} \\ \frac{\|\boldsymbol{\tau}_p\|}{\|\mathbf{B}_E\|} \hat{\mathbf{B}}_E \times \hat{\boldsymbol{\tau}}_p &= \|\mathbf{M}\| \hat{\mathbf{M}} = NA \|\mathbf{I}\| \hat{\mathbf{I}} \\ \frac{\|\boldsymbol{\tau}_p\|}{\|\mathbf{B}_E\|} \frac{1}{NA} \hat{\mathbf{B}}_E \times \hat{\boldsymbol{\tau}}_p &= \|\mathbf{I}\| \hat{\mathbf{I}} = \mathbf{I} \end{aligned} \quad (6.53)$$

The components of the current vector found through Equation 6.53, are the x, y and z-magnetorquer currents required to produce the torque corresponding to the projected torque vector, $\boldsymbol{\tau}_p$.

6.3.2 Controller Parameters

The requirements for the controller, stated in section 2.1, is to be able to maintain a nadir pointing or pointing in the direction of travel. In section 1.6, the actuation speed for this types of pointing is calculated to 0.0012 rad/s. According to item 2.1.5 of the requirement specification, a pointing accuracy of $10^\circ = 0.17$ rad must be obtained.

The actuation velocity can be considered as a ramp input, hence for a type 1 system a steady state error will occur. To stay within the required pointing accuracy when disturbance torques are present, a controller which does not include disturbance torques in the computation of control torque is desired to have disturbance suppression by a factor of 10, giving a pointing accuracy of $1^\circ = 0.017$ rad.

With an actuation speed of 0.0012rad/s the maximum allowable steady state error, e_{ss} , is found as:

$$e_{ss} = \frac{0.0012}{0.017} = 14.16 \quad (6.54)$$

The relation between the proportional and derivative gains for a type 1 system is given in terms of the ramp error, $1/K_v$, found from the direct term of Figure 6.3 as:

$$K_v = \lim_{s \rightarrow 0} \left(s \frac{K_p}{J s^2 + K_d s} \right) = \frac{K_p}{K_d} \quad (6.55)$$

With the maximum allowable steady state error determined to 14.16 from equation 6.54, the gain values can be found as:

$$e_{ss} = \frac{1}{K_v} = \frac{1}{\frac{K_p}{K_d}} = \frac{K_d}{K_p} \leq 14.16 \quad (6.56)$$

Confer Equation 6.45 the proportional and derivative gains may be given in terms of the closed loop natural frequency, ω_n , and the damping factor, ζ , as:

$$\frac{K_p}{J} = \omega_n^2, \quad \frac{K_d}{J} = 2\zeta\omega_n \quad \Leftrightarrow \quad \frac{K_p}{K_d} = \frac{\omega_n}{2\zeta} \quad (6.57)$$

It is desired to have a maximum overshoot, M_p , of 5 %, setting the damping factor value to $\zeta = 0.7$. Combining Equation 6.55 and 6.57, solving the former for the equality, the natural frequency can be found to $\omega_n = 98.87 \cdot 10^{-3}$ rad/s.

With the inertia given in equation 6.5, the proportional and derivative gains are found to be:

$$\mathbf{K}_p = \begin{bmatrix} 14.8 \\ 919.9 \\ 920.6 \end{bmatrix} \cdot 10^{-6} \quad \mathbf{K}_d = \begin{bmatrix} 0.21 \\ 13.03 \\ 13.04 \end{bmatrix} \cdot 10^{-3} \quad (6.58)$$

The controller gain values for K_p and K_d are determined for all the satellite axes, and the controller can be implemented and tested together with the satellite dynamics.

6.3.3 Evaluation of the Controller

An evaluation of the controller parameters is needed to test if the chosen gain values, \mathbf{K}_p and \mathbf{K}_d , meets the requirements for the controller, as stated in section 2.1.

The controller is subjected to a ramp input, see figure 6.5, to test if the steady state error is within the specified values. Seeing that there is a steady state error on the ramp response a plot of the

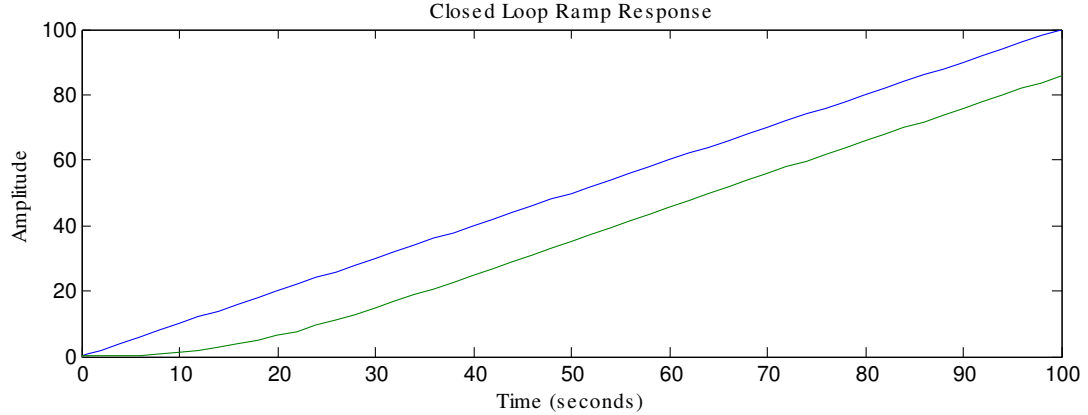


Figure 6.5: Closed loop reponse for the controller.

steady state error is made to further analyse the magnitude of the steady state error in figure 6.6.

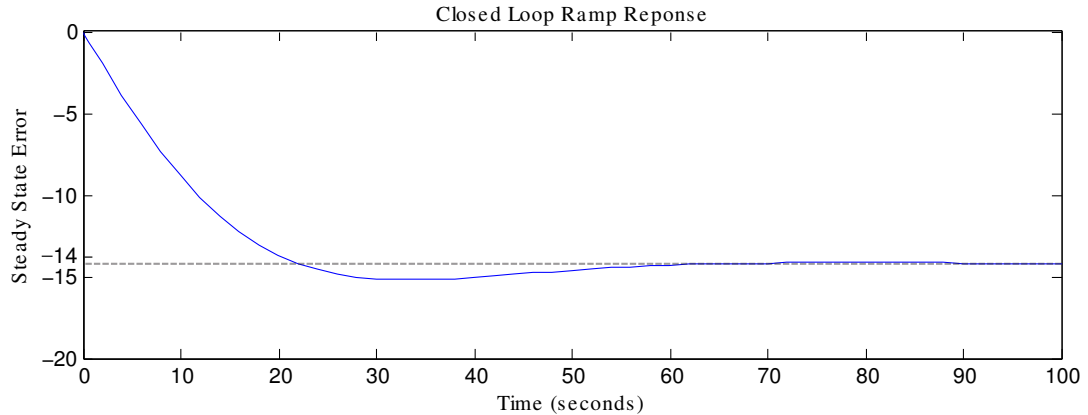


Figure 6.6: A plot of the steady state error for the controller with a ramp input, shows a steady state error of 14.19.

The steady state error is just above the margin of 14.16. Even though it is higher than the margin it is of an acceptable magnitude. The criteria for a steady state error less than 14.16 is a factor 10 higher than the maximum error allowed for the system.

It is seen from Equation 6.58 that the derivative term, consisting of the angular velocity, is weighing more in the torque determination than the proportional term consisting of the attitude quaternion. This means that the system is dampening the control torque heavily in order to suppress overshoot, ensuing a long settling time of approximately 66 s and a rise time of 18.2 s. Seeing that the duration of an orbit is approximately 5400 s, this is regarded a reasonable settling and rise time.

The step response made in figure 6.7 shows the overshoot, rise- and settling time with values similar to those previously calculated.

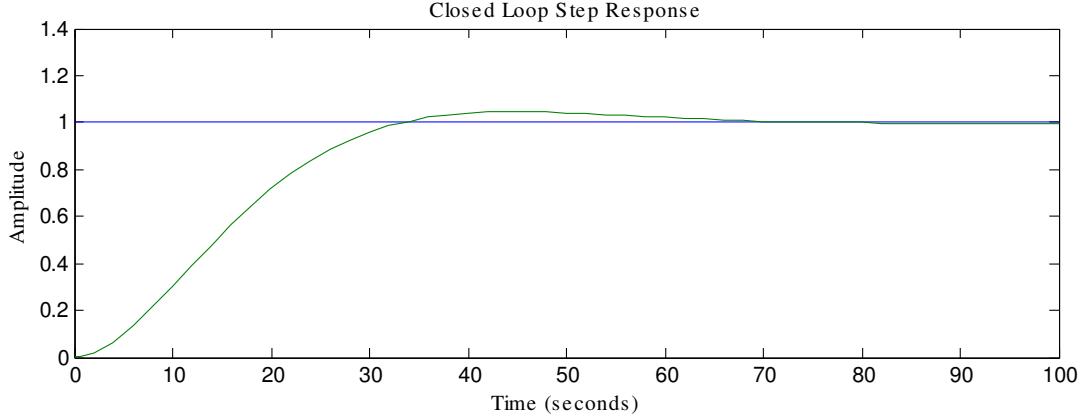


Figure 6.7: Closed loop step response shows an overshoot of less than 5%, a rise time of approximately 18 s and settling time of approximately 66 s.

By applying a ramp input to the controller with a slope of 0.0012, similar to the actuation speed of the satellite, the steady state error is found in radians, shown in figure 6.8.

A steady state error of approximately 0.017 rad is visible in the plot, which shows that the

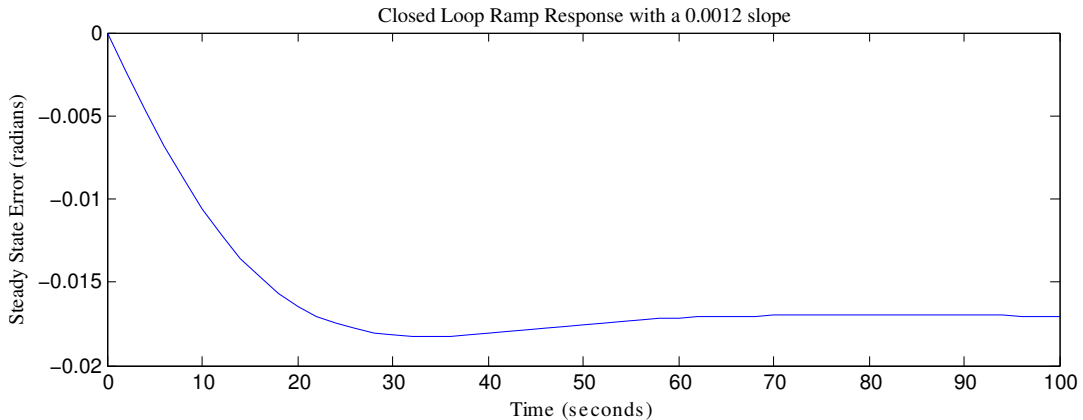


Figure 6.8: A plot of the steady state error magnitude with a 0.0012 slope applied to the controller, shows that the steady state error is approximately 0.017 rad.

controller is within 1° from the specified pointing direction.

The proportional and derivative controller gains found in equation 6.58 shows good behavior for the linear control system, as they are within or very near the specified margins, and the slow rise time and settling time is not an issue as these are of a reasonable length, compared to the orbit duration.

Controller Error

With the controller designed to obtain a maximum steady state error of 0.0017 rad, a calculation of the complete closed loop error is needed to confirm the disturbance suppression rate of 10 is sufficient to meet to requirement of less than a 10° pointing error.

The closed loop error E_{cl} is given as:

$$E_{cl} = R - \left(\frac{GD}{1+GD} R + \frac{G}{1+GD} W - \frac{D}{1+GD} V \right) \quad (6.59)$$

where

G is the plant transfer function

D is the controller transfer function

R is the reference input

W is the disturbances

V is the sensor noise

Assuming the sensor noise to be zero and using the designed PD-controller the controller error is found from equation 6.59 to be:

$$E_{cl} = R - \left(\frac{K_p}{Js^2 + K_d s + K_p} R + \frac{1}{Js^2 + K_d s + K_p} W \right) \quad (6.60)$$

In section 6.1.2 the maximum aerodynamic disturbance torque is found in equation 6.36 to be $0.258 \cdot 10^{-6}$ Nm. Including this disturbance in the model a closed loop ramp response is made for the system, shown in figure. The ramp response in figure 6.9 shows that even with the aerodynamic

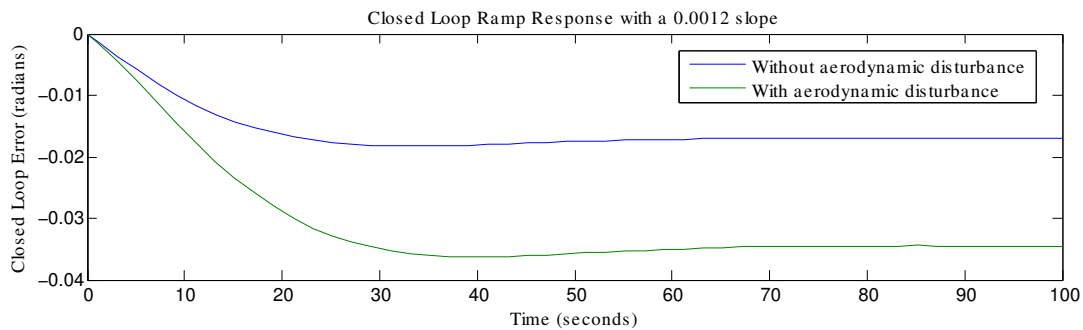


Figure 6.9: A plot of the closed loop error with a 0.0012 slope applied to the controller, shows that the closed loop error with aerodynamic torque disturbance is 0.0345 rad, compared to the steady state error of 0.0017, which is without aerodynamic disturbance.

disturbance torque, the controller is well within the specified requirements. As the closed loop error with maximum aerodynamic torque is of 0.0345 rad, and the requirement for the controller is to be within 0.17 rad from the desired pointing direction. This shows that the controller has a high margin of error for sensor noise and other environmental disturbance torques.

Compensating For The Inertial Torques

The total torque of the satellite, given in equation 6.37, is the collective torques of the inertial torques, control torques and the disturbance torques. Controlling the satellite requires keeping the total torque of the satellite as close to or equal to the control torque as possible. Thus the controller has to compensate for the inertial torque created by the cross-product of the angular velocities and satellite inertia.

$$\tau_{\text{sat}} = -\omega \times \bar{\mathbf{J}}\omega \quad (6.61)$$

When applying a torque to one of the satellite axes, it also creates an angular velocity around the other satellite axes as a result of the cross-product shown in equation 6.61. A compensation for the cross-product has to be introduced to the control law equation to counteract this unwanted rotation. The cross-product gives rotation around the satellite axes in the SBRF as shown:

$$\begin{bmatrix} {}^s\tau_{\text{sat},x} \\ {}^s\tau_{\text{sat},y} \\ {}^s\tau_{\text{sat},z} \end{bmatrix} = \begin{bmatrix} \omega_z(J_{yx}\omega_x + J_{yy}\omega_y + J_{yz}\omega_z) - \omega_y(J_{zx}\omega_x + J_{zy}\omega_y + J_{zz}\omega_z) \\ -\omega_z(J_{xx}\omega_x + J_{xy}\omega_y + J_{xz}\omega_z) + \omega_x(J_{zx}\omega_x + J_{zy}\omega_y + J_{zz}\omega_z) \\ \omega_y(J_{xx}\omega_x + J_{xy}\omega_y + J_{yz}\omega_z) - \omega_x(J_{yx}\omega_x + J_{yy}\omega_y + J_{yz}\omega_z) \end{bmatrix} \quad (6.62)$$

Calculating the cross-product for the CRF, the expression for the rotation in equation 6.62 is reduced because all the off-diagonal elements in the inertia matrix, $\bar{\mathbf{J}}$, are zero in the CRF, and

the cross-product is then given as:

$$\begin{bmatrix} {}^c\boldsymbol{\tau}_{\text{sat},x} \\ {}^c\boldsymbol{\tau}_{\text{sat},y} \\ {}^c\boldsymbol{\tau}_{\text{sat},z} \end{bmatrix} = -\boldsymbol{\omega} \times \bar{\mathbf{J}}\boldsymbol{\omega} = \begin{bmatrix} (J_{yy} - J_{zz})\omega_z\omega_y \\ (J_{zz} - J_{xx})\omega_z\omega_x \\ (J_{xx} - J_{yy})\omega_y\omega_x \end{bmatrix} \quad (6.63)$$

Inserting the CRF cross-product from equation 6.63 into the control law equation 6.48, gives a new controller which corrects the applied control torque to compensate for the inertial torques.

$${}^s\boldsymbol{\tau}_{c,\text{comp}} = \mathbf{K}_p \begin{bmatrix} q_{e1} \\ q_{e2} \\ q_{e3} \end{bmatrix} \text{sign}(q_{e4}) - \mathbf{K}_d \begin{bmatrix} \omega_x \\ \omega_y \\ \omega_z \end{bmatrix} - {}^s_c\bar{\mathbf{R}} \begin{bmatrix} ({}^cJ_{yy} - {}^cJ_{zz})\omega_z\omega_y \\ ({}^cJ_{zz} - {}^cJ_{xx})\omega_z\omega_x \\ ({}^cJ_{xx} - {}^cJ_{yy})\omega_y\omega_x \end{bmatrix} \quad (6.64)$$

Using the new compensated control torque from equation 6.64 in the satellite dynamic equation 6.37, gives a total satellite torque as:

$$\bar{\mathbf{J}}\dot{\boldsymbol{\omega}} = \boldsymbol{\tau}_{\text{sat}} + \underbrace{\boldsymbol{\tau}_c - \boldsymbol{\tau}_{\text{sat}}}_{\boldsymbol{\tau}_{c,\text{comp}}} + \boldsymbol{\tau}_d \quad (6.65)$$

The compensated control torque, $\boldsymbol{\tau}_{c,\text{comp}}$, is the control torque produced by the pointing control system. This gives only the disturbance torque as an unknown torque, which has to be suppressed by the controller.

Evaluation of the compensated controller is done through the Simulink simulation in section 7 together with the attitude determination and ephemeris model, no evaluation is done separately on the compensated controller.

Chapter 7

Simulation of the ADS and ACS

This section will describe the setup and configuration of the simulation environment using Simulink. The simulation environment comprises several primary system blocks. These blocks include: spacecraft dynamics, sensor measurements, attitude determination, and attitude control, as depicted in Figure 7.1. Several smaller system blocks are used as well, though their function is primarily concerned with quaternion rotations, and space environmental parameters e.g. position of the sun, and disturbance torques.

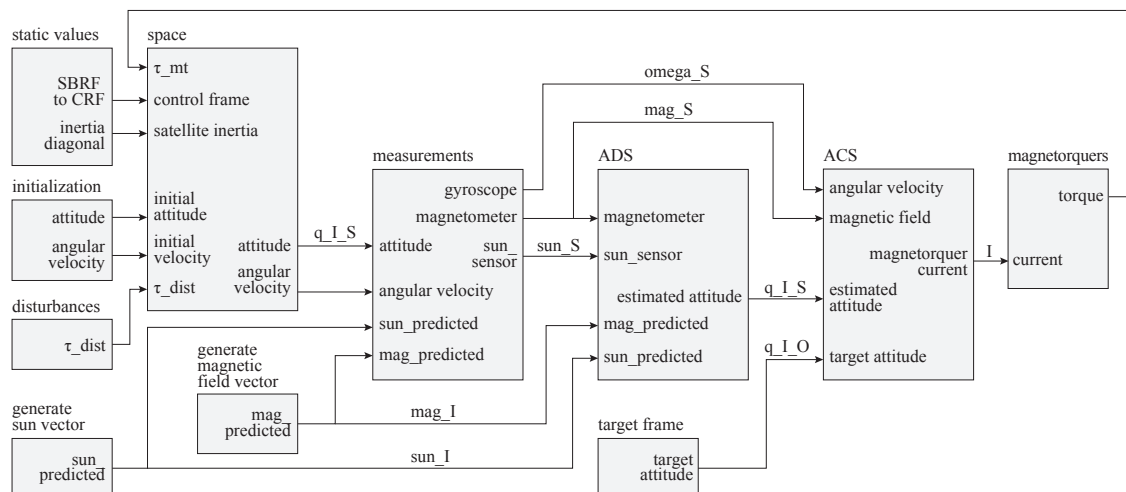


Figure 7.1: The block diagram above shows the simulation blocks together with the signal paths. The diagram shows the path from the spacecraft dynamics to the actuation on the magnetorquer from the controller.

7.1 Simulation of the Orbital Environment

The orbital environment comprises several sub-elements. These include sun position, magnetic field, and several disturbance torques, as described in subsection 6.1.2. The simulation interpretation of these elements are briefly described in the following.

7.1.1 Sun Position

The satellite sun vector is simulated using a predicted sun vector in the ECI reference frame. The predicted sun vector is found using the ephemeris model, as mentioned in subsection 5.1.3. This model uses the inputs Julian Date and a vector from the ECI reference frame to the spacecraft. The predicted sun vector is fed to a measurement block simulating the sun sensors in the SBRF. This outputs a sun vector represented as measured from the satellite.

7.1.2 Magnetic Field

The magnetic field is simulated using a magnetic field model, called IGRF as described in subsection 5.1.2. This magnetic field is found as an array of vectors depicting the magnetic field around the Earth at different altitudes. The IGRF model simply requires a position given in the ECI frame and a magnetic vector is returned at the given position, also represented in the ECI frame. This magnetic field vector is interpreted by the measurement block simulating the magnetometers, and returned as a measured magnetic vector in the SBRF.

7.1.3 Disturbance Torques

The disturbances modeled in section 6.1.2 are implemented as Matlab scripts, and imported into Simulink. In the case of aerodynamic torque disturbance, the simulation block needs both an SBRF attitude and a velocity vector as inputs. This in turn outputs a disturbance vector for use in the spacecraft dynamics block as seen in Figure 7.1.

7.2 Simulation of the spacecraft dynamics

The spacecraft dynamics primarily comprises the model equations described in section 6.1. The simulation block consists of six inputs and two outputs. The six inputs are initial velocity, initial attitude, controller frame, satellite inertia, torque from magnetorquers, and disturbance torques. Inside the spacecraft dynamics block lies the model of the satellite which is implemented as a C-source code file, *scdynamics.c*. The inputs to the C-file are torque from the magnetorquers, disturbance torques and the satellite inertia. The torques are combined with the initial velocity to determine the angular velocity of the satellite. The inertia is set as an input port which makes it possible to change the inertia without changing the source code. The output from the scdynamics block is an angular velocity used to determine the actual angular velocity and the actual attitude. The inputs are to be rotated from the CRF to the SBRF, which is done by using the inverse of the control rotation matrix in Equation 5.21. The initial attitude is a quaternion describing a given orientation in ECI. The initial angular velocity can be set to a given initiating velocity.

7.3 Simulation of the ADS

The attitude determination block is simulated as a Matlabscript containing the SVD function. There are four inputs to the block and one output (see figure 7.1). The inputs are called *sun_S*, *sun_I*, *mag_S*, and *mag_I* and the output is a quaternion denoted *q_I_S*. The inputs *sun_S* and *mag_S* is the sensor data retrieved from the magnetometer and the sun sensor given in the SBRF. The inputs *sun_I* and *mag_I* are the predicted vectors determined by the *mag_predicted* and *sun_predicted* block given in the ECI frame. The SVD is applied to the matrix generated by taking the sum of the outer product between each pair of vectors as seen equation 7.1).

$$\bar{\mathbf{A}} = \text{sun_S} \cdot \text{sun_I}^T + \text{mag_S} \cdot \text{mag_I}^T \quad (7.1)$$

By using the SVD method (as described in 5.2) the optimal rotation matrix is determined and a quaternion is generated using said matrix.

7.3.1 Verification of the ADS

The ADS is tested and verified by running simulations without any control algorithms connected. Furthermore the simulation conditions are kept within a controlled set of parameters. This is done in the first verification simulation of the ADS by having a static sun vector aligned with ECI x-axis, while creating a magnetic vector rotating in the plane perpendicular to the sun vector. This scenario is a simplified version of a satellite in a sun synchronous orbit. All initial rotational speed of the satellite is set to zero, along with all disturbance torques.

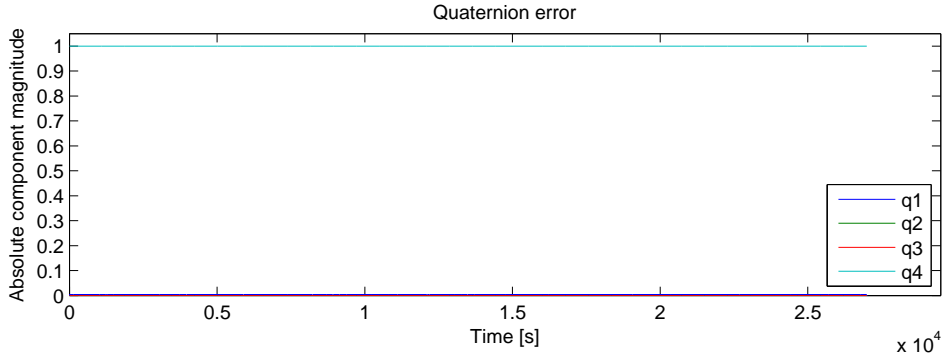


Figure 7.2: Simulation of the ADS with a static sun vector and a magnetic vector rotating in the plane perpendicular to the sun vector.

The simulation using this scenario resulted in the output displayed in Figure 7.2. The graph displayed is the error quaternion which describes the relative error between the actual and estimated attitudes. This error quaternion is obtained by taking the inverse of the actual attitude quaternion and making a quaternion multiplication with the estimated attitude quaternion. If the error is zero the error quaternion will obtain the values (0,0,0,1) which is the representation of zero rotation between the two attitude quaternions. As can be seen in Figure 7.2 the ADS performs almost flawlessly under these test conditions.

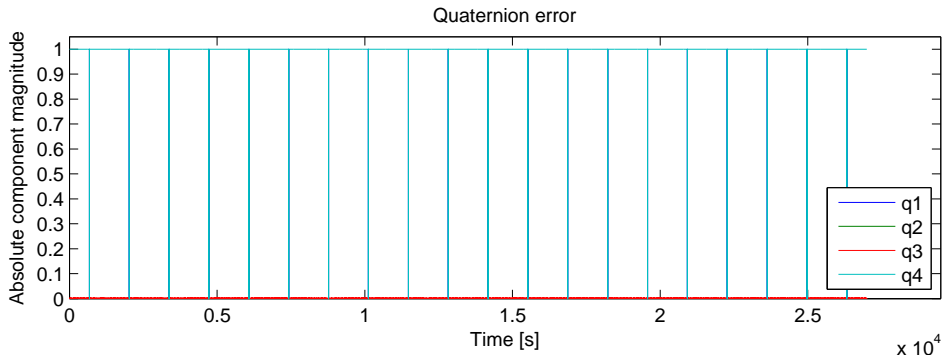


Figure 7.3: Simulation of the ADS with a static sun vector and a magnetic vector rotating in the same plane as the sun vector. The x-axis is time given in seconds and the y-axis are magnitudes of the quaternion components.

Another simulation is made with the intent to determine the severity of error when the SVD method fails estimation. This is tested by having the magnetic vector rotating in the same plane as the sun vector is oriented. This will inadvertently result in faulty estimation when the sun- and magnetic vectors align (become parallel). This simulation will give a general idea of the threshold where the ADS will begin to fail.

The results of this simulation can be seen in Figure 7.3. As seen from the error quaternion the ADS has proven to be very robust and the region of faulty estimation is very narrow. Within the

simulation environment the time region of faulty estimation is determined to be two simulation steps, and therefore almost momentary.

With these two initial simulation tests, it is concluded that the ADS is working as intended and is able to determine any attitude as long as the sun- and magnetic vectors do not align.

7.4 Simulation of the Controller

The controller is implemented as a Matlab script interpreting the control laws given in Equation 6.48. This results in a Simulink block with five inputs and one output. The five inputs consists of: q_{altitude} , q_{target} , k_{th} , k_{om} , and ω_C while the output is simply τ_c which acts as the control torque parameter. Both q_{altitude} and q_{target} are used to determine the error quaternion within the control block. The values k_{th} and k_{om} are the adjustable gain factors for the controller, while ω_C is the input variable for gyroscope measurements.

A seperate Matlab function is constructed in order to interpret magnetorquers and the projection it implies (as described in section 6.3.1). This block has two inputs (τ_c and B_E) and two outputs (τ_{act} and I). The two input elements are the control torque vector and the magnetic field vector, which are used to calculate the desired current vector, I (which is also an output). The two output elements consist of a current vector, I , which is only used for data collection, and a resulting torque vector for the simulated physical feedback of the system.

While a complete and complex model of the orbit environement is available for use, the following simulations are primarily made with controlled input vectors. This is primarily done in order to easily identify errors and optimise the control algorithms accordingly.

This in turn means that the sun vector is static in the ECI frame, while the magnetic vector is either also static or rotating in a plane with a frequency according to the change the magnetic vector would have in orbit.

Two different target quaternions will be used in the simulations as well: a static quaternion with the values $(0,0,0,1)$, and a varying quaternion describing a rotating vector basis evolving around its z-axis at the same rate of an orbital period (emulating the rotation of nadir pointing or ORF). Finally all simulations will be executed over a total duration of 20 orbits.

The first simulations made with the controller is done with both a static sun vector and a perpendicular static magnetic vector. The sun vector is aligned with the ECI x-axis and the magnetic vector is aligned with the ECI y-axis. The initial position of the satellite is defined with the quaternion $(\frac{1}{\sqrt{2}}, 0, 0, \frac{1}{\sqrt{2}})$ and the target quaternion defined as $(0,0,0,1)$. This means that the satellite is oriented with a 90° offset with respect to the ECI frame and the target is to get the satellite to align with the ECI frame.

With this set-up the initial simulation results showed that the controller was unstable. By tuning the parameters, a stable result was obtained as seen in Figure 7.4. The parameters used in order to obtain these results are given in Equation 7.2.

$$\mathbf{K}_p = \begin{bmatrix} 14.8 \\ 919.9 \\ 920.6 \end{bmatrix} \cdot 10^{-10} \quad \mathbf{K}_d = \begin{bmatrix} 0.21 \\ 13.03 \\ 13.04 \end{bmatrix} \cdot 10^{-5} \quad (7.2)$$

As seen the parameters has been dampened with factors of 10000 and 100 respectively, when compared to the determined values given in Equation 6.58. It is expected that this error is a combination of two factors. One is the fact that the quaternion error is proportional to the angular error, but the proportionality factor is unknown. The second factor is the lack of a dimension of actuation seeing how the magnetic field restricts the desired three dimensional torque to a maximum of two dimensions. This can result in overshoots seeing how it is possible to actuate in some directions, but not possible to counteract when reaching the desired orientation, which in turn means that a large overshoot will be observed.

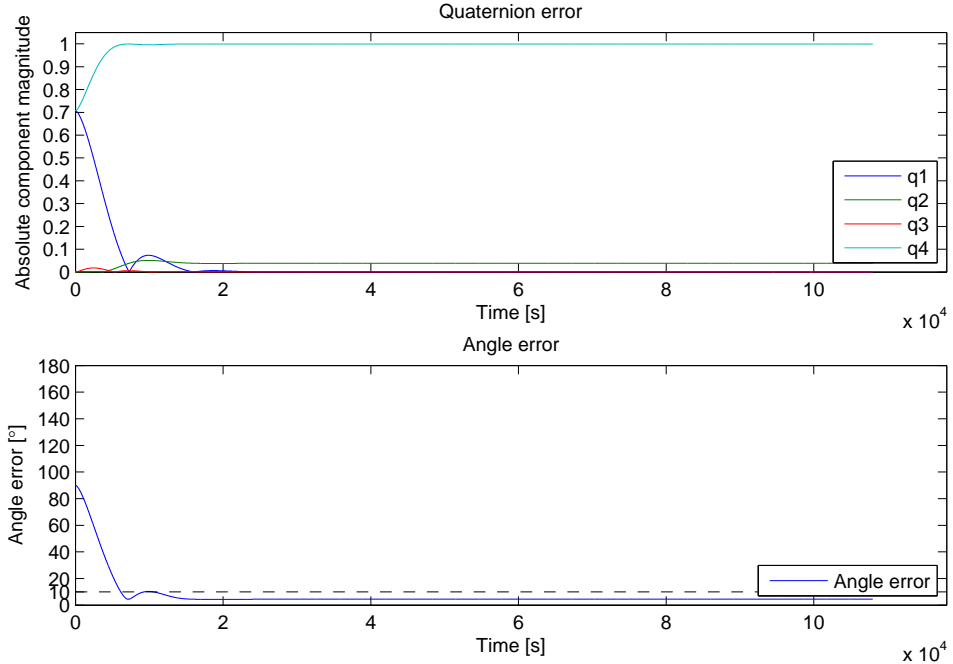


Figure 7.4: Simulation of the ACS with a static sun vector and a perpendicular static magnetic vector. Initial quaternion attitude is equal to $(\frac{1}{\sqrt{2}}, 0, 0, \frac{1}{\sqrt{2}})$ and target quaternion is equal to $(0, 0, 0, 1)$.

The results from the simulation with the tuned parameters from Equation 7.2 can be seen in Figure 7.4 where both the quaternion error and angular error are displayed. As seen on the angular error, the controller is able to keep within the limit of $\pm 10^\circ$. From the error quaternion it can be seen that the controller is not able to reduce the rotation around the y-axis all the way, which is an expected effect of the magnetic field being oriented in the same direction as the y-axis.

The second set of simulations was made with a static sun vector aligned with the ECI x-axis, along with a magnetic field rotating perpendicular to the sun vector. Since this simulation was expected to be more problematic due to the constraints of the magnetic field, the magnetorquer block was bypassed. This was done in order to verify that the controller would work regardless of the limitations of magnetic actuation. The results of this simulation can be seen in Figure 7.5 where both the quaternion error and angular error is displayed. Since the controller is working properly with a rotating magnetic field it is expected that any errors encountered during the following simulations is due to the limitations of magnetic actuation, and not the controller itself.

After it was verified that the controller worked without the magnetorquer block, a simulation was made including said simulation block. The results of this simulation can be seen in Figure 7.6. As seen the results hardly vary from the previous simulation, and the angular error is still within the required limit of $\pm 10^\circ$.

The final simulations were made using a rotating target reference frame. This frame is simply a vector basis rotating around its z-axis at the same rate as the ORF. This vector basis is converted to a quaternion with respect to the ECI frame. The results of this simulation can be seen in Figure 7.7, where it is easily observed that the controller is unstable. Following these results several simulations were made and it was determined that when using magnetic actuation with linear controllers, the frequency, or rate, of the target frame has to be significantly lower than the change in the magnetic field used to actuate.

A test using this set-up, with a significantly slower target rate, is shown in Figure 7.8, where it is

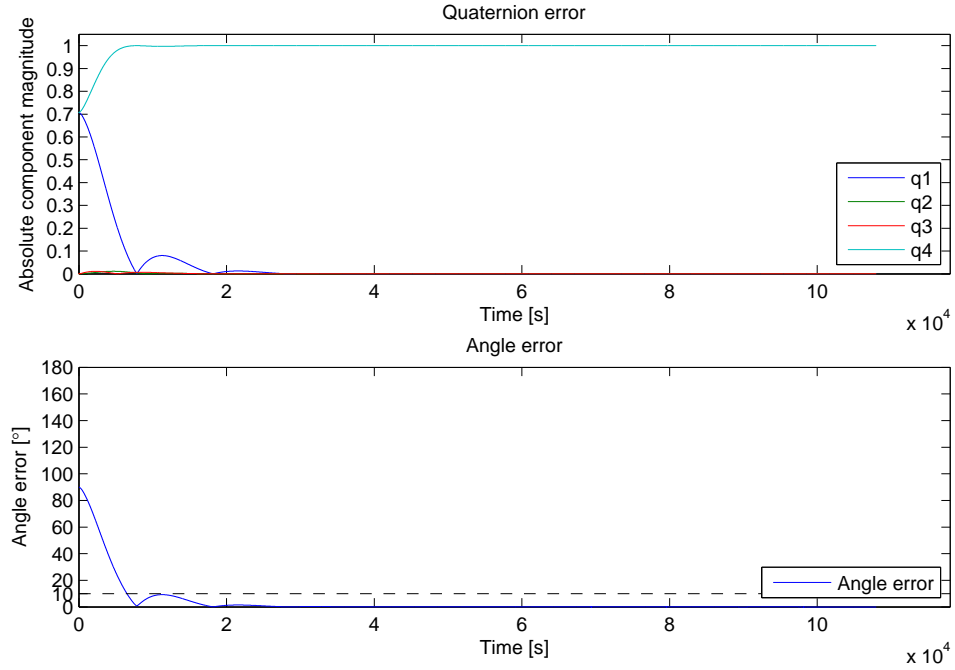


Figure 7.5: Simulation of the ACS with a static sun vector and a perpendicular rotating magnetic vector. Initial quaternion attitude is equal to $(\frac{1}{\sqrt{2}}, 0, 0, \frac{1}{\sqrt{2}})$ and target quaternion is equal to $(0, 0, 0, 1)$. The magnetorquer simulation block is bypassed, and the control torque is fed directly back in the system.

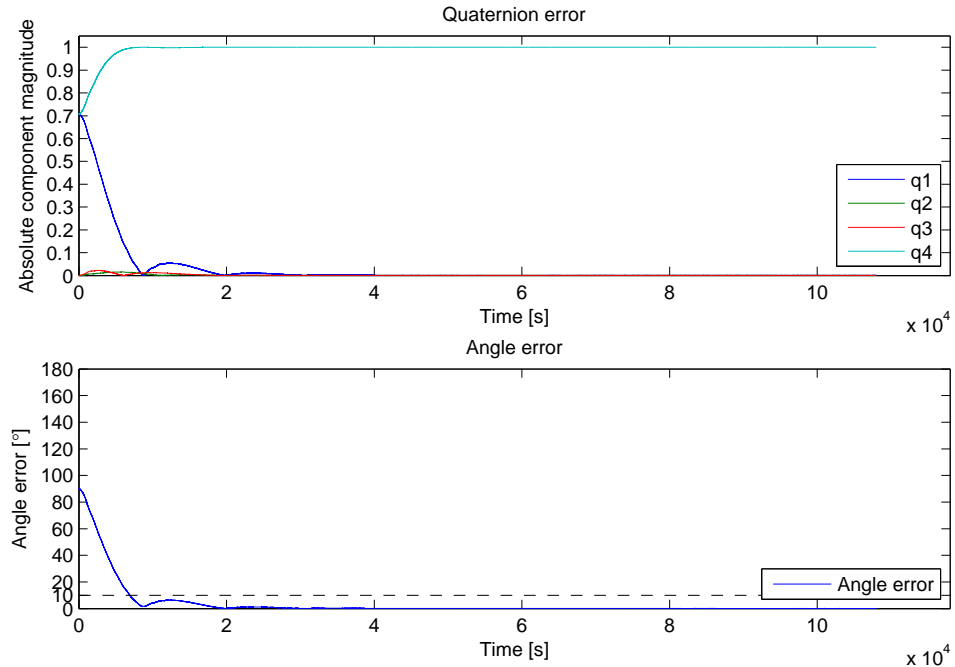


Figure 7.6: Simulation of the ACS with a static sun vector and a perpendicular rotating magnetic vector. Initial quaternion attitude is equal to $(\frac{1}{\sqrt{2}}, 0, 0, \frac{1}{\sqrt{2}})$ and target quaternion is equal to $(0, 0, 0, 1)$.

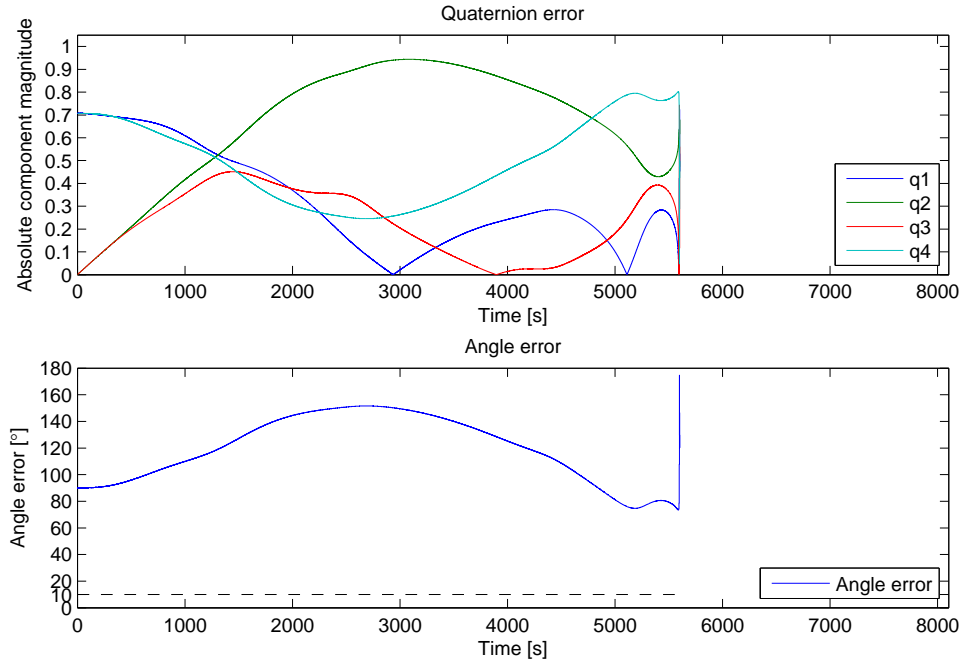


Figure 7.7: Simulation of the ACS with a static sun vector and a perpendicular static magnetic vector. Initial quaternion attitude is equal to $(\frac{1}{\sqrt{2}}, 0, 0, \frac{1}{\sqrt{2}})$ and a target frame rotating at the same frequency as the ORF.

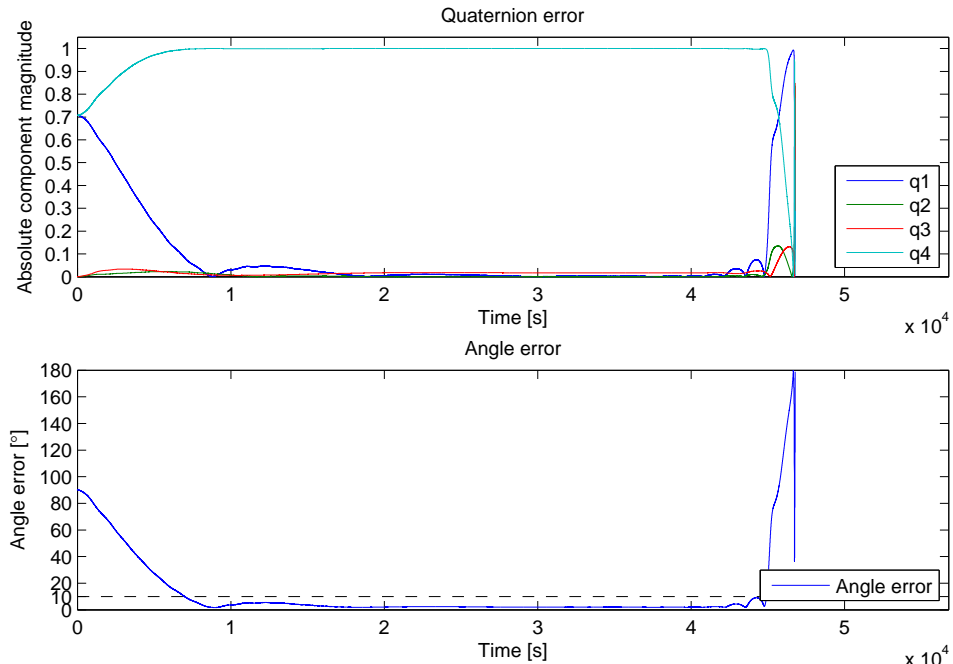


Figure 7.8: Simulation of the ACS with a static sun vector and a perpendicular static magnetic vector. Initial quaternion attitude is equal to $(\frac{1}{\sqrt{2}}, 0, 0, \frac{1}{\sqrt{2}})$ and a target frame rotating at a frequency significantly slower than the ORF.

possible to see that the controller is becoming unstable during the final set of orbits. This in turn resulted in further finetuning of the controller parameters in order to obtain a stable controller under the test conditions. These parameters are given in Equation 7.3.

$$\mathbf{K}_p = \begin{bmatrix} 14.8 \\ 919.9 \\ 920.6 \end{bmatrix} \cdot 10^{-10} \quad \mathbf{K}_d = \begin{bmatrix} 0.21 \\ 13.03 \\ 13.04 \end{bmatrix} \cdot 7 \cdot 10^{-6} \quad (7.3)$$

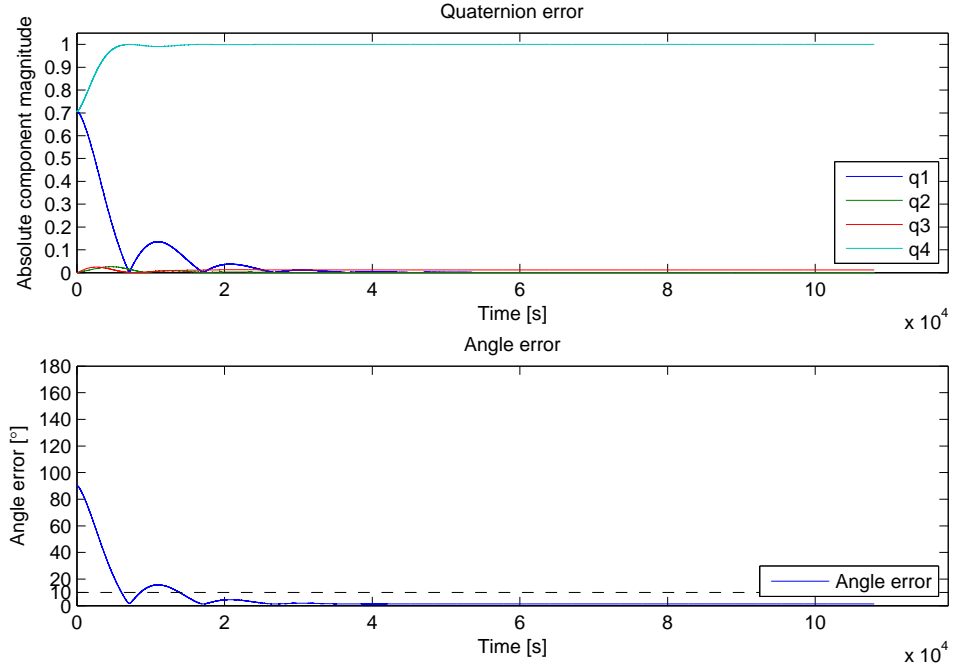


Figure 7.9: Simulation of the finetuned ACS with a static sun vector and a perpendicular static magnetic vector. Initial quaternion attitude is equal to $(\frac{1}{\sqrt{2}}, 0, 0, \frac{1}{\sqrt{2}})$ and a target frame rotating at a frequency significantly slower than the ORF.

A final simulation was made using the updated parameters and the results can be seen in Figure 7.9. Though the initial overshoot passes the upper limit, the controller overall is still within the bounds of $\pm 10^\circ$ as required.

While the final iteration of the controller is within the requirements set forth in requirement 2.2.2 it is still not able to function under the condition where the target frame is rotating at a rate equal to that of the ORF (and even less so with respect to the TRF). When using linear controllers in combination with magnetic actuation in three dimensions, the magnetic field has to rotate at a significantly faster rate than the target vector basis.

Chapter 8

Integration of the ADCS

This chapter describes the integration of the two main subsystems developed and those obtained from pre-existing repositories. The first part of the integration describes the way the attitude determination system is intended to be integrated for the full system along with the attitude control system. The second part describes the integration of the system elements for the acceptance test.

The general flow for the ADCS is described in figure 8.1. As it can be seen the system is intended to retrieve the data from the sensors. Afterwards the sensor data is used for the attitude determination along with calculated vectors for the sun and magnetic field in the ECI frame. Then the target frame is calculated, be it the ORF or the TRF. The present attitude of the satellite given in the ECI frame and the wanted attitude in the ECI frame is then used to determine an error quaternion, which is used to calculate the needed control torque. By using the measurements of the magnetic field vector given in the SBRF, the best current vector, needed for actuation, can be determined. After determining the required current, it is also possible to determine the PWM duty cycles needed to produce the determined currents. After the PWM duty cycles has been determined, the PWM signal is used to control the magnetorquers until the magnetometer routine interrupts the PWM signal to perform measurements. This entire sequence is then repeated for the system to be able to control its attitude.

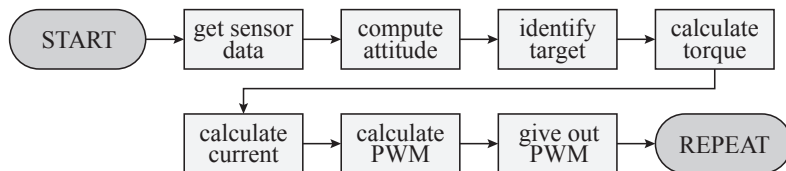


Figure 8.1: General flowchart for the ADCS.

A satellite mockup is available for mounting the constructed ADCS PCB and sun sensor (see Appendix F). As described in Appendix F the sun sensor and ADCS PCB are mounted within the satellite mockup, to use for the acceptance test. The desired final integration is for the mockup to have six sun sensors mounted to be able to get more accurate measurements from the sun sensors and to be able to rotate the satellite in all direction and still be able to determine the attitude of the satellite. Furthermore, in order for the satellite mockup being able to actuate, magnetorquers are to be mounted for the final integration. However, as the ADCS2 (which is to be used for pointing the satellite) is not currently able to produce a PWM signal, the magnetorquers are not mounted on the mockup to use for the acceptance test.

The software integration for the acceptance test is much different from the one desired in the final

integration. For the acceptance test, only the system for attitude determination is implemented in software, as is also the case for the hardware. Furthermore, implementations of time dependent functions, like the model for determining the rotation between ECI and ECEF and sun vector in ECI, are not performed. The SGP4 and IGRF models for determining position of the satellite and the magnetic field surrounding the satellite are not implemented either. Instead, static sun- and magnetic field vectors are generated in ECI for the acceptance test. Software for determining rotation between other frames than ECI and SBRF has not been implemented in the test software either.

During integration of the software, some minor problems were encountered with including the functions that have been developed during this project. One of the problems encountered is that, when trying to implement the math function `sqrt()` it was not possible to run the software even though it was possible to compile. To fix this problem the `sqrt()` function was replaced by the `pow()` function, and raising the number to the power of $\frac{1}{2}$ instead.

Another problem encountered during the integration of the software is the fact that it does not seem possible to include the developed code by using header files. This means that all of the required functions for the attitude estimation have to be manually included in the file containing the code for USB JTAG communication with the satellite. The problem is suspected to be caused by not adding the header files in all necessary files.

With the system assembled and integrated, an acceptance test can now be conducted in order to verify that the system requirements are met.

Chapter 9

Acceptance Test

The acceptance test is conducted to verify the functionality of the developed software with the existing hardware. Mainly, this acceptance test will focus on the test of the ADS, due to the ADCS2 (ARM processor) on the AAUSAT3 ADCS PCB not being able to give a PWM output to the magnetorquers, which is why the requirement 2.2.2 cannot be tested.

From the system requirements, seen in chapter 2 requirement 2.2.1, it is known that the CubeSat has to have a pointing knowledge of $\pm 2^\circ$ from its initial launch altitude at 350 km down to at least 200 km. This means that it is needed to be able to determine the attitude of the satellite with a precision of $\pm 2^\circ$. This is also the only requirement available for the ADS.

The test of the ADS is performed in the laboratory. A sketch of the test set-up is seen in figure 9.1. The satellite is placed in the center of a set of Helmholtz coils, creating a magnetic field in one direction, and with a spotlight pointing at the satellite from another direction. The direction of the magnetic field is chosen to be the x-axis of the TECI (the test ECI created in the laboratory) and the spotlight points in the negative y-direction of this TECI. The z-axis of the TECI is chosen to always be aligned with the z-axis of the satellite. As only one sun sensor is available for the test, it is chosen that the y-axis of the satellite is the direction normal to the side where the sun sensor is attached.

The execution of the test is done by first placing the satellite with the spotlight pointing perpendicular to the plane in which the sun sensor is placed. Instead of uploading the ephemeris software for predicting the sun vector in ECI, and the IGRF software for determining the magnetic field vector, the predicted unit length sun vector in TECI is set to be (0,-1,0) and the predicted unit length magnetic field vector is set to (1,0,0). Furthermore, the magnetic field vector obtained by the magnetometer is manipulated to not having any magnetic field strength in the direction of the z-axis. This is done due to the fact that Earth's magnetic field vector has a strength that is almost as high as the one that is produced by the Helmholtz coils. When manipulating this part of the vector to being zero, it means that there will be only a "measured" magnetic field in the x- and y-axis.

As mentioned, the spotlight is kept still during the test, and the measurements are made while rotating the satellite from -75° to 75° with 15° steps. The data from the test is shown in the test protocol in appendix G. From the columns showing the measured angles on the sun sensor, it is seen that this angle deviates with about 33% from the actual angle every time. At the same time the sun sensors have been given the highest weighing coefficient (see section 5.2.2), due to measurements showing less noise on the sun sensors compared to the magnetometer. However, it seems that the magnetometer gives much more precise measurements, which also means that the magnetometer should have been weighted higher than the sun sensor. But as the test was done during daytime, a lot of reflecting light could potentially be affecting the sun sensor measurements.

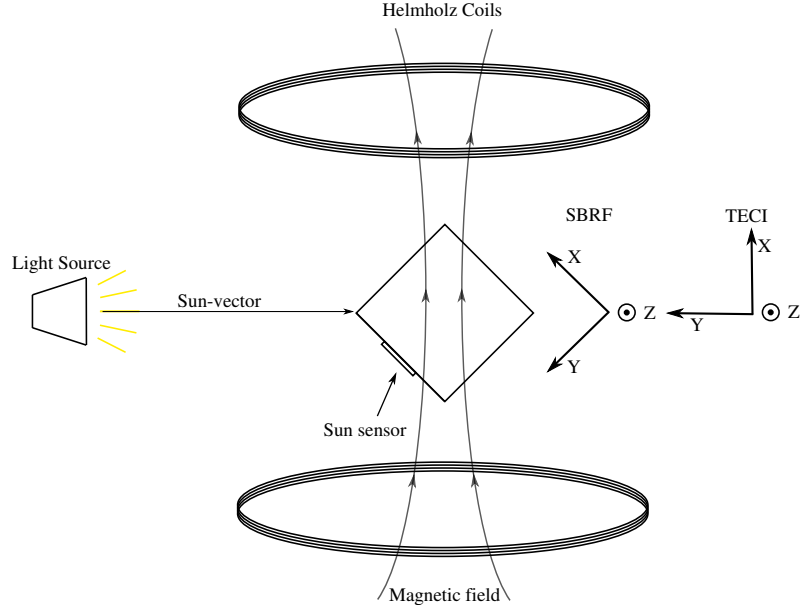


Figure 9.1: The figure shows the test set-up for the acceptance test. In the figure the satellite has been rotated 45° counterclockwise.

The data shown in the test protocol indicates that the smallest angle error is 2.73° and the biggest is 26.9° , which both are errors that are higher than the allowed $\pm 2^\circ$. This means that for the conducted test, the system is not able to comply with the requirement. This may be improved by testing in an environment with no disturbing light. This is also why the attitude determination test has been re-evaluated in Matlab, only using the magnetometer measurements. This test is a special case where rotation about the magnetic field vector is not possible. When determining the attitude only using the magnetometer data, the biggest angle error is 1.9° and the smallest error measured is 0.0021° . However, it is important to mention that it will not be possible to determine the attitude unambiguously by only using the magnetic field vector in all cases.

Additionally, according to the request posed in requirement 2.1.9 it is desired to test if the sun sensors are saturating, as it is suspected to be a problem on AAUSAT3. The tests indicate that this is indeed the case because of the 33% deviation and because of the sun sensor having reached its limit, showing an incident angle of 93° when the actual angle is 60° and -91° when the angle is -60° .

Chapter 10

Closure

10.1 Conclusion

The primary concern of this conclusion is to review the three main requirements described in chapter 2.

Requirement 2.2.1 is verified under the idealised conditions both via the simulation environment and through the acceptance test. In the simulations the ADS performed outstandingly and proved very robust to near parallelity of the vector inputs. The simulation was performed using near LEO conditions. Confer the acceptance test the ADS was not able to estimate the attitude within the bounds of $\pm 2^\circ$. The primary source of error was determined to originate from the sun sensor. It is expected that this error may be caused by saturation of the photo diodes within the sun sensor.

Requirement 2.2.2 is solely tested through the simulation environment. While it was possible to control the satellite, and point it at a moving target reference under controlled conditions, it was not possible to obtain the actuation speed needed to perform nadir pointing. This is primarily suspected to be an effect of the target change rate being close to equal to the magnetic field change rate, thereby impairing the effectiveness of the controller. The acceptance test of this requirement was unperformable due to the lack of a PWM driver for the actuators.

Requirement 2.2.3 is verified confer the acceptance test of the ADS. It is expected to be possible to test the ACS with the PWM driver available.

10.2 Further Development

It has been concluded that it is possible to obtain a reliable pointing control with a linear controller with magnetorquers as the only means of actuating. With the constraint of the magnetorquers not being able to induce torque components parallel to the magnetic field, it is inferred to be difficult to attain an arbitrary attitude with a linear controller. For a linear controller, it is proposed to look into the development of a reaction wheel, and dimensioning one or more reaction wheels to fit into a CubeSat. This actuator addition would also have the benefit of facilitating a much faster target attitude acquisition, and the magnetorquers permit momentum cancellation (de-spinning the reaction wheels), which is the important constraint of reaction wheels. Including reaction wheels in the satellite, however, the satellite can no longer be regarded a rigid body, and the rigid body dynamics posed will cease to apply, thus requiring new modelling of the satellite dynamics.

Pointing with only magnetorquer actuation available is possible with a linear controller, but it is considered desirable to develop a non-linear controller for the existing hardware as this would facilitate more precise control. This requires knowledge of non-linear controller theory, which

is beyond sixth semester literacy. With this in mind, the development of a non-linear pointing control system as a continuation of this project poses a valid project for sequent semesters.

For a future AAUSAT4 ADCS project it is also reckoned an obvious refinement to scrutinise attitude determination using other and more advanced methods than SVD, to overcome the limitation of not being able to determine the attitude when the sun vector and the geomagnetic field vector are parallel. Additionally a more advanced method, such as Kalman Filtering, should pose a better attitude propagation, taking more factors into account, and hence being better at computing a more accurate attitude, also when in eclipse and no sun vector is available.

Appendix A

Cubesat Standard

This section is written with knowledge from [Munukata 09].

A CubeSat is a small satellite of dimensions $10 \times 10 \times 11.35$ cm and a weight of max. 1.33 kg per unit. CubeSats are deployed into space using a Poly Picosatellite Orbital Deployer (P-POD). The standard was introduced in 1999 to increase the accessibility to space for small payloads, by lower cost, decreased development time and sharing of development documentation. The CubeSat standard is used by over 100 universities, high schools, and private firms.

A.1 CubeSat General Specifications

- All parts shall remain attached to the CubeSat during launch, ejection, and operation. No additional space debris shall be created.
- Pyrotechnics shall not be permitted.
- No pressure vessel over 1.2 atmosphere shall be permitted.
- Total stored chemical energy shall not exceed 100 Wh.
- No hazardous materials shall be used on a CubeSat.
- Total Mass Loss shall be $\leq 1\%$.
- Collected Volatile Condensable Material shall be $\leq 0.1\%$.

A.2 CubeSat Mechanical Requirements

- The CubeSat's Z axis shall be inserted first into the P-POD.
- The CubeSat's X and Y dimensions shall be 100.0 ± 0.1 mm.
- The CubeSat's Z dimension shall be 113.5 ± 0.1 mm.
- All components shall not exceed a 6.5 mm normal of the surface of the cube.
- Exterior CubeSat components shall not have contact to the inside of the P-POD, other than the designated CubeSat rails.
- The CoM shall be located within a sphere of 2 cm from the geometric centre of the CubeSat.

A.3 CubeSat Electrical and Operational Requirements

- No electronics shall be activated during launch, due to electrical and RF interference.
- CubeSats with batteries shall have the capability to receive a transmitter shutdown command, as per Federal Communications Commission regulation.
- All deployables such as booms, antennas, and solar panels shall wait to deploy a minimum of 30 minutes after the CubeSat's deployment switches are activated from P-POD ejection.
- RF transmitters greater than 1 mW shall wait to transmit a minimum of 30 minutes after the CubeSat's deployment switches are activated from P-POD ejection.
- Operators shall obtain and provide documentation of proper licenses for use of frequencies.
- The orbital decay lifetime of the CubeSats shall be less than 25 years after end of mission.

A.4 CubeSat Testing Requirements

- Random vibration testing shall be performed according to requirements specified by the launch vehicle.
- Thermal Vacuum Bake-out shall be performed to ensure proper out gassing of components, according to requirements specified by the launch vehicle.
- Visual inspection and measurements of the CubeSat shall be performed.
- The CubeSat must undergo and survive protoflight testing, specified by the launch vehicle provider, after which the CubeSat shall not be modified.

CubeSats are obliged to meet these requirements as an occurrence of damage to the main payload due to a faulty CubeSat, could jeopardise the launching of CubeSats into space in the future.

Appendix B

QB50

Source: [Smith 12]

QB50 is a joint ESA project, where a network of 50 CubeSats are launched into a Low Earth Orbit at around 320 km altitude. The satellite network is to conduct a series of scientific in-situ measurements in the lower thermosphere, planned for launch in early 2015.

B.1 Measuring in the Lower Thermosphere

The lower thermosphere is the least explored layer of the atmosphere, due to the high atmospheric drag at these altitudes, which causes a short lifetime for satellites. The only way to have satellites conduct measurements at these low altitudes has been to launch into a highly elliptical orbit resulting in a very short time spent in the region of interest per orbit. Sending a satellite into circular orbit at this altitude would simply be too costly because of the orbital decay.

A network of low-cost CubeSats for continuous in-situ measurements is an option which has not yet been organised, and the QB50 is the first project to do so. By itself, a CubeSat is too small to be able to carry out measurements of scientific value, but in a large network, where the loss of a few satellites is insignificant, the CubeSats pose a unique opportunity to conduct measurements of fundamental scientific value.

The mission of the QB50 CubeSats will be to study the re-entry process by measuring the constituents of the lower thermosphere from the deployment altitude of 320 km during decay to an expected altitude of about 90 km where they are expected to burn up in the atmosphere. The measured trajectories will be compared to the predicted, and this will be used to develop more accurate models of this part of the atmosphere and to better estimate the drag coefficients of CubeSats.

B.2 The QB50 CubeSat Network

The satellite network will consist of 40 double-unit CubeSat satellites which are to conduct the scientific measurements, and another 10 double- or triple-unit CubeSat satellites for In-Orbit-Demonstration (IOD) of new technologies and sensors.

The 40 double-unit CubeSat satellites will have one of two scientific units as payload, the first focusing on measurements of the neutral constituents in the lower thermosphere whereas the second focuses on measuring charged particles and the ambient plasma in the ionosphere.

The very low orbit altitude entails that the duration of the longest pass above one ground station will be around 2-5 min. As part of the QB50 collaboration, all participants will be able to receive data from any CubeSat in the network, allowing for a much higher uplink and downlink capability for each satellite, and hence a much higher payoff in terms of measurement data.

Appendix C

AAUSAT3 Sun Sensor design

The sun sensor included on the AAUSAT3 ADCS is built by the AAUSAT3 team and consists of two SLCD-61N8 photo diodes per sensor, a pair of two sensors are used per side of the satellite for bi-axis measurements.

C.1 Determination of the Sun Vector

From the surface of the side panel PCB where the diodes are mounted, there is a distance h to the surface of the satellite. In the metallic surface of the satellite, an oblong slot 90° on the photo diode array lets the sunray reach the photo diode at a distance x from directly below the edge of the slot. This allows for the calculation of the sun vector, see Figure C.1.

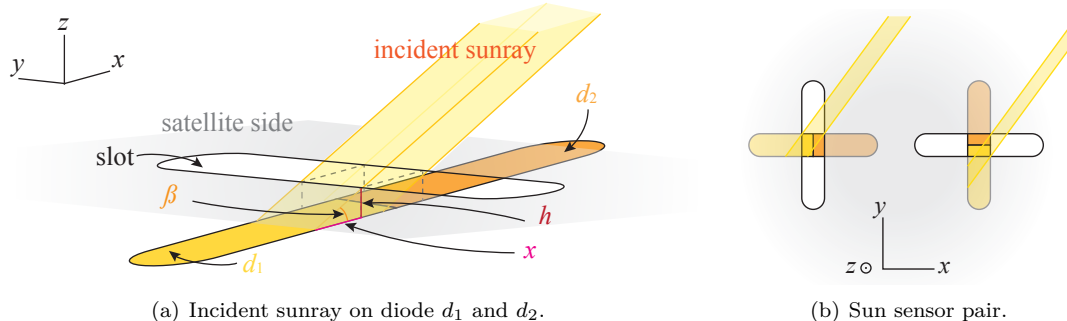


Figure C.1: Figure C.1(a) depicts a sun sensor, where the distance from the slot to the diode array, h , and the distance x determines the angle β . In figure C.1(a) the angle gives the xz-direction to the sun in the sun sensor reference frame. Figure C.1(b) depicts both sun sensors, the right giving the xz-angle and the left the yz-angle, which can be combined to the sun vector.

The distance x cannot be directly calculated, since each diode does not contain an array of diodes. Each diode outputs a current relative to the number of incident photons and the angle at which they are arriving. In the AAUSAT3 software, a ratio between the outputs of the two diodes, d_1 and d_2 , is used to determine the angle $\alpha = 90^\circ - \beta$. This angle, describing the direction of the sun vector, is determined as the ratio between the difference in output and the total output from

the two diodes, similar to a reflection coefficient:

$$\alpha_1 = \frac{d_1 - d_2}{d_1 + d_2} \cdot 100 \text{ [°]} \quad (\text{C.1})$$

In Equation C.1 the output is in degrees measured from the normal vector to the sensor plane, and a negative angle implies that the vector lies in the d_1 half plane and a positive angle that the vector lies in the d_2 half plane. The second angle is calculated replacing d_1 and d_2 with d_3 and d_4 , respectively. Each vector must be rotated into SBRF using the frames in Figure C.2.

C.2 Sun Sensor Coordinate System and Interfacing

The sun sensors on AAUSAT3 are mounted on the satellite according to Figure C.2, depicting the relation to the SBRF, and Table C.1, clarifying the sensitive direction of each sensor pair.

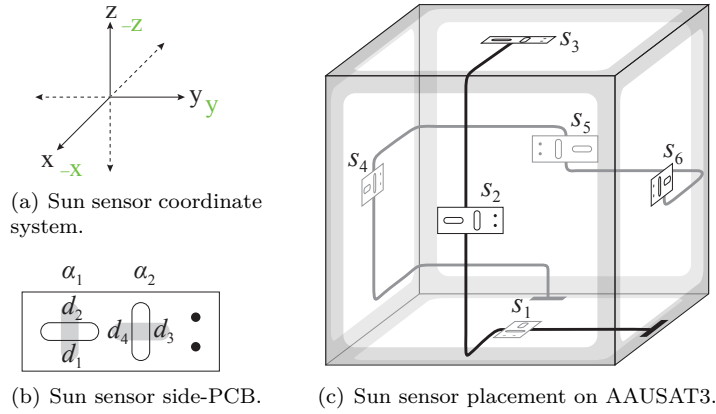


Figure C.2: In figure C.2(a) the reference frame of the sun sensors is depicted, the green axis-coordinates indicating SBRF. This reference frame is directly applied in in C.2(c), which depicts the orientation of each sensor pair and the number convention of side-PCBs on AAUSAT3. Figure C.2(b) displays the numbering of the photo diodes on each side-PCB.

Angle		Sensor 1	Sensor 2	Sensor 3	Sensor 4	Sensor 5	Sensor 6
α_1	Half plane	yz, z<0	xz, x>0	xz, z>0	yz, y<0	xz, x<0	yz, y>0
	Pos. angle	y<0	z>0	x<0	z<0	z>0	z<0
α_2	Half plane	xz, z<0	xy, x>0	yz, z>0	xy, y<0	xy, x<0	xy, y>0
	Pos. angle	x<0	y<0	y<0	x>0	y>0	x<0

Table C.1: Sun sensor measure planes, all given in the sun sensor reference frame, see figure C.2(a) and C.2(c). The positive angles relate to the diode numbering convention, see figures C.2(b) and C.1.

The power supply for the sun sensors is led through a circuit breaker switch, TPS2553-1, which will latch off during over or reverse current. The signals from the photo diodes are connected to a 16 bit ADC, ADS1148, which encompasses a standard SPI interface.

Appendix D

Additional Sensors and Actuators Considered for AAUSAT4

D.1 Star Tracker

Sources: [Schmidt 08, Hutchin 10, Liebe 02, Shucker 01]

Star trackers have traditionally been the preferred attitude determination technology for satellites due to its hight precision. In recent years, the development within MEMS and CMOS technology have brought the achievable size down to fit into CubeSats.

An autonomous star tracker consists of an electronic camera connected to a microcomputer. This holds an internal star catalogue and algorithms for identifying star patterns, hence enabling the attitude of the satellite to be determined. The star camera consists of a lens and the small CMOS sensor. When the starlight passes through the lens, it travels the focal length (distance from the lens to the photodiode array) and is projected onto the sensor elements.

The microcomputer of the star tracker contains a star catalogue which is a list of pairs of stars containing interstellar angles, distances and magnitudes of a chosen number of stars on the celestial sphere. The star detection includes determining the centre of a star from a weighing of the pixels in the defocused image, and comparing the star pattern to the internal star catalogue.

The star tracker has been deemed both too expensive (€ 20 000 [Buhl 13]) and too big ($30 \times 30 \times 38.1$ mm, 50 g [BST 12]) for the AAUSAT4 mission. General development of star tracker technology for CubeSats is still in progress, and it is recommended for future generations of AAUSATs that the star tracker should be reconsidered.

D.2 Sun Sensor Based on Solar Panels or Image Sensor

Other types of sensor technology can be used for sun sensors than the photocell design used for AAUSAT3. Instead of actual sensors, the solar panels can be used, which are already a part of the satellite design. By measuring the power output generated by each solar panel, it is possible to give a rough estimate of the inclination of the incident sunlight. Using solar panels offers less accuracy than other types of sun sensors, and are prone to measurement errors due to dazzling, caused by reflected sunlight off another object, thus giving a faulty sun vector.

Another type of sun sensor is an image based sun sensor, which lets the sunlight pass through a small pinhole in a mask plate onto an image sensor, as depicted in Figure D.1. The light will only illuminate certain pixels of the image sensor, and from this measurement, a determination of the inclination of the sunlight is possible. When using an image sensor, the angles of the light can be measured in two axes at the same time, unlike the photocell based sun sensor design. This type

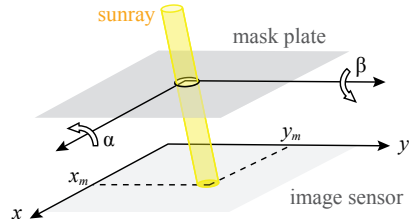


Figure D.1: Sun sensor based on an image sensor. The sunray let in through the pinhole illuminates a certain area on the image sensor. With the measured x_m and y_m values from the image sensor, the angles α and β can be determined.

of sun sensor is more precise than the other types mentioned, but it is also more complex and requires more computational power.

Utilisation of the solar panels as a way to determine direction will not be a focus of this project. However, seeing as it is purely a question of developing software, the possibility of using this method of attitude determination is still present in the future. The sun sensor design relying on an image sensor has been declined due to higher cost and more complex construction compared to the existing sun sensor design.

D.3 Horizon Sensor

A horizon sensor detects infrared light emitted from the Earth's atmosphere. This infrared radiation is of great contrast to the cold of space and it is therefore possible to detect the area between the Earth's atmosphere and space, i.e. the horizon of the Earth. Horizon sensors can be either of a static type, or a scanner. A static horizon sensor has a field of view large enough to sense the curvature of the Earth, and can only determine attitude when a crossing of the horizon is made.

While the horizon sensor is both small and relatively cheap, it has been discarded due to being too circumstantial with regards to giving usable attitude measurements. This is due to the fact that a considerable piece of visible horizon has to be in the field of view of the sensor.

D.4 Accelerometer

Source: [Omega 12]

An MEMS accelerometer measures the acceleration along its sensitive axis. When accelerated, the piezoelectrical material inside the microelectromechanical accelerometer will convert the applied mechanical force into a proportional electric charge.

Conceptually the accelerometer can be described as a device comprising a spring, a movable mass, and a sensor to measure displacement of the mass. The spring ensures that after ended acceleration the displacement of the mass will be reset. Furthermore, deceleration of the accelerometer will be interpreted in the same way as an acceleration. An accelerometer can be used to measure rotation of a given device, however, in order to do so the accelerometer must be displaced from the centre of rotation of the body. The displacement of the accelerometer needs to be taken into account when calculating the rotation of the device.

Hence, it is possible to use an accelerometer to determine rotation of the satellite, however, the gyroscope has been deemed superior, as the accelerometer is more prone to measurement errors due to vibration or acceleration.

D.5 Reaction Wheels

Source: [Inc. 13]

A reaction wheel consists of a motor for spinning a mass with a substantial amount of inertia. The concept of the reaction wheel is preservation of angular momentum. The reaction wheels are mounted along each of the three axes of the subject. The speed in either direction is controlled by a microprocessor.

$$L_{\text{total}} = J_{\text{satellite}} \cdot \omega_{\text{satellite}} + \sum_i J_{\text{wheel},i} \cdot \omega_{\text{wheel},i} \quad (\text{D.1})$$

Equation D.1 shows that the preservation of angular momentum requires a trade-off between the momentum of the satellite and the momenta of the reaction wheels. It is also seen how the velocity and inertia of the wheels have an effect on the spin rate of the satellite. Over time it is possible for the angular momentum of the wheels to reach an upper speed limit. This might result in the need for angular momentum cancellation, which can be done by other attitude control mechanisms. A spinning reaction wheel can act as a gyro stabilizer, which means that small disturbances has no effect on the orientation of the body.

In order for the AAUSAT4 attitude control to actuate fast enough, reaction wheels are considered necessary, the magnetorquers being able to allocate the possible occasional excess energy. The reaction wheels should be custom made at AAU in a future AAUSAT4 ADCS project, but will not be included in this project.

D.6 Thrusters

Sources: [Bellis 12] [NASA 13]

Thrusters are one of the most basic kinds of spacecraft propulsion systems. It is purely a utilisation of Newton's third law, that any applied force will produce an opposite force of equal magnitude. This is realized by ejecting some mass in one direction and having the spacecraft react in the opposite direction. The ejection of mass is what defines the thruster propulsion system, and the mass ejected is often a defining factor of what kind of thruster is in question. Most thrusters simply use pressure as a way of ejecting the mass, while other forms use electromagnetic fields.

D.6.1 Pressure Propulsion

The simplest of thrusters is merely a pressurised container with a nozzle attached that ejects mass in a given direction. This method of propulsion can be used for satellites in orbit to either rotate or change their position.

The most classic and well known thruster is the liquid fuel rocket propulsion, which burns fuel in order to generate overpressure and eject its fuel mass from a rocket nozzle. It utilises two liquid components: oxidiser and fuel, which is mixed and burned in the rocket engine in order to obtain thrust. The liquid fuel rocket propulsion is among the most powerful available with today's technology. However, the storage of both oxidiser and fuel poses an array of challenges, including very low temperature for certain oxidisers as well as extremely corrosive and/or acid fuels.

Solid fuel rocket propulsion utilises the same principle, however, with the solid fuel both the oxidiser and fuel component is combined in a mutual solid state material which is then burned, the exposed surface area of the solid fuel being proportional to the amount of thrust. A variety of different methods for obtaining the right thrust can be used, but all of them aim to supply a constant thrust level. The solid fuel is easier to store than the liquid fuel, but once a solid fuel source is ignited it will burn until all the fuel has been used, with no way of turning it off.

D.6.2 Ion Propulsion

A more advanced type of thruster is the ion propulsion. With this type of propulsion the fuel source is an inert gas, which is excited into plasma (it is also possible to have an ion fuel source that is solid). By using an inert gas, negative effects like oxidisation, hydrolysis, and sudden chemical reactions (explosions) can be avoided. In order to propel the spacecraft, the ion propulsion system uses electrical fields to accelerate the positive ions of the plasma, and thereby ejecting them away from the spacecraft. Since the main thrust is consisting of positive ions, a negative ion beam is added in order to retain the plasma state of the inert gas and also having a neutrally charged exhaust beam. While the ion propulsion can obtain the highest speeds for spacecrafts with current technology, the amount of acceleration force is extremely low.

All thruster types have been discarded in this project due to size, complexity, limited operational time due to fuel amount, and hazards related to liquid and/or solid fuels. However, if a small and cheap ion propulsion system, using solid fuel, would become available in the future, this would be an actuator method of interest.

Appendix E

Determination of Magnetorquer Torque

The derivations in this appendix are used to outline the general expressions for determining the torque produced by a magnetorquer. The derivations are first shown for one axis, and the rest of the derivations are done without further explanations. The bottom part of the appendix includes the dimensioning of a magnetorquer to be used for pointing the satellite.

The force applied to the satellite from the magnetorquers is the current through the coil times the length of the wire crossed with the magnetic field, as expressed in equation E.1.

$$\mathbf{F} = \mathbf{I}l \times \mathbf{B} \quad (\text{E.1})$$

where

- \mathbf{I} is the current running through the different sides of the coil,
represented as a vector going in the direction of the current flow.
- l is the length of the wire.
- \mathbf{B} is the surrounding magnetic field vector.

Four current vectors and a magnetic field vector can then be defined as shown, and the force vectors can be determined as shown in equation E.4.

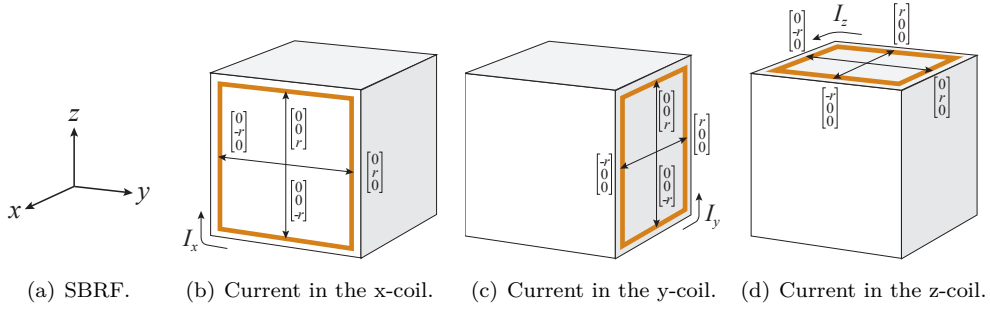
$$\mathbf{I}_{x,1} = \begin{bmatrix} 0 \\ -I_x \\ 0 \end{bmatrix} \quad \mathbf{I}_{x,2} = \begin{bmatrix} 0 \\ 0 \\ -I_x \end{bmatrix} \quad \mathbf{I}_{x,3} = \begin{bmatrix} 0 \\ I_x \\ 0 \end{bmatrix} \quad \mathbf{I}_{x,4} = \begin{bmatrix} 0 \\ 0 \\ I_x \end{bmatrix} \quad (\text{E.2})$$

$$\mathbf{B} = \begin{bmatrix} B_x \\ B_y \\ B_z \end{bmatrix} \quad (\text{E.3})$$

$$\begin{aligned} \mathbf{F}_{x,1} &= \begin{bmatrix} 0 \\ -I_x l \\ 0 \end{bmatrix} \times \begin{bmatrix} B_x \\ B_y \\ B_z \end{bmatrix} = \begin{bmatrix} -I_x B_z l \\ 0 \\ I_x B_x l \end{bmatrix} & \mathbf{F}_{x,2} &= \begin{bmatrix} 0 \\ 0 \\ -I_x l \end{bmatrix} \times \begin{bmatrix} B_x \\ B_y \\ B_z \end{bmatrix} = \begin{bmatrix} I_x B_y l \\ -I_x B_x l \\ 0 \end{bmatrix} \\ \mathbf{F}_{x,3} &= \begin{bmatrix} 0 \\ I_x l \\ 0 \end{bmatrix} \times \begin{bmatrix} B_x \\ B_y \\ B_z \end{bmatrix} = \begin{bmatrix} I_x B_z l \\ 0 \\ -I_x B_x l \end{bmatrix} & \mathbf{F}_{x,4} &= \begin{bmatrix} 0 \\ 0 \\ I_x l \end{bmatrix} \times \begin{bmatrix} B_x \\ B_y \\ B_z \end{bmatrix} = \begin{bmatrix} -I_x B_y l \\ I_x B_x l \\ 0 \end{bmatrix} \end{aligned} \quad (\text{E.4})$$

The results of these calculations are used to calculate the torque exerted on the satellite. The torque is calculated by crossing the lever arm vectors (shown in figure E.1) from the CoM to each side of the magnetorquer with the force applied by the given side of magnetorquer as shown in equation E.5.

$$\boldsymbol{\tau} = \mathbf{r} \times \mathbf{F} \quad (\text{E.5})$$



(a) SBRF. (b) Current in the x-coil. (c) Current in the y-coil. (d) Current in the z-coil.

Figure E.1: Definition of positive current direction through the magnetorquer coils in each axis. The lever arm length, r , is indicated for all current directions in the magnetorquers.

where

τ is the torque exerted on the satellite.

\mathbf{r} is a vector from CoM of the satellite side towards the side of the magnetorquer

Each of the vectors describing the lever arms to the four sides of the magnetorquers can be defined as shown below, and thereby the torques for the x-axis magnetorquer can be determined.

$$\mathbf{r}_{x,1} = \begin{bmatrix} 0 \\ 0 \\ r \end{bmatrix} \quad \mathbf{r}_{x,2} = \begin{bmatrix} 0 \\ -r \\ 0 \end{bmatrix} \quad \mathbf{r}_{x,3} = \begin{bmatrix} 0 \\ 0 \\ -r \end{bmatrix} \quad \mathbf{r}_{x,4} = \begin{bmatrix} 0 \\ r \\ 0 \end{bmatrix} \quad (\text{E.6})$$

$$\boldsymbol{\tau}_{x,1} = \begin{bmatrix} 0 \\ 0 \\ r \end{bmatrix} \times \begin{bmatrix} -I_x B_z l \\ 0 \\ I_x B_x l \end{bmatrix} = \begin{bmatrix} 0 \\ -r I_x B_z l \\ 0 \end{bmatrix} \quad \boldsymbol{\tau}_{x,2} = \begin{bmatrix} 0 \\ -r \\ 0 \end{bmatrix} \times \begin{bmatrix} I_x B_y l \\ -I_x B_x l \\ 0 \end{bmatrix} = \begin{bmatrix} 0 \\ 0 \\ r I_x B_y l \end{bmatrix}$$

$$\boldsymbol{\tau}_{x,3} = \begin{bmatrix} 0 \\ 0 \\ -r \end{bmatrix} \times \begin{bmatrix} I_x B_z l \\ 0 \\ -I_x B_x l \end{bmatrix} = \begin{bmatrix} 0 \\ -r I_x B_z l \\ 0 \end{bmatrix} \quad \boldsymbol{\tau}_{x,4} = \begin{bmatrix} 0 \\ r \\ 0 \end{bmatrix} \times \begin{bmatrix} -I_x B_y l \\ I_x B_x l \\ 0 \end{bmatrix} = \begin{bmatrix} 0 \\ 0 \\ r I_x B_y l \end{bmatrix} \quad (\text{E.7})$$

The total torque in the x-axis is then determined by a summation of all of the torques as shown in equation E.8.

$$\boldsymbol{\tau}_{x,\text{tot}} = \sum_{k=1}^4 \boldsymbol{\tau}_{x,k} = 2rlI_x \begin{bmatrix} 0 \\ -B_z \\ B_y \end{bmatrix} \quad (\text{E.8})$$

The rest of the axes are calculated explicitly below.

The arm, r , is the half length of the wire of one side of the coil, l , and the area that the coil encloses can be determined as the square of this length.

$$r = \frac{1}{2}l \quad l^2 = A \quad (\text{E.9})$$

The above calculations is for a one winding coil, so for the expression to apply for any number of windings, the expression is multiplied with the number of windings in the coil, N . An expression describing all the axes can then be made, as shown in equation E.10.

$$\begin{aligned} \boldsymbol{\tau}_{x,\text{tot}} + \boldsymbol{\tau}_{y,\text{tot}} + \boldsymbol{\tau}_{z,\text{tot}} &= AN \left(I_x \begin{bmatrix} 0 \\ -B_z \\ B_y \end{bmatrix} + I_y \begin{bmatrix} B_z \\ 0 \\ -B_x \end{bmatrix} + I_z \begin{bmatrix} -B_y \\ B_x \\ 0 \end{bmatrix} \right) \\ &= AN \begin{bmatrix} 0 & B_z & -B_y \\ -B_z & 0 & B_x \\ B_y & -B_x & 0 \end{bmatrix} \cdot \begin{bmatrix} I_x \\ I_y \\ I_z \end{bmatrix} \\ &= AN(\mathbf{I} \times \mathbf{B}) \end{aligned} \quad (\text{E.10})$$

The calculations using the magnetic field vector in the y- and z-axis can be seen below:

Calculations for the Y-axis

$$\mathbf{I}_{y,1} = \begin{bmatrix} I_y \\ 0 \\ 0 \end{bmatrix} \quad \mathbf{I}_{y,2} = \begin{bmatrix} 0 \\ 0 \\ I_y \end{bmatrix} \quad \mathbf{I}_{y,3} = \begin{bmatrix} -I_y \\ 0 \\ 0 \end{bmatrix} \quad \mathbf{I}_{y,4} = \begin{bmatrix} 0 \\ 0 \\ -I_y \end{bmatrix} \quad (\text{E.11})$$

$$\mathbf{F}_{y,1} = \begin{bmatrix} I_y l \\ 0 \\ 0 \end{bmatrix} \times \begin{bmatrix} B_x \\ B_y \\ B_z \end{bmatrix} = \begin{bmatrix} 0 \\ -I_y B_z l \\ I_y B_y l \end{bmatrix} \quad \mathbf{F}_{y,2} = \begin{bmatrix} 0 \\ 0 \\ I_y l \end{bmatrix} \times \begin{bmatrix} B_x \\ B_y \\ B_z \end{bmatrix} = \begin{bmatrix} B_x \\ I_y B_x l \\ 0 \end{bmatrix}$$

$$\mathbf{F}_{y,3} = \begin{bmatrix} -I_y l \\ 0 \\ 0 \end{bmatrix} \times \begin{bmatrix} B_x \\ B_y \\ B_z \end{bmatrix} = \begin{bmatrix} 0 \\ I_y B_z l \\ -I_y B_y l \end{bmatrix} \quad \mathbf{F}_{y,4} = \begin{bmatrix} 0 \\ 0 \\ -I_y l \end{bmatrix} \times \begin{bmatrix} B_x \\ B_y \\ B_z \end{bmatrix} = \begin{bmatrix} I_y B_y l \\ -I_y B_x l \\ 0 \end{bmatrix} \quad (\text{E.12})$$

$$\mathbf{r}_{y,1} = \begin{bmatrix} 0 \\ 0 \\ r \end{bmatrix} \quad \mathbf{r}_{y,2} = \begin{bmatrix} -r \\ 0 \\ 0 \end{bmatrix} \quad \mathbf{r}_{y,3} = \begin{bmatrix} 0 \\ 0 \\ -r \end{bmatrix} \quad \mathbf{r}_{y,4} = \begin{bmatrix} r \\ 0 \\ 0 \end{bmatrix} \quad (\text{E.13})$$

$$\boldsymbol{\tau}_{y,1} = \begin{bmatrix} 0 \\ 0 \\ r \end{bmatrix} \times \begin{bmatrix} 0 \\ -I_y B_z l \\ I_y B_y l \end{bmatrix} = \begin{bmatrix} r I_y B_z l \\ 0 \\ 0 \end{bmatrix} \quad \boldsymbol{\tau}_{y,2} = \begin{bmatrix} -r \\ 0 \\ 0 \end{bmatrix} \times \begin{bmatrix} -I_y B_y l \\ I_y B_x l \\ 0 \end{bmatrix} = \begin{bmatrix} 0 \\ 0 \\ -r I_y B_x l \end{bmatrix}$$

$$\boldsymbol{\tau}_{y,3} = \begin{bmatrix} 0 \\ 0 \\ -r \end{bmatrix} \times \begin{bmatrix} 0 \\ I_y B_z l \\ -I_y B_y l \end{bmatrix} = \begin{bmatrix} r I_y B_z l \\ 0 \\ 0 \end{bmatrix} \quad \boldsymbol{\tau}_{y,4} = \begin{bmatrix} r \\ 0 \\ 0 \end{bmatrix} \times \begin{bmatrix} I_y B_y l \\ -I_y B_x l \\ 0 \end{bmatrix} = \begin{bmatrix} 0 \\ 0 \\ -r I_y B_x l \end{bmatrix} \quad (\text{E.14})$$

$$\boldsymbol{\tau}_{y,\text{tot}} = \sum_{k=1}^4 \boldsymbol{\tau}_{y,k} = 2rlI_y \begin{bmatrix} B_z \\ 0 \\ -B_x \end{bmatrix} \quad (\text{E.15})$$

Calculations for the Z-axis

$$\mathbf{I}_{z,1} = \begin{bmatrix} -I_z \\ 0 \\ 0 \end{bmatrix} \quad \mathbf{I}_{z,2} = \begin{bmatrix} 0 \\ -I_z \\ 0 \end{bmatrix} \quad \mathbf{I}_{z,3} = \begin{bmatrix} I_z \\ 0 \\ 0 \end{bmatrix} \quad \mathbf{I}_{z,4} = \begin{bmatrix} 0 \\ I_z \\ 0 \end{bmatrix} \quad (\text{E.16})$$

$$\mathbf{F}_{z,1} = \begin{bmatrix} -I_z l \\ 0 \\ 0 \end{bmatrix} \times \begin{bmatrix} B_x \\ B_y \\ B_z \end{bmatrix} = \begin{bmatrix} 0 \\ I_z B_z l \\ -I_z B_y l \end{bmatrix} \quad \mathbf{F}_{z,2} = \begin{bmatrix} 0 \\ -I_z l \\ 0 \end{bmatrix} \times \begin{bmatrix} B_x \\ B_y \\ B_z \end{bmatrix} = \begin{bmatrix} -I_z B_z l \\ 0 \\ I_z B_x l \end{bmatrix}$$

$$\mathbf{F}_{z,3} = \begin{bmatrix} I_z l \\ 0 \\ 0 \end{bmatrix} \times \begin{bmatrix} B_x \\ B_y \\ B_z \end{bmatrix} = \begin{bmatrix} B_x \\ -I_z B_z l \\ I_z B_y l \end{bmatrix} \quad \mathbf{F}_{z,4} = \begin{bmatrix} 0 \\ I_z l \\ 0 \end{bmatrix} \times \begin{bmatrix} B_x \\ B_y \\ B_z \end{bmatrix} = \begin{bmatrix} I_z B_z l \\ 0 \\ -I_z B_x l \end{bmatrix} \quad (\text{E.17})$$

$$\mathbf{r}_{z,1} = \begin{bmatrix} 0 \\ r \\ 0 \end{bmatrix} \quad \mathbf{r}_{z,2} = \begin{bmatrix} -r \\ 0 \\ 0 \end{bmatrix} \quad \mathbf{r}_{z,3} = \begin{bmatrix} 0 \\ -r \\ 0 \end{bmatrix} \quad \mathbf{r}_{z,4} = \begin{bmatrix} r \\ 0 \\ 0 \end{bmatrix} \quad (\text{E.18})$$

$$\boldsymbol{\tau}_{z,1} = \begin{bmatrix} 0 \\ r \\ 0 \end{bmatrix} \times \begin{bmatrix} 0 \\ I_z B_z l \\ -I_z B_y l \end{bmatrix} = \begin{bmatrix} -r I_z B_y l \\ 0 \\ 0 \end{bmatrix} \quad \boldsymbol{\tau}_{z,2} = \begin{bmatrix} -r \\ 0 \\ 0 \end{bmatrix} \times \begin{bmatrix} -I_z B_z l \\ 0 \\ I_z B_x l \end{bmatrix} = \begin{bmatrix} 0 \\ r I_z B_x l \\ 0 \end{bmatrix}$$

$$\boldsymbol{\tau}_{z,3} = \begin{bmatrix} 0 \\ -r \\ 0 \end{bmatrix} \times \begin{bmatrix} 0 \\ -I_z B_z l \\ I_z B_y l \end{bmatrix} = \begin{bmatrix} -r I_z B_y l \\ 0 \\ 0 \end{bmatrix} \quad \boldsymbol{\tau}_{z,4} = \begin{bmatrix} r \\ 0 \\ 0 \end{bmatrix} \times \begin{bmatrix} I_z B_z l \\ 0 \\ -I_z B_x l \end{bmatrix} = \begin{bmatrix} 0 \\ r I_z B_x l \\ 0 \end{bmatrix} \quad (\text{E.19})$$

$$\boldsymbol{\tau}_{z,\text{tot}} = \sum_{k=1}^4 \boldsymbol{\tau}_{z,k} = 2rlI_z \begin{bmatrix} -B_y \\ B_x \\ 0 \end{bmatrix} \quad (\text{E.20})$$

Dimensioning of the Magnetorquer

The satellite travels with a velocity of approximately 7800 km/s around Earth. If the satellite is set to point at MCC at all times in orbit, the maximum needed angular acceleration of the satellite, when assuming it already has been detumbled, is $0.8992 \cdot 10^{-3}$ rad/s². Using Newton's second law for rotational motion, presented in section 6.2, it is possible to calculate the maximum torque needed to point the satellite in one direction by placing this torque in the worst axis (the y-axis has the highest inertia according to the inertia matrix) and multiplying this vector by the inertia matrix. Thereby maximum torque the magnetorquer is to carry out is calculated to be 83752 nNm.

The area of the magnetorquers are chosen to be the maximum area that the satellite can contain, which is 7.5x7.5 cm. The lowest magnetic field strength in an orbit with an altitude of 320 km, is approximately 20000 nT. This value is found using a magnetic field contour map using IGRF11. It is known that the maximum current allowed to run through coils used on the AAUSAT3 magnetorquers is 20 mA. With these different informations, the size of the magnetorquer can then be calculated by rearranging equation 6.17. The angle θ is set to be 90° to make the calculation easier.

$$N = \frac{\|\boldsymbol{\tau}\|}{\|\mathbf{I}\| A \|\mathbf{B}_E\| \sin \theta} = 37223$$

The discrepancy between the number of windings needed for AAUSAT3 and the number of windings estimated for AAUSAT4 is very significant, up to a factor of ~150. It is expected that this deviation is caused by stricter requirements for actuation of the satellite as well as the use of two different inertia matrices. Furthermore, the inertia matrix used for the AAUSAT3 magnetorquer dimensioning is 50 times smaller than the inertia matrix used for the AAUSAT4 dimensioning.

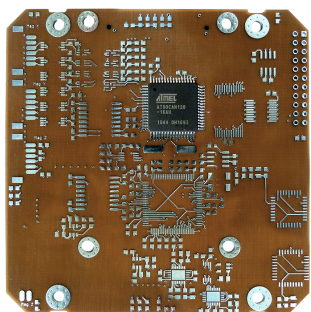
This amount of windings seems excessive, which will result in an increase in coil resistance and thereby require a higher voltage in order to obtain the same current of 20 mA. Another possibility would be to increase the cross sectional area of the wire used for the coils, but this would mean an increase in the weight of the magnetorquer. Either way it does not seem like magnetorquers would be the optimal way of trying to follow the TRF. The magnetorquers should not have a problem with nadir pointing, as long as they are able to produce more torque than needed to overcome the disturbance torques.

From earlier development for the AAUSAT3, a magnetorquer of 250 windings is available. With the software already available for the ADCS PCB for AAUSAT3 it is only possible to actuate for 88% of the time [Vinther 10]. Also it is assumed that the $\sin(\theta)$ has a mean (RMS) value of $\frac{1}{\sqrt{2}}$. With these constraints, the maximum torque that these magnetorquers are able to apply is calculated to be approximately 270 nNm. As the aerodynamic disturbance torque calculated in section 6.1.2 is approximately 259 nNm it should be possible to use this magnetorquer for nadir pointing.

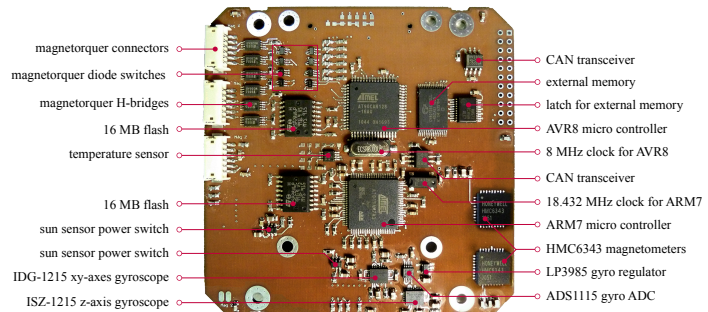
Appendix F

Constructing the ADCS PCB for the Acceptance Test

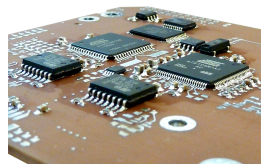
In order to be able to conduct the acceptance test, a PCB had to be prepared. Adapting the hardware design from AAUSAT3, a spare PCB has been soldered with SMD components, see Figure F.1. Additionally a sun sensor (side) PCB had to be assembled for the acceptance test, requiring reflow soldering of the photo diodes, see Figure F.2.



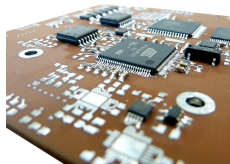
(a) Early stage assembly of PCB.



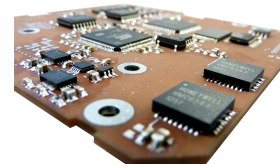
(b) Final assembled PCB.



(c) MCUs and external memory.

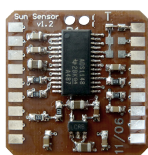


(d) Before gyro soldering.

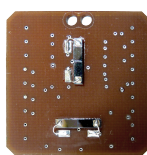


(e) After gyro and magnetometer reflow soldering.

Figure F.1: Assembly of SMD components on the ADCS PCB.



(a) Sun sensor circuitry.



(b) Sun sensor photo diodes.



(c) Front cover, sensor side.



(d) Front cover, outside.

Figure F.2: Sun sensor side PCB and aluminium cover.

The PCBs are mounted inside a CubeSat mock-up in order to be able to conduct the acceptance test. The magnetorguers were not included in the test set-up, as a magnetorquer PWM driver was unavailable.



Figure F.3: Assembled mock-up of the CubeSat with ADCS PCB, sun sensor and their interconnection.

Appendix G

Test Protocol for Acceptance Test

Description

The test is used to determine the precision of the attitude determination. This is done by setting up an environment similar to what the satellite experiences in orbit. The goal is to determine a predefined attitude and then compare this data to the data achieved from the attitude determination on the satellite. A light acting as the sun and a set of Helmholtz coils acting as the magnetic field of the Earth define the test set-up.

Test Set-up



Figure G.1: Test set-up for the acceptance test in the satellite laboratory.

Figure G.1 shows a picture of the set-up used to test the attitude determination. The satellite is placed within a set of Helmholtz coils with a magnetic field pointing in the direction of the x-axis in the TECI (ECI frame of the test environment). A spotlight is used to imitate the sun so it is possible to measure an angle of the sun vector. The satellite is placed as close to the centre of the magnetic field induced by the Helmholtz coils as possible, to ensure that the magnetic field is as uniform as possible. The satellite is placed on an angle chart (see figure G.2) to make it possible to turn the satellite with a known angle, to be able to make attitude determination in Matlab which can be compared to the results from the test.

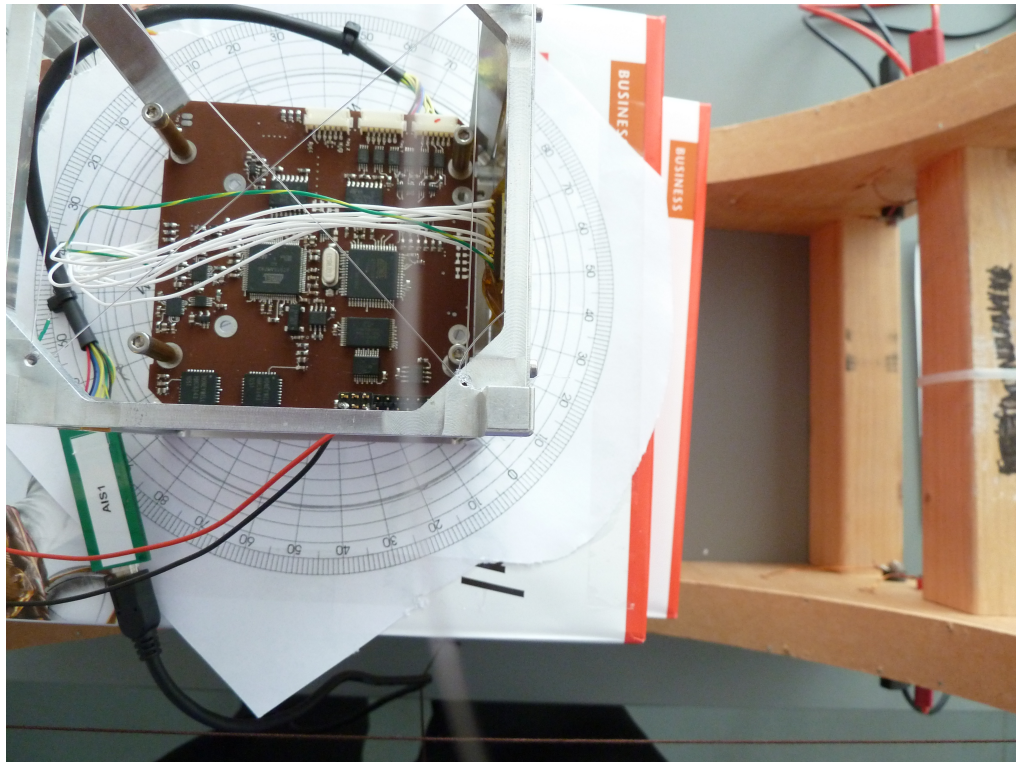


Figure G.2: The picture shows the angle chart used to compare the measured angle to the real angle of the sun vector.

Calculations

The calculations for the determination of the error angles are mainly done in the Matlab file *acceptance_test.m* included on the CD. This script determines the expected attitude quaternion and multiplies it with the conjugated attitude quaternion obtained during the test. This produces the error quaternion which is converted to an angle error. As angles determined by the sun vectors, deviates a lot from the actual angle, the satellite is actually rotated, the script also determines the error quaternion and angle error only using the magnetometer measurements.

Results

Angle on Chart [°]	Sun Sensor Angle [°]	Calculated Quaternion	Estimated Quaternion	Error Angle[°]	Sun Vector	MAG Vector	Magnet Error Quaternion	Magnet Error Angle [°]
0 (-9,-3)	$\begin{bmatrix} 0 \\ 0 \\ -0.6088 \\ 0.7934 \end{bmatrix}$	$\begin{bmatrix} 0.069851 \\ -0.002809 \\ -0.008923 \\ 0.997514 \end{bmatrix}$	$\begin{bmatrix} 0.034560 \\ -0.989665 \\ 0.139173 \\ 0 \end{bmatrix}$	2.7333	$\begin{bmatrix} 9855 \\ -308 \\ 0 \\ 0 \end{bmatrix}$	$\begin{bmatrix} 0 \\ 0 \\ -0.0128 \\ 0.9999 \end{bmatrix}$	$\begin{bmatrix} 0 \\ 0 \\ 1.4670 \\ 0 \end{bmatrix}$	
15 (-9,14)	$\begin{bmatrix} 0 \\ 0 \\ -0.5000 \\ 0.8660 \end{bmatrix}$	$\begin{bmatrix} 0.068875 \\ -0.012019 \\ 0.121601 \\ 0.990114 \end{bmatrix}$	$\begin{bmatrix} 0.222762 \\ -0.964888 \\ 0.139173 \\ 0 \end{bmatrix}$	23.2277	$\begin{bmatrix} 9673 \\ -2939 \\ 0 \\ 0 \end{bmatrix}$	$\begin{bmatrix} 0 \\ 0 \\ -0.0076 \\ 1.0000 \end{bmatrix}$	$\begin{bmatrix} 0 \\ 0 \\ 0.8717 \\ 0 \end{bmatrix}$	
30 (-9,34)	$\begin{bmatrix} 0 \\ 0 \\ -0.3827 \\ 0.9239 \end{bmatrix}$	$\begin{bmatrix} 0.067546 \\ -0.017826 \\ 0.293305 \\ 0.953463 \end{bmatrix}$	$\begin{bmatrix} -0.567994 \\ -0.811180 \\ 0.139173 \\ 0 \end{bmatrix}$	13.3268	$\begin{bmatrix} 8654 \\ -5383 \\ 0 \\ 0 \end{bmatrix}$	$\begin{bmatrix} 0 \\ 0 \\ -0.0005 \\ 1.0000 \end{bmatrix}$	$\begin{bmatrix} 0 \\ 0 \\ 0.0587 \\ 0 \end{bmatrix}$	
45 (-9,59)	$\begin{bmatrix} 0 \\ 0 \\ -0.2588 \\ 0.9659 \end{bmatrix}$	$\begin{bmatrix} 0.059103 \\ -0.0020164 \\ 0.467664 \\ 0.881698 \end{bmatrix}$	$\begin{bmatrix} -0.850778 \\ -0.511199 \\ 0.121869 \\ 0 \end{bmatrix}$	11.2867	$\begin{bmatrix} 7031 \\ -7482 \\ 0 \\ 0 \end{bmatrix}$	$\begin{bmatrix} 0 \\ 0 \\ 0 \\ 1.0000 \end{bmatrix}$	$\begin{bmatrix} 0 \\ 0 \\ 0.0021 \\ 0 \end{bmatrix}$	
60 (-9,93)	$\begin{bmatrix} 0 \\ 0 \\ -0.1305 \\ 0.9914 \end{bmatrix}$	$\begin{bmatrix} 0.075609 \\ -0.0026265 \\ 0.657124 \\ 0.749521 \end{bmatrix}$	$\begin{bmatrix} 0.990268 \\ -0.0000 \\ 0.139173 \\ 0 \end{bmatrix}$	9.0811	$\begin{bmatrix} 5091 \\ 8961 \\ 0 \\ 0 \end{bmatrix}$	$\begin{bmatrix} 0 \\ 0 \\ 0.0092 \\ 1.0000 \end{bmatrix}$	$\begin{bmatrix} 0 \\ 0 \\ 1.0521 \\ 0 \end{bmatrix}$	
75 (-9,52)	$\begin{bmatrix} 0 \\ 0 \\ 0 \\ 1.0000 \end{bmatrix}$	$\begin{bmatrix} 0.130595 \\ -0.134610 \\ 0.482854 \\ 0.855381 \end{bmatrix}$	$\begin{bmatrix} -0.740488 \\ -0.578583 \\ 0.342020 \\ 0 \end{bmatrix}$	8.0818	$\begin{bmatrix} 2621 \\ -9999 \\ 0 \\ 0 \end{bmatrix}$	$\begin{bmatrix} 0 \\ 0 \\ 0.0156 \\ 0.9999 \end{bmatrix}$	$\begin{bmatrix} 0 \\ 0 \\ 1.7901 \\ 0 \end{bmatrix}$	

Angle on Chart [°]	Sun Sensor Angles [°]	Calculated Quaternion	Estimated Quaternion	Error Angle [°]	Sun Vector	MAG Vector	Magnet Error Quaternion	Magnet Error Angle [°]
-15	(-9, 20)	$\begin{bmatrix} 0 \\ 0 \\ 0.1305 \\ 0.9914 \end{bmatrix}$	$\begin{bmatrix} 0.070077 \\ 0.005336 \\ -0.166244 \\ 0.983577 \end{bmatrix}$	8.0793	$\begin{bmatrix} 0.354880 \\ -0.924495 \\ 0.139173 \\ 0 \end{bmatrix}$	$\begin{bmatrix} 9470 \\ 2352 \\ 0 \\ 0 \end{bmatrix}$	$\begin{bmatrix} 0 \\ 0 \\ 0.0166 \\ 0.9999 \end{bmatrix}$	1.9006
-30	(-9, -39)	$\begin{bmatrix} 0 \\ 0 \\ 0.2588 \\ 0.9659 \end{bmatrix}$	$\begin{bmatrix} 0.077778 \\ 0.016060 \\ -0.313580 \\ 0.946235 \end{bmatrix}$	9.0435	$\begin{bmatrix} 0.621572 \\ -0.767578 \\ 0.156435 \\ 0 \end{bmatrix}$	$\begin{bmatrix} 8398 \\ -4849 \\ 0 \\ 0 \end{bmatrix}$	$\begin{bmatrix} 0 \\ 0 \\ 0.0164 \\ 0.9999 \end{bmatrix}$	1.8826
-45	(-9, -59)	$\begin{bmatrix} 0 \\ 0 \\ 0.3827 \\ 0.9239 \end{bmatrix}$	$\begin{bmatrix} 0.060412 \\ 0.018425 \\ -0.470032 \\ 0.880387 \end{bmatrix}$	13.0221	$\begin{bmatrix} 0.859570 \\ -0.496273 \\ 0.121869 \\ 0 \end{bmatrix}$	$\begin{bmatrix} 6822 \\ -6836 \\ 0 \\ 0 \end{bmatrix}$	$\begin{bmatrix} 0 \\ 0 \\ 0.0155 \\ 0.9999 \end{bmatrix}$	1.7799
-60	(-9, -91)	$\begin{bmatrix} 0 \\ 0 \\ 0.5000 \\ 0.8660 \end{bmatrix}$	$\begin{bmatrix} 0.037643 \\ 0.013317 \\ -0.660642 \\ 0.749638 \end{bmatrix}$	24.2639	$\begin{bmatrix} 0.997564 \\ 0.0000 \\ 0.06756 \\ 0 \end{bmatrix}$	$\begin{bmatrix} 4707 \\ 8447 \\ 0 \\ 0 \end{bmatrix}$	$\begin{bmatrix} 0 \\ 0 \\ 0.0035 \\ 1.0000 \end{bmatrix}$	0.3979
-75	(-9, -78)	$\begin{bmatrix} 0 \\ 0 \\ 0.6088 \\ 0.7934 \end{bmatrix}$	$\begin{bmatrix} -0.013747 \\ -0.010753 \\ -0.621508 \\ 0.783214 \end{bmatrix}$	26.9054	$\begin{bmatrix} 0.973776 \\ -0.224814 \\ -0.034899 \\ 0 \end{bmatrix}$	$\begin{bmatrix} 2281 \\ -9477 \\ 0 \\ 0 \end{bmatrix}$	$\begin{bmatrix} 0 \\ 0 \\ 0.0027 \\ 1.0000 \end{bmatrix}$	0.3117

Part I

Litterature

Bibliography

- [Arovas 08] Daniel Arovas. *Winter 2008: UCSD Phys 110B Lecture Notes chap 13.* 2008. http://physics.ucsd.edu/students/courses/winter2008/physics110b/LECTURES/CH13_RIGID_BODIES.pdf.
- [Bak 02] Thomas Bak. Lecture notes - modeling of mechanical systems. Master's thesis, Aalborg University, 2002. Aalborg University.
- [Bellis 12] Mary Bellis. *How Rockets Work*, 2012. <http://inventors.about.com/od/rstartinventions/a/SolidPropellant.htm>.
- [Bougher 97] Stephen W. Bougher & Raymond G. Roble. *Thermosphere*. vol. Encyclopedia of Planetary Science, 1997. <http://www.springerreference.com/docs/html/chapterdbid/30926.html#min>.
- [BST 12] Berlin Space Technologies BST. *Star Tracker ST-200*, 2012. <http://www.berlin-space-technologies.com/index.php?id=10>.
- [Buhl 13] Matthias Buhl. *Star Tracker BST-200 price*. e-mail, March 2013. e-mail can be found on the attached cd.
- [Cai 12] Yongyao Cai, Yang Zhao, Xianfeng Ding & James Fennelly. *Magnetometer basics*. 2012. http://www.memsic.com/userfiles/files/publications/Articles/Electronic_Products_Feb_%202012_Magnetometer.pdf.
- [Celestrak 13] Celestrak. *NORAD CubeSat TLE*, 2013. <http://www.celestrak.com/NORAD/elements/cubesat.txt>.
- [Honeywell 07] Honeywell. *HMC6343 Datasheet*, 2007.
- [Hoots 80] Felix R. Hoots & Ronald L. Roehrich. *Spacetrack Report No. 3: Models for Propagation of NORAD Element Sets*. December 1980. <http://www.amsat.org/amsat/ftp/docs/spacetrk.pdf>.
- [Hutchin 10] Richard A. Hutchin & Gail Erten. *Miniaturized Interferometric Star Tracker for Cubesats (C-MiST)*. 2010.
- [Inc. 13] Microsat Systems Canada Inc. *What is a Reaction Wheel*. 2013. <http://www.reactionwheel.com/resources/reactionwheel.pdf>.
- [InvenSense 08] InvenSense. *IDG-1215 Datasheet*, 2008.
- [InvenSense 09] InvenSense. *ISZ-1215 Datasheet*, 2009.

BIBLIOGRAPHY

- [J. Peraire 09] S. Widnall J. Peraire. *Lecture L26 - 3D Rigid Body Dynamics: The Inertia Tensor.* 2009. http://ocw.mit.edu/courses/aeronautics-and-astronautics/16-07-dynamics-fall-2009/lecture-notes/MIT16_07F09_Lec26.pdf.
- [Jewett 08] John W. Jewett & Raymond A. Serway. Physics for scientists and engineers with modern physics. David Harris, seventh edition, 2008.
- [Kelso 12] T. S. Kelso, David A. Vallado, Paul Crawford & Richard Hujksak. *Revisiting Spacetrack Report #3: Rev 2.* August 2012. <http://celestrak.com/publications/AIAA/2006-6753/AIAA-2006-6753-Rev2.pdf>.
- [Lewin 99] Walter Lewin. *Physics I: Classical Mechanics.* video, 1999. <http://ocw.mit.edu/courses/physics/>.
- [Liebe 02] Carl Christian Liebe. *Accuracy Performance of Star Trackers A Tutorial.* IEEE Transactions on Aerospace and Electronic Systems, vol. 38, no. 2, April 2002. <http://ieeexplore.ieee.org/stamp/stamp.jsp?tp=&arnumber=1008988>.
- [Markley 99] F. Landis Markley & Daniele Mortari. *How to estimate attitude from vector observations.* 1999. http://www.malcolmdshuster.com/FC_MarkleyMortari_Girdwood_1999_AAS.pdf.
- [Markowitz 10] Alex Markowitz. *Fall 2010: UCSD Phys 1B Lecture Notes.* 2010. http://www-physics.ucsd.edu/students/courses/fall2010/physics1b/documents/LECT17_2262211.pdf.
- [Munukata 09] Riki Munukata. *Cubesat Design Specifications.* 2009. http://cubesat.org/images/developers/cds_rev12.pdf.
- [NASA 71] NASA, Robert Lyle & Pericles Stabekis. *Spacecraft Aerodynamic Torques.* January 1971. NASA Space Vehicle Design Criteria (Guidance & Control) <http://www.dept.aoe.vt.edu/~cdhall/courses/aoe4065/NASADesignSPs/sp8058.pdf>.
- [NASA 13] NASA. *Ion Propulsion.* 2013. <http://www.nasa.gov/centers/glenng/about/fs21grc.html>.
- [of Geomagnetism 10] International Association of Geomagnetism & Aeronomy. *International Geomagnetic Reference Field.* January 2010. <http://www.ngdc.noaa.gov/IAGA/vmod/igrf.html>.
- [Omega 12] Omega. *Accelerometers.* 2012. <http://www.omega.co.uk/prodinfo/accelerometers.html>.
- [Schmidt 08] Marco Schmidt & Klaus Schilling. *Pico-satellite Capabilities for Telecommunication and Earth Observation.* Space Exploration Technologies, Proc. of SPIE, vol. 6960, no. 696005, 2008. http://proceedings.spiedigitallibrary.org/data/Conferences/SPIEP/22045/696005_1.pdf.
- [Sensors 99] Sensors. *A Micromachined Quartz Angular Rate Sensor for Automotive and Advanced Inertial Applications.* no. -, 1999. <http://www.sensorsmag.com/sensors/position-presence-proximity/a-micromachined-quartz-angular-rate-sensor-automotive-and-ad-1071>.
- [Sensors 03] Sensors. *An Overview of MEMS Inertial Sensing Technology.* no. -, 2003. <http://www.sensorsmag.com/sensors/acceleration-vibration/an-overview-mems-inertial-sensing-technology-970>.

- [Shucker 01] Brian Shucker. *Ground-Based Prototype of CMOS Navigational Star Camera for Small Satellite Applications*. 15th AIAA/USU Conference on Small Satellites, 2001.
- [Sidi 97] Marcel J. Sidi. Spacecraft dynamics & control - a practical engineering approach. Numeéro 7 in Cambridge Aerospace. Press Syndicate of the University of Cambridge, 1997.
- [Silonex 09] Silonex. *SLCD-61N8 Datasheet*, 2009.
- [Singarayar 13] Fiona Singarayar, R. Reinhard, C. Asma, C. Bernal, W. Wegelaar & D. Kataria. *QB50 System Requirements and Recommendations*. February 2013. <https://www.qb50.eu/download/requirements/QB50SystemRequirementsDocument-20130206.pdf>.
- [Smith 12] A. Smith, T. Beuselinck, J. F. Dalsgaard Nielsen, J. De Keyser, A. Gregorio, D. Kataria, V. Lappas, F. J. Lübben, J. Moen, S. Palo, R. Reinhard, A. Ridley, J. Rotteveel, G. Schmidtke & T. Schmiel. *QB50 Sensor Selection Working Group*. March 2012. https://www.qb50.eu/sswg_report.pdf.
- [Sørensen 06] Sofie Louise Sandberg Sørensen. Oersted as a gravity mission satellite. Master's thesis, 2006. Master's Thesis, Niels Bohr Institute.
- [Texas Instruments 09] Texas Instruments. *ADS1115 Datasheet*, 2009.
- [Texas Instruments 10] Texas Instruments. *ADS1148 Datasheet*, 2010.
- [Vinther 10] Kasper Vinther & Kasper Fuglsang Jensen. Attitude determination and control system for aausat3. Master's thesis, Aalborg University, June 2010.
- [Wahba 65] Grace Wahba. *A Least Squares Estimate of Spacecraft Attitude*. 1965. <http://www.stat.wisc.edu/~wahba/ftp1/oldie/wahbasproblem.pdf>.
- [Wertz 78] James R. Wertz. Spacecraft attitude determination and control. D. Reidel Publishing Company, 1978.
- [Wertz 99] James R. Wertz & Wiley J. Larson. Space mission analysis and design. Space Technology. Space Technology Library, third edition, 1999.
- [Winetraub 06] Yonatan Winetraub & San Bitan. *Attitude Determination – Advanced Sun Sensors for Pico-satellites*. January 2006. <http://www.agi.com/downloads/corporate/partners/edu/advancedSunSensorProject.pdf>.
- [Wiśniewski 99] Rafał Wiśniewski. *Lecture Notes on Modeling of a Spacecraft*. 1999. Aalborg University.

